Morphodynamic optimisation study of the design of semi-permeable dams for rehabilitation of a mangrove-mud coast

A case study of the Building-with-Nature project in Demak, Indonesia

Technische Universiteit Delft

Master thesis

B.P. Smits

October 17, 2016

TU Delft

Morphodynamic optimisation study of the design of semi-permeable dams for rehabilitation of a mangrove-mud coast

A case study of the Building-with-Nature project in Demak, Indonesia

By

B.P. (Bob) Smits

4086686

in partial fulfillment of the requirements for the degree of

Master of Science

in Civil Engineering

at Delft University of Technology

to be defended publicly on Friday November 4, 2016 at 11:00 AM.

An electronic version of this thesis is available at http://repository.tudelft.nl/.

Thesis committee

Prof.dr.ir. J.C. Winterwerp

Dr. K. Cronin

Prof.dr.ir M.J.F. Stive

Dr.ir. M. Van der Wegen

Dr. B.K. Van Wesenbeeck

F. Van der Goot, MSc

Delft University of Technology

Faculty Civil Engineering and Geosciences

Department of Hydraulic Engineering

Section of Environmental Fluid Mechanics

Deltares

Enabling Delta Life

TU Delft

Delft University of Technology

Abstract

Due to the removal of mangrove forests, the coastal zone of Demak district has suffered from severe erosion. One of the proposed solutions to restore the sediment balance and encourage mangrove re-establishment, is the construction of semi-permeable dams. This study aims to optimise the design of such structures.

A 2DH site-specific model was set up in Delft3D Flexible Mesh to simulate the large-scale morphodynamics of the area. As Demak coastal zone is a data poor environment, the model validation was largely based on qualitative observations and expert judgement.

In order to capture sediment behind the dams, the system mainly depends on locally eroded sediment. Waves dominate the availability of sediment in the area. After waves have stirred up the sediment on the foreshore, the tidal current transports the suspended sediment towards shore.

The model results show that the dams successfully attenuate waves and capture sediment. Important design aspects were studied, aiming to formulate more generic guidelines for the design of such structures. New dams were found to have a negative influence on the sedimentation rate behind surrounding dams that are located backward or sidewards. For comparable mangrove-mud coasts, single coast-parallel dams are expected to capture more sediment than closed off cells. It is recommended to use the model to test new dam configurations and to study other design aspects. In order to fully validate the model, more data should be gathered.

Preface

This thesis reports on my graduation work for the master program Hydraulic Engineering at Delft University of Technology. The work is part of the Building with Nature project in Demak (Indonesia), which attracted my attention because of the interesting combination of a challenging physical environment and an innovative approach. Even though at times the software did not cooperate, I quite enjoyed working on the project. I sincerely hope my contributions will form a small step towards the regrowth of the mangrove ecosystem and renewed safety for local residents in Demak.

The research was carried out at Deltares, where there is expertise on ecological and hydrological aspects of mangrove forests, as well as numerical modeling of hydrodynamics, fine sediments and morphology in D-Flow Flexible Mesh. The basis of this model is constructed in collaboration with Eric Julianus who was simultaneously doing his MSc thesis work for the same project (Building with Nature, Indonesia), researching the potential of a fine sediment nourishment.

I would like to express my gratitude to the people who contributed to my thesis or supported me personally. First of all I would like to thank Katherine Cronin for her great daily supervision, her vigilance and her constructive feedback. I would like to thank professor Han Winterwerp, head of my graduation committee, for the fruitful meetings, his guidance and his incredible involvement with the project. Thanks to professor Marcel Stive for his focus on the research goals and to Mick van der Wegen for sharing his experience in modeling mud flats and helping to interpret the model results. Bregje van Wesenbeeck and Fokko van de Goot thanks for linking the research to the daily practice of the project. Thanks to Arthur, Adri and Michal for all the support with the Delft3D Flexible Mesh software. Lastly, I would like to thank the students at Deltares for the necessary distraction with animated conversations during the breaks.

Bob Smits
Delft, September 2016

Contents

Chapter 1

Introduction

This chapter gives an introduction to the topic of this thesis. It starts with a motivation for research and a brief introduction of the Demak coastal zone in section 1.1. Next, in section 1.2 a problem analysis is given. Subsequently, the objectives and research questions are discussed in section 1.3. Section 1.4 explains the project approach. Finally the outline of the report is presented in section 1.5.

1.1 Motivation for research

The coastal zone of Demak district has suffered from severe erosion and related floodings, mainly due to the removal of mangrove forests. The loss of the flood protection that the mangrove forests once offered has caused coastal retreat from a few hundred meters up to a kilometer (at some places) in recent decades (Ecoshape, 2015). An integrated, site-specific strategy has been implemented in Demak district applying a Building with Nature approach. The main solution proposed is to bring back a healthy mangrove ecosystem. Proposed measures to restore the sediment balance and encourage mangrove re-establishment are the construction of semi-permeable dams and a nourishment of fine sediment. The research presented here is focussed on the design conditions and impact of these semi-permeable dams.

1.2 Problem analysis

Historically, the coastal zone of Demak district was protected from flooding by a mangrove greenbelt that attenuates waves and captures and stabilises sediment, see figure 1.1. However, the conversion of mangrove belts into aquaculture ponds has impeded this protective function (Van Wesenbeeck *et al.*, 2015). Additionally, the sediment supply to the intertidal area is diminished, as aquaculture pond systems disconnect the river from the natural floodplain. This situation is exacerbated by land subsidence and the impacts of

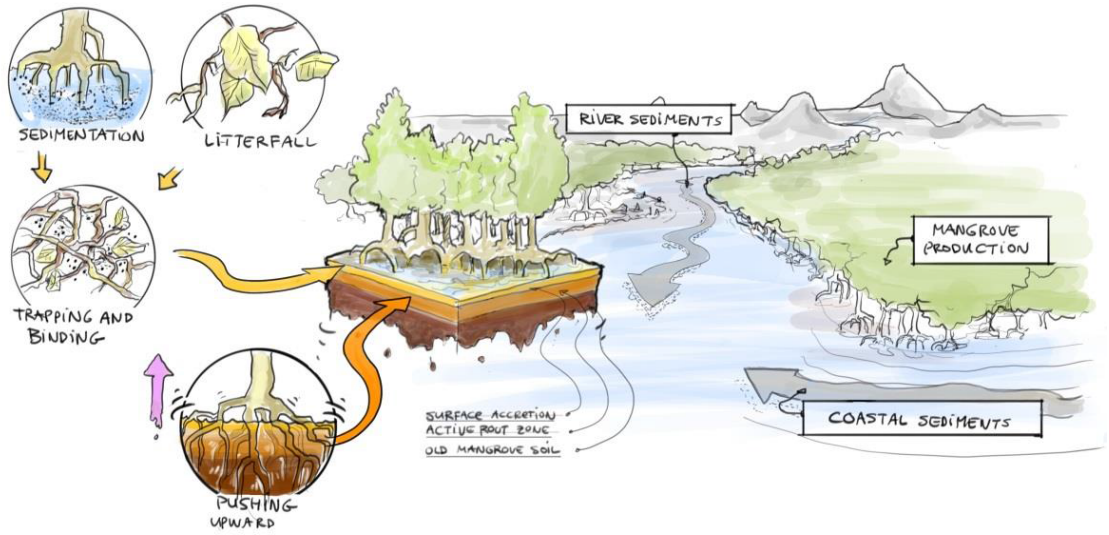

Figure 1.1: Schematisation mangrove-sediment interaction (Ecoshape, 2015)

climate change, particularly by the increased intensity and frequency of storms and associated floods and by sea level rise. During storm surges, high tides and periods of excessive rainfall, this has severely increased flood risk in the area. The past decades rapid shoreline degradation and erosion have been recorded at an average rate of 100 m/year (Winterwerp *et al.*, 2014). In figure 1.2 the positions of the Demak coastline in years between 2003 and 2013 are indicated, as well as the locations of local villages, roads and rivers. The coastline has now retreated upto the road between Bogorame and Timbulsloko, which is about to collapse, thus exposing kilometers of hinterland to flooding. Moreover, the removal of mangroves has led to loss of other economic, environmental and social services.

As the soil consists of very fine, cohesive sediments, conventional engineering measures failed due to lack of stability. Locally, these hard structures were even found to intensify erosion by blocking sediment transport towards the coast and by enhancing wave effects due to wave reflection (Winterwerp *et al.*, 2013). Moreover, they are too expensive, unable to adapt to climate change and do not have the economic, environmental and social benefits that healthy mangrove ecosystems offer. A building with nature approach, on the other hand, could solve the erosion problems in a way that is more resilient to the impacts of climate change by using natural processes for mangrove rehabilitation. Simple mangrove planting was also unsuccessful, as the conditions (e.g. sediment input) were not suitable for growth of mangrove seedlings.

According to Bradshaw (1987): “In order to restore a healthy mangrove belt, the currently degraded system needs to be restored to its original state in terms of ecological, physical and chemical system properties.” The erosion in the Demak coastal zone is caused by disturbance of the fine sediment balance. A first step is to restore this balance is to stop the

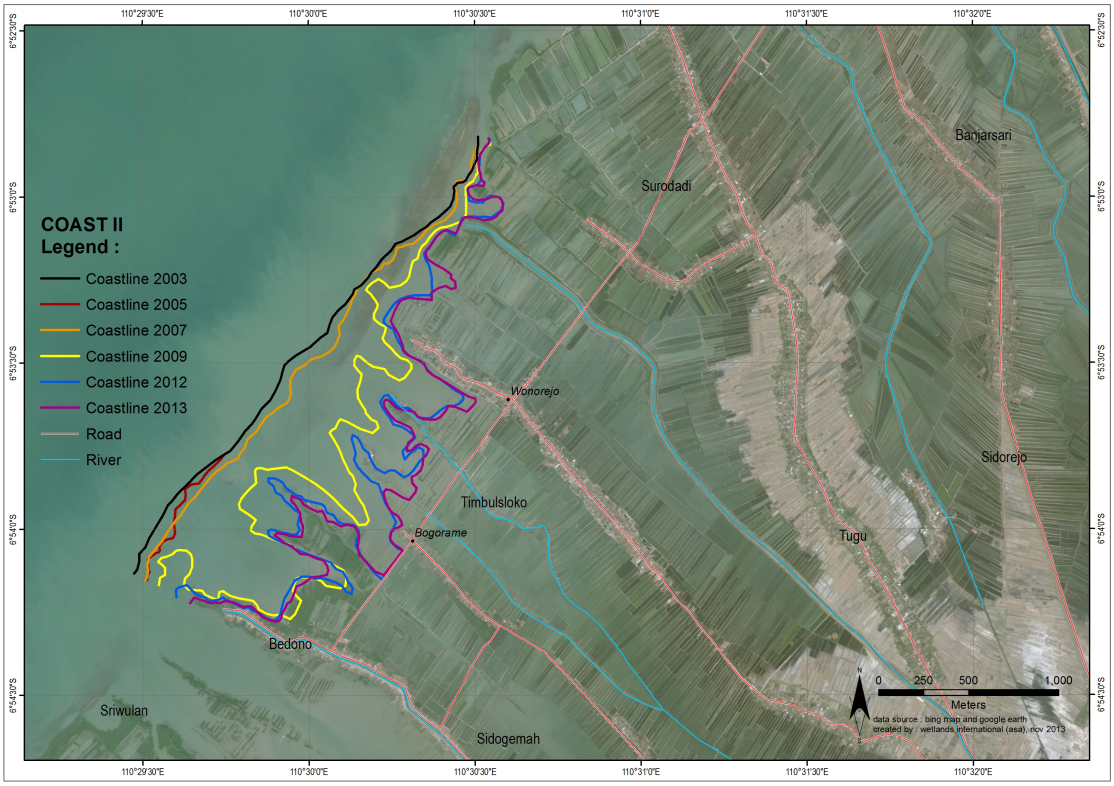

Figure 1.2: Development of Demak coastline between 2003 and 2013.

erosion process and regain a stable coastline. More sediment needs to be deposited on the coast than the amount being washed away. Thus removing the causes for degradation and providing suitable environmental conditions for natural regeneration of mangroves.
Semi-permeable dams made of bamboo piles and brushwood have successfully reduced erosion and stimulated sedimentation in comparable muddy environments (Schmitt *et al.*, 2013; Van Cuong *et al.*, 2015; Saengsupavanich, 2013). It uses local, biodegradable materials and is easy to establish using simple equipment. An ongoing pilot study for which a dam was constructed in the field, is showing promising results. However, little is known about the spatial design of such dams to obtain optimal sedimentation and a favourable environment for mangrove recovery, which is the focus of this research.

1.3 Research objectives

This research aims to get a better understanding of the large-scale morphodynamics of the Demak coastal area, including hitherto disregarded phenomena such as wave-induced effects and feedback from bed level change on hydrodynamic processes. It focusses on the design of semi-permeable dams to restore sediments along the coast, aiming to simulate the effect of interaction between multiple dams on sediment transport and sedimentation patterns. Moreover, the research aims to provide more generic guidelines on the spatial

arrangement of dams for large scale implementation.

For this purpose, the following research questions have been formulated:

- What factors play a critical role in the sediment transport in the Demak coastal zone? Which physical phenomena determine the availability of sediment and from which sources does that sediment originate?
- What is the settling pattern of fine sediments behind the semi-permeable dams? Can the initial deposition that was observed behind the pilot dam be simulated?
- How does the interaction between multiple semi-permeable dams affect sediment transport and sedimentation patterns? How can the spatial arrangement of the dams be optimised for sedimentation and (ultimately) mangrove recovery in Demak coastal zone?
- Can more generic guidelines be formulated for the design of semi-permeable structures in a muddy environment?

1.4 Approach

First, a literature study was performed. The functions of mangrove forests for coastal resilience in muddy environments were studied, as well as favourable conditions for rehabilitation of mangrove forests. Moreover, coastal processes affecting the Demak coast and the use of semi-permeable structures for wave damping were investigated. A better understanding of the large-scale and long term coastal system of Demak is necessary, in order to identify the physical phenomena play an important role in the sediment transport in the area. For this purpose, a system analysis of Demak coastal zone was undertaken.
Next, a numerical model was set up in Delft3D Flexible Mesh (FM) to assess the potential and optimise the spatial design of semi-permeable structures for sedimentation of fine sediments. This model helps to establish whether favourable conditions for mangrove recovery are achieved. If this is the case, it is assumed mangrove regrowth will indeed occur, thereby stabilising the coastline. More generically, such a numerical model helps to formalise the knowledge and experience gained during the proposed regional-scale Building with Nature application, potentially making these applicable to other conditions.
It should be noted that the availability of data in the area of interest is very limited, i.e. modeling a data-poor environment. Model validation was therefore only partially be possible and was largely based on expert judgement.

1.5 Outline report

Before diving into the details of Demak coastal zone, first some theoretical background is given about hydrodynamic coastal processes, fine sediment dynamics, mangrove forests

and semi-permeable structures. This is subject of in chapter 2. Once the basic theoretical concepts are described, they can be applied to Demak coastal zone in chapter 3. The physical parameters that play an important role in sediment transport at Demak coastal zone are quantified, including hydrodynamics (e.g. tides, waves) and morphodynamics (sediment sources and sinks). Next, chapter 4 discusses the most important design considerations for the semi-permeable structures, based on reference projects and a pilot study.
Chapter 5 describes the numerical research method. It contains a model description, as well as the model set-up and validation. Chapter 6 gives the results of the numerical research and a sensitivity analysis. These results are discussed and related to theory and observed behaviour of the system in chapter 7. Finally, in chapter 8 the conclusions of the research are given, along with some recommendations for further research.

Chapter 2

Theoretical background

Before describing the area in more detail, the most important theoretical concepts that are essential to get a better understanding of the erosion problems are described in this chapter, along with criteria for mangrove restoration. First the hydrodynamic processes that play a role in a coastal zone are introduced in section 2.1. Section 2.2 describes properties of fine sediments and the processes of sedimentation and erosion. Moreover, the impacts of the discussed hydrodynamic processes on large-scale sediment transport on mud coasts are considered. Mangrove forests are the subject of section 2.3, including its ecosystem services and rehabilitation. Lastly, semi-permeable structures are discussed in section 2.4, including their interaction with flow and spatial design of such structures.

2.1 Hydrodynamic coastal processes

The important hydrodynamic nearshore processes that influence tides and waves as they move towards shore are described here. The main focus is on processes that affect sediment transport.

2.1.1 Tides

Definitions
The vertical rise and fall of the water level is called *tide*. High tide means high water levels, whereas low tide means low water levels. The time it takes for the water level to rise from lowest to highest elevation is called the *rising period*. The subsequent time it takes to reach the lowest level again is called the *falling period*. The length of the rising period does not necessarily equal that of the falling period. Tidal currents are the related horizontal movements back and forward, where flood currents have velocities in the tidal propagation direction and ebb current velocities are oppositely directed. Due to the phase relationship between vertical and horizontal tide, a falling tide does not necessarily coincide with ebb currents.

Slack water is the name used for the reversal of tidal flow. Flow reversal from ebb to flood occurs around low water and is therefore called *low water slack*. For flow reversal from flood to ebb *high water slack* occurs around high water.

Tidal character
The tidal character is determined by the tidal constituents, that originate from influences of the moon, sun and irregularities in the Earth's movement. The tidal constituents are named accordingly, with a letter representing the origin of the constituent and an index representing the number of daily cycles. For example the component M2 represents the influence of the moon. Similarly, the component S2 represents the influence of the sun. Both these components are called semi-diurnal components as they occur twice daily, indicated by the index. It is important to note that the main lunar tide has a slightly longer period that the main solar tide, resulting in spring-neap tide variability. When the moon and the sun are aligned, the M2 and S2 components are in phase causing spring tide. When the components are out of phase it is neap tide.
A measure for the tidal character is the form factor F. The form factor is defined as the relative amplitude of the main diurnal components compared to the amplitude of the main semi-diurnal components:

$$F = \frac{K1 + O1}{M2 + S2} \tag{2.1}$$

with the symbols of the constituents in this case indicating their respective amplitudes.
Based on the form factor, four categories are distinguished. An overview of these categories and examples of corresponding tidal curves are given in appendix A.

Tidal propagation
The slowly varying tide propagates as a tidal wave with a large wave length relative to the amplitude and is therefore a long wave. On its way towards coastal waters, the tidal wave is distorted by local differences in water depth and by restriction of the width or reflection, both due to land masses. As the wave period does not change, the wave length is affected by changes in the propagation speed. The wave celerity is proportional to the square root of the water depth. When tidal waves get into shallower water the celerity decreases, which results in a concentration of energy and thus an increase in tidal amplitude (comparable to the shoaling effect of wind waves in shallow water).

2.1.2 Waves

Wave transformation
As waves propagate from deep water towards the coast, they are affected by the seabed and transform through processes such as *refraction, diffraction shoaling, bottom friction* and *wave-breaking*. The following definitions were taken from Lighthill (1978) and Holthuijsen (2007) and were slightly altered for the purpose of this report.
Refraction is the turning of waves towards shallower water due to depth- or current-induced changes in the phase speed along the wave crest. For gentle slopes and parallel depth contours, refraction causes waves to turn to a more shore-parallel orientation. *Diffraction* is

wave transformation due to sheltering by obstacles such as islands or breakwaters (Penney & Price, 1952). *Shoaling* is the variation of waves in their direction of propagation due to depth-induced changes of the group velocity in that direction. When waves approach the shore, the wave celerity is reduced. The wave height increases in order to conserve wave energy. *Bottom friction* becomes more important wherever the water depth is about half the wavelength so that the waves induce significant horizontal motions near the bottom. When the wave height becomes larger than a certain fraction of the water depth waves start to break. This is called *depth-induced breaking* since the limiting wave height is governed by a water depth limitation. This fraction is between 0.78 (for solitary wave theory) and 0.88 (for Stokes wave theory), which is explained in more detail in appendix B. Breaking waves form a surface roller (which can be observed from the foam in the breaker zone) that temporarily stores energy and momentum. The wave energy is first converted into turbulent kinetic energy and subsequently dissipated through the production of turbulence.

Wave orbital motion & wave boundary layer

Underneath the wave surface the fluid particles follow an orbital path, because of the oscillatory horizontal and vertical flow velocities. In deep water the orbits are circular, but in shallow water the orbits transform to an elliptical shape, see figure 2.1. Looking at the vertical distribution, the vertical displacement diminishes towards the bottom. The horizontal displacement, however, remains almost constant.

Close to the bed, a thin wave boundary layer will form, due to the wave-induced motion of the water particle. It is the transition between the bed and the 'normal' oscillating flow. Here, vorticity is generated that is not accounted for in linear wave theories (that assumes irrotational fluid). Energy dissipation takes place in this boundary layer. Moreover, streaming causes a non-zero wave-averaged horizontal flow in the wave propagation direction in the wave boundary layer (Longuet-Higgins, 1953). Outside the breaker zone, it is therefore potentially important for transporting sediment onshore.

Bed shear stresses & turbulence modelling

Flow induces turbulent stresses on the soft sediment bed, the so-called *Reynold stresses*. These stresses are characterised by large spatial and temporal fluctuations. Orbital velocities from waves also induce an additional bed shear stress component. The flow in the wave boundary layer is generally turbulent due to the presence of sediment on the bed. Because of the thin boundary layer, the velocity gradients perpendicular to the bed are large, giving rise to large stresses in the wave boundary layer (Hinze, 1975). Hence, wave energy is dissipated and sediment can be mobilised.

The local velocity thus consists of a mean, a wave and a turbulent part. This makes it more difficult to distinguish between fluctuations induced by turbulence and by the mean flow when waves are present. Detailed modeling of the wave boundary layer is there a complex research field. In order to refrain from turbulence modelling, often empirical friction laws are used, introducing friction coefficients. In order to take into account mixing effects, the concept of turbulent eddy viscosity is widely used.

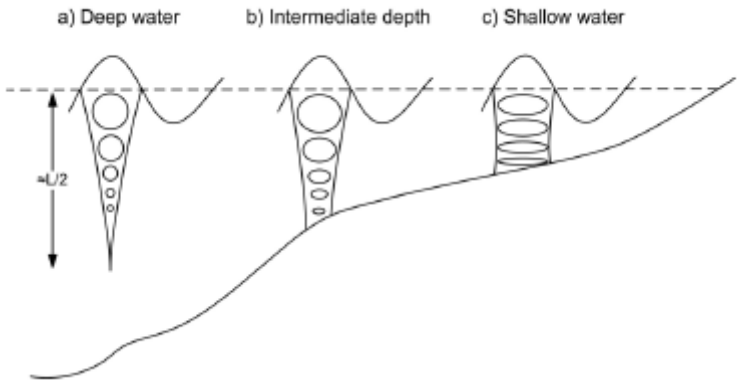

Figure 2.1: Trajectories of water particles in orbital motion for deep water, at intermediate depth and in shallow water (Ippen, 1966)

Radiation stress

Besides energy, waves also transfer momentum. This can be regarded equivalent to a stress, according to Newton's second law. Depth-integrated and wave-averaged flux of momentum due to waves is defined as *radiation stress* (Longuet-Higgins & Stewart, 1962). Horizontal variations in this stress may act as forces on the water. In shallow waters these forces can be important, particularly in the surf zone, which may lead to considerable set-up, set-down and strong currents.

Due to wave dissipation in the breaker zone, momentum is transferred from the wave motion to the mean flow. In alongshore direction this gives rise to a wave-induced *longshore current*. The driving force behind this current (acting in longshore direction) is the cross-shore gradient in radiation shear-stress. The longshore current is therefore limited to the surf zone and can strongly influence the sediment transport in that area.

In the area of interest, however, the coastal slope is very gentle, hence the cross-shore gradient in radiation stress is much smaller. Set-up, set-down and wave-induced currents will therefore not be so large. Note that, besides this wave-induced current, also tidal and wind forces can generate a current along the coast.

Considering the vertical distribution of the forces, a secondary circulation pattern may arise that can potentially influence sediment transport. The imbalance between the cross-shore wave radiation stress gradient and the pressure gradient over the vertical is indicated by figure 2.2. The pressure gradient due to set-up is constant over the vertical, whereas the radiation stress term is particularly large near the surface due to the strong pressure and velocity variations in the surface roller of breaking waves (above the wave trough level). Fluid particles above mean trough level will therefore experience a net force in shoreward direction (averaged over the wave period), creating a surface current (and mass flux) towards the coast. Fluid particles below mean trough level, on the other hand, will be forced seaward, thereby creating a seaward current called *undertow*.

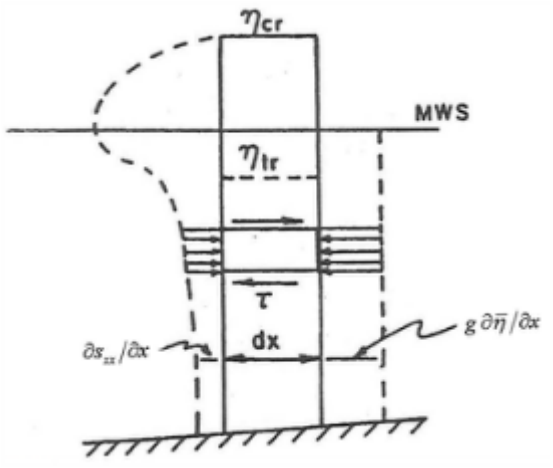

Figure 2.2: Schematisation of vertical distribution of stresses acting on a water column in the surfzone (Svendsen, 2006)

2.2 Sediment dynamics

In order to understand the morphodynamic behaviour of a (muddy) coastline, this section describes sediment dynamics for fine sediment. First, some fine sediment properties are described, including cohesion, flucculation and settling velocity. Next, erosion of fine sediments is considered on particle scale, including several types of erosion models and transport formulae. Finally, the implications for large scale sediment transport on mud coasts are regarded.

2.2.1 Fine sediment properties

The information in this section is largely based on Winterwerp & Van Kesteren (2004) and corresponding lectures on sediment dynamics course at TU Delft.
Mud mixtures consist of fine sediments, such as silt and clay. For sufficiently large clay content, when individual sand or silt particles can no longer settle out in suspension, these mud mixtures have cohesive properties. Clay particles are negatively charged at their face, attracting cations. These cations align in a so-called diffusive double layer, at the edge of which the net electrical charge is zero. Therefore particles can approach each other. As a result of the Van der Waals forces, clay particles can aggregate forming flocs. This process is limited by the Kolmogorov length scale, as turbulent stresses rapidly increase beyond this scale (Batchelor, 1960). Therefore, flocs have a typical equilibrium size of hundreds of micrometers. It is important to keep in mind that flocculation is a dynamic process (dependent on space, time, organic composition, etc.) that takes time. Therefore flocs may not be in equilibrium. Mud flocs are loose structures that exhibit a large water content of typically 80-95%, that grows with floc size. The bearing capacity of mud is therefore much lower than for sand. Moreover, mud mixtures have small permeabilities, because of the small grain size. The combination of large water content and small permeability

can cause risk of liquefaction, where the soil loses all strength and stiffness and starts to behave like a liquid.

When fine sediment particles are in suspension, they start to settle. In sandy beds with some fine sediment, larger particles tend to settle faster than smaller particles, which causes segregation (i.e. sorting of sediment). The fine sediment particles settle on top of the bed, forming a very soft layer on the scale of millimeters, called *fluffy layer*. Tidal flow mixes these fine sediment particles over the water column through turbulent entrainment. At slack water, where velocities are small, fines get time to settle again and are deposited on top of the consolidated bed again, thereby reforming the fluffy layer. This is a continuous process over the tidal cycle.
For Euclidian particles (such as sand), Stokes presumed that a particle settling in a viscous fluid at constant settling velocity, drag forces balance gravity forces. Mud flocs, however, are not massive Euclidean particles and Stokes' classical settling law does not apply. Since settling occurs while flocs are aggregating, settling velocity increases with floc size. From field measurements, it is known that settling velocity first increases with Suspended Particle Matter (SPM) concentration, due to enhanced flocculation. However, beyond a certain concentration the settling velocity decreases as a result of *hindered settling* (Dankers & Winterwerp, 2007). As SPM concentration increases rapidly at the bottom of the water column, flocs higher in the water column are in the wake flow of flocs that are lower in the water column, see figure 2.3. The resulting buoyancy effect is particularly relevant for flocs, because of the large volume/mass ratio (i.e. large water content) and already occurs at relatively small SPM concentrations. Because of flocculation and hindered settling, the settling velocity is not constant.
Once fine sediment particles have settled to the bottom of the water column, they are deposited on the bed forming a soft soil. After deposition the soil consolidates, gradually increasing the density and strength of the soil. During consolidation water is squeezed out of the soil, as porosity decreases. If no new sediment particles are added, the bed will lower as consolidation continues.

2.2.2 Erosion of fine sediments

In the classic Partheniades-Krone erosion model, the difference between the flux of sediment from the bed (erosion) and the flux of sediment towards the bed (deposition) equals the increase in SPM concentration (Partheniades, 1965). The deposition rate of sediment particles on the bed is governed by the SPM concentration and the settling velocity. For the erosion rate, simply a threshold is taken for the onset of erosion (Kandiah, 1974; Ariathurai & Arulanandan, 1978). This model cannot adequately represent steady or slowly varying flow, as the threshold for erosion is either exceeded (causing unlimited erosion) or not exceeded (leading to continuous siltation).
Therefore a two-layer buffer model was suggested by Van Kessel *et al.* (2011). In that model a distinction is made between an upper (active) layer, which is characterised by short time scales, and a lower layer, which is characterised by long time scales. Deposition

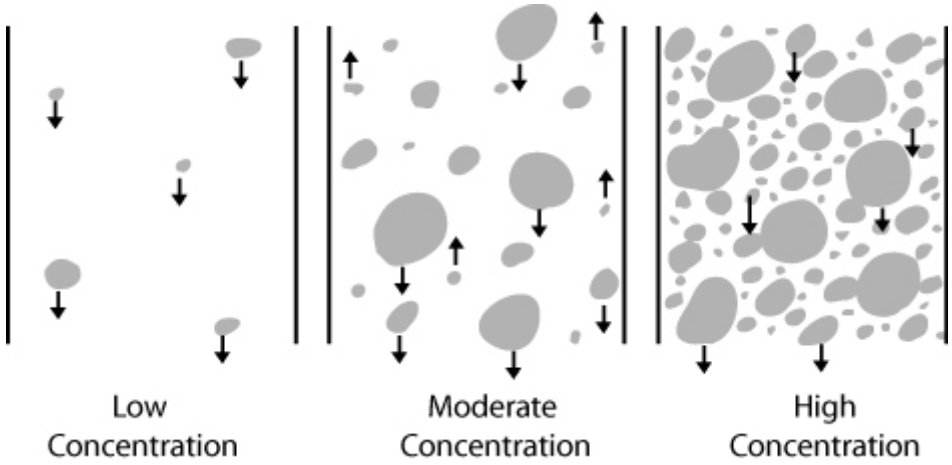

Figure 2.3: Schematisation of hindered settling for different sediment concentrations (Major, 2003)

and erosion of both layers are considered separately, as a function of physical and biological processes (including bed form migration, pore water underpressures and bioturbation).

Classic (coarse) sediment transport formulae (e.g. Engelund-Hansen) are only valid if the availability of sediment is not limited (i.e. in alluvial conditions). In starved bed conditions, where the availability of sediment is limited (e.g. a consolidated muddy bed), the entrainment of fines is governed by the strength distribution within the bed. This is important for understanding the erosion of muddy coasts. Entrainment is the re-suspension of particles from the bed through turbulent vertical mixing, which is enhanced by a thickening of the flow boundary layer as an effect of waves, as explained in section 2.1.2.
Three erosion modes can be distinguished for mud-mixtures: floc, mass and surface erosion (Mehta *et al.*, 1989), see figure 2.4. Floc erosion is the disruption of individual sediment flocs (or part of these flocs) from the bed when flow-induced peak stresses exceed the drained strength of unconsolidated flocs. When flow-induced stresses become even larger and locally exceed the undrained bed strength, undrained erosion of lumps of material from an over-consolidated bed may occur. This is called mass erosion and is caused by failure within the bed through crack formation. Surface erosion is a drained process during which layers of flocs are removed from the consolidating bed (Kandiah, 1974), i.e. the sediment particles are replaced by water. Turbulent flows change the stress state of a soil, which induces small deformations of the bed and, consequently, negative pore water pressure gradients. This over-consolidated state initiates an inflow of water into the bed according to Darcy's law. As a result, pore water pressure gradients dissipate and the sediment strength decreases. Thus, a surface erosion threshold can be established at the decreased bed strength upon exceedance by flow-induced stresses. It is important to note that peaks in turbulence-induced bed shear stresses can be large, so erosion can even occur when the mean bed shear stress is lower than the mean bed strength (Van Prooijen & Winterwerp, 2010).

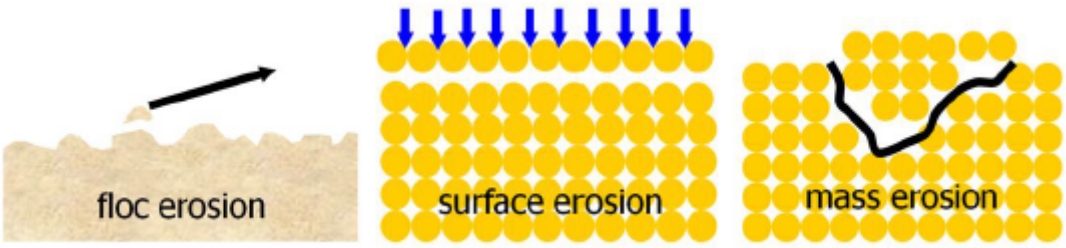

Figure 2.4: Schematisation of erosion types for cohesive sediment (courtesy of prof. Winterwerp)

2.2.3 Sediment transport on mud coasts

Mud coasts in equilibrium are characterised by a convex-up profile and mild slopes (1:1000 to 1:1500). Due to refraction, tides and long (swell) waves approach the coastline more or less perpendicularly. Waves damp more by viscous dissipation on the mild slope, than by wave-breaking, hence long-shore currents are small. Sediments pathways are therefore largely perpendicular to the coast.
As explained in section 2.1.2, waves stir up fine sediments from the bed. Under non-breaking waves, turbulent conditions occur only very close to the bed as the turbulent boundary layer is very thin. Hence, waves stir up the sediment from the bed through erosion or re-suspension, but they do not mix sediments over the water column. Wave-induced streaming close to the bed may then result in an onshore directed transport, although this will be much smaller than the transport by the tidal current. Inside the breaker zone, on the other hand, depth-induced breaking enhances vertical mixing. Additionally, waves may weaken the soil by oscillatory wave stresses that can even liquefy the soil. The energy required to mobilise fine, loosely packed, cohesive sediments from the bed is much smaller than the energy required to keep that sediment in suspension. As a result, waves dominate erosion of the seabed. After waves have mobilised sediments, wave- and flow-induced currents tend to mix and transport the sediment. Wave-induced currents tend to be an order of magnitude smaller than tidal currents, because fine sediments can only accumulate in areas with low wave action. Therefore the transport of sediments is governed by tidal flow.
So generally, where waves erode the mangrove-mud coast, tidal currents bring sediment to the coast. It should be noted, however, that large waves do not only erode the coast, but also stir up fine sediments from the foreshore. During rising water, the mobilised sediments are mixed over the water column and transported towards the coast. According to Winterwerp *et al.* (2005), this is also the reason why coast-parallel breakwaters work contra-productive along mud coasts, as the offshore sediment source is reduced.

It is important to note that coastal retreat is a net effect as a result of a balance between two gross effects, viz. sedimentation and erosion. The dynamic location of the coastline therefore results from the sediment transport towards the coast by tidal filling and large waves and erosion by both large and small waves. Eroding mudflats tend to attain a

concave-up profile, where wave effects become even larger. All mangrove habitat is lost in these areas, which results in loss of coastal protection by mangroves (forming a positive feedback), on which section 2.3.1 elaborates.

2.3 Mangrove forests

Mangrove forests are coastal forests found along tropical and sub-tropical coastlines. They exist largely in intertidal areas (see figure 2.5), i.e. areas that are sloped and raised above mean sea level, flooded approximately 30% of the time during tidal high waters. More frequent flooding can cause stress and ultimately death of mangroves.
In order to live in intertidal areas, mangrove trees have special physiological adaptations to deal with salt in their tissues. Their root systems are adapted in such a way to support themselves in soft mud sediment (which are largely anaerobic) and transport oxygen from the atmosphere to their roots (Lewis III, 2005).

2.3.1 Ecosystem services

Mangrove forests provide a wide variety of ecosystem services, including ecological, socio-economic and coastal protection services. For example, they enhance fisheries (Hutchison *et al.*, 2014), carbon storage, (non-timber) forest products and recreation (Lewis III, 2005). Here, the focus will be on the coastal protection service that mangrove forests provide.

Wave height attenuation
Mangrove greenbelts can offer protection from damage due to wave impact (i.e. erosion and flooding) by reducing the wave energy and wave height of wind and swell waves. The mangrove trees act as obstacles for the oscillatory flow in waves, creating drag. Wave energy is dissipated by flow around the mangrove vegetation, performing work to change flow direction and against the friction of the mangrove surface, thereby reducing wave height (Mazda *et al.*, 1997).
Although mangrove forests are usually found on shores with little incoming wave energy, during storms, hurricanes or periods of strong winds (e.g. the monsoon period) they can be subject to larger waves. 100 m of mangroves can reduce the wave height by 13 to 66% (McIvor *et al.*, 2012). Thus the wave height of wind and swell waves can be reduced over relatively short distances.

According to McIvor *et al.* (2012), factors influencing wave height attenuation as waves pass through mangroves include travelled distance, water depth and various mangrove characteristics (e.g. species, age, size). The height and period of the waves also affect wave attenuation by mangroves, as well as the slope of the shore. Mangroves often grow on very gently sloping shores and may indirectly increase wave energy dissipation by increasing surface elevation, which is explained in more detail below.
Water depth is a function of bathymetry (or topography on land) and tidal phase. Combined with the mangrove structure and properties, this determines the nature of obstacles

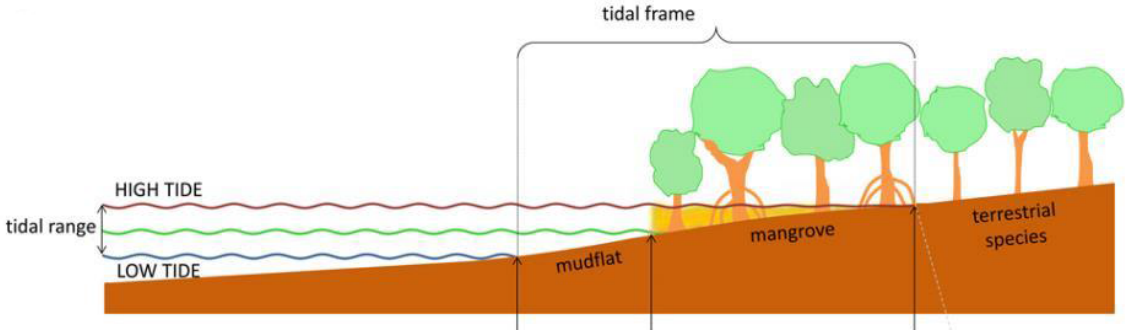

Figure 2.5: Mangrove growing area

encountered by waves as they pass through the mangrove forest. When they pass through a greater density of obstacles, waves are reduced more rapidly. Mangroves with aerial roots will attenuate waves in shallow water more rapidly than those without. At greater water depths, waves may pass above aerial roots, but the lower branches can perform a similar function (McIvor *et al.*, 2012).
Bao (2011) studied wave height reduction by coastal mangrove forests in Vietnam, measuring wave height and mangrove forest structures at different cross-shore locations and derived an integrated exponential equation as a function of initial wave height and canopy closure, height and density. The wave height is reduced exponentially by travelled cross-shore distance. Quartel *et al.* (2007) already hypothesised that this exponential relation can be explained by the dense network of trunks, branches and aerial roots of mangrove trees, increasing bed roughness, causing more friction and thus dissipating more wave energy.

Bed level elevation
Besides dampening effects that mangroves have on waves, their influence on land accretion and compaction also contributes to coastal safety. By slowing water flows and reducing wave energy, mangroves allow increased deposition of sediments. Additionally, through the growth of subsurface roots, mangroves may increase the soil volume. Together this can cause an increase in the sediment surface level if the sediment inputs exceed sediment losses.
Processes that influence the mangrove surface elevation can occur at or above the mangrove soil surface, as well as subsurface. Surface processes include the deposition of material on the surface of the soil (sedimentation), the binding of material in its place (accretion) and the loss of surface material (erosion). Factors influencing surface erosion have been treated in section 2.2.2. By reducing hydraulic loads on the sediment surface, the mangrove vegetation reduces the frequency at which the bottom shear stress exceeds the critical threshold for erosion.
Sedimentation, on the other hand, can involve (allochthonous) material carried into the mangrove area in suspension, but also locally generated (autochthonous) material. The first category consists of deposited material by rivers (terrigenous sources) and longshore

transport, biologically produced material or precipitated material. Locally generated material originates from mangrove vegetation and benthic species (organisms living on and inside the muddy substrate). Factors influencing sedimentation rates are the amount of incoming sediment and locally generated material, as well as factors that affect suspended material to settle or quickly re-suspend, such as period of inundation, flow rates and flocculation of particles.
Sedimentation contributes to surface accretion, which is affected by growth of mangrove roots into the newly deposited layer. The network of living and dead roots increase the shear strength of the mangrove soil surface, presumably by binding the soil together (Scoffin, 1970), and prevents them from being washed away by waves and tidal flows (Cahoon & Lynch, 1997). Moreover dewatering and consolidation of fluid muds increases soil shear strength and thereby the ability to resist resuspension and erosion by waves (Wells & Roberts, 1980).

Subsurface processes occur below the soil surface but above the consolidated basement layer. Processes expected to act over short time scales include swelling and shrinkage of soils related to water content and compression and rebound of soils due to changes in the weight of the material above. Tidal levels, rainfall and groundwater level are of importance for these short time scales, as well as the soil composition. The long term surface elevation is mainly influenced by growth and decomposition of roots and compaction of soils (Cahoon *et al.*, 2006). Tree health, salinity, temperature, availability of nutrients and soil consolidation are important factors for these long term influences.

According to McIvor *et al.* (2013), historical observations and literature suggest that soil surface elevation due to mangroves have kept up with sea level rise over thousands of years in some locations. This mainly depends on local factors, the most important of which are supply of (allochthonous) sediment, wave climate, tidal range and rate of sub-surface root growth.

2.3.2 Rehabilitation of mangrove-mud coasts

According to Ellison (2000) ecological restoration of mangrove habitat is feasible, has been done on a large scale in various parts of the world, and can be done cost-effectively. Nevertheless, mangrove rehabilitation efforts have often been unsuccessful, because not all limiting factors for mangrove growth were taken into account (Balke *et al.*, 2011). Failed measures include hard coastal defence structures (Anthony & Gratiot, 2012), as well as mangrove planting (Lewis III, 2005).
A sufficient understanding of ecological, hydrological and morphodynamic conditions for mangrove recovery is essential, as well as cooperation with local communities. Ecological, hydrological (and socio-economic) requirements have adequately been covered in literature and are briefly summarised here. The main focus is on morphodynamic requirements for successful mangrove rehabilitation.

Ecological requirements
Most mangrove species have propagules that are produced anually in large numbers and that are waterborne, i.e. seeds float to new sites for colonisation. Following the basic principles of secondary succession, mangrove propagule availability may be the limiting factor for mangrove growth due to removal of mangroves, hydrological restrictions or blockages that prevent natural transport of mangrove propagules to the restoration site. Thus, as long as abundant supply of propagules is available and the environmental conditions are favourable, mangroves can emerge autonomously (Lewis III, 2005).

Hydrological requirements
Balke *et al.* (2011) defined a sequence of phases for establishment of pioneer mangrove species *Avicennia alba*, based on experimental studies and field observations. First stranded propagules need an inundation-free period, in order to rapidly develop roots that are long enough to withstand displacement by flooding. Then roots need to become long enough to resist against seedling dislodgement by hydrodynamic forces from waves and currents. In this phase, the required root length is proportional to the force that needs to be withstood. Finally, in order to survive high energy wave events that may cause sheet erosion (thereby inducing seedling dislodgement), even longer roots are needed. This stresses the importance of rapid root expansion to pass all the thresholds.
Besides flooding stress, increased salinity due to reductions in freshwater availability, increased anaerobic conditions and free sulfide availability can also kill or stress mangroves at restoration sites (McKee & Faulkner, 2000). Therefore sufficient free exchange of seawater with the adjacent ocean or estuary should be allowed and fresh water outflows from rivers should not be blocked (Lewis III, 2009).

Morphodynamic requirements
In particular on eroding coastlines, as is the case in Demak coastal zone, morphodynamic requirements are critical to stop further land losses and ensure successful mangrove rehabilitation. Many mangrove-mud coasts do not form rigid, stable coastlines, but are instead often highly dynamic with cycles of coastal progradation and coastal retreat. The theory on sediment dynamics treated in section 2.2 is crucial to understand the natural processes along muddy coastlines and intertidal mudflats.
From theory, it can be concluded that tides and rivers supply sediment to the coast. Erosion occurs as waves stir up sediment, which is subsequently transported by currents. In a healthy mangrove ecosystem these processes are in balance, so that the coastline is in (dynamic) equilibrium. The mangroves' root system helps to trap and accumulate sediment. The tidal flat is convex up, with a gentle slope and shallow water at the seaward edge of the mangrove forest. In areas that are suffering from erosion, however, an in-balance of (fine) sediments exists, which causes an erosion process at a larger scale through which the shape of the mudflat becomes progressively concave-up, enhancing the wave affects even further (Winterwerp *et al.*, 2013).
Sedimentation is primarily governed by tidal processes, sediment trapping by the mangroves and consolidation of freshly deposited sediments. Erosion is largely governed by

surface waves. Destabilisation of mangrove trees can already be caused by a few decimeters of erosion, as mangrove roots anchor only about 0.5 m deep into the soil (Tomlinson, 1986). Therefore, although large waves presumably have the largest effect (and may erode large amounts of sediment in a short period of time), small capillary waves can stir up fine sediments from the bed as well, which causes erosive processes to occur throughout the year. However, as explained in section 2.2.1, large waves may have a smaller erosion effect than small waves, since they also stir up sediments in the foreshore.

Winterwerp *et al.* (2013) proposes the following strategy for rehabilitation of eroding mangrove-mud coasts: a first step for mangrove rehabilitation is to restore the sediment balance in order to stop the erosion and regain a stable coastline. The amount of sediment being washed away should be surmounted by the amount of material that is deposited. In order to increase the onshore flux of fine sediment it is necessary to accomplish a well-managed buffer zone or green belt of several hundreds of meters in width, in which incoming tides can freely flow, and to remove all obstacles in this buffer zone (e.g. levees and artificial mounds). Next, fine sediments need to be trapped on the mudflat in a natural way (to enhance sediment accretion) and longshore currents need to be reduced to lower transport of fine sediments away from the area, thereby creating an environment in which fine sediments can settle. Moreover, wave heights should be reduced in such a way that wave reflection does not induce additional, local scour. Hydrological conditions should be restored in order to ensure appropriate tidal inundation characteristics and sufficient fresh water flow towards the mangrove stands (Lewis III, 2005). This involves rehabilitation of creeks and removal of small dams further inland, but also considering restoration of aquaculture ponds to mangroves (e.g. partial removal of pond dikes). The latter would also help to stabilise the coast by providing protection from erosion by storm waves. If necessary, mangroves can be planted at suitable locations in the areas where natural propagule supply is a limiting factor.

2.4 Semi-permeable structures

One of the proposed solutions to protect the coastline and restore the sediment balance, is the construction of semi-permeable structures. Semi-permeable dams or pile breakwaters are structures that reduce wave energy, while allowing flow (and thereby transport of sediment) through the structure, see figure 2.6 for an example. Presumably, such structures could create a calm area to stop erosion and accelerate sediment deposition, as indicated in figure 2.7. In Europe semi-permeable structures made from wood have been deployed over centuries to reclaim land from the sea. More recently, such wooded structures have been tested in mangrove-mud coasts in Vietnam (Schmitt *et al.*, 2013) and Thailand (Saengsupavanich, 2013). In this section the relevant theory from literature is given. The design of the semi-permeable structures is treated in more detail in chapter 4.

Figure 2.6: Example of brushwood groyne

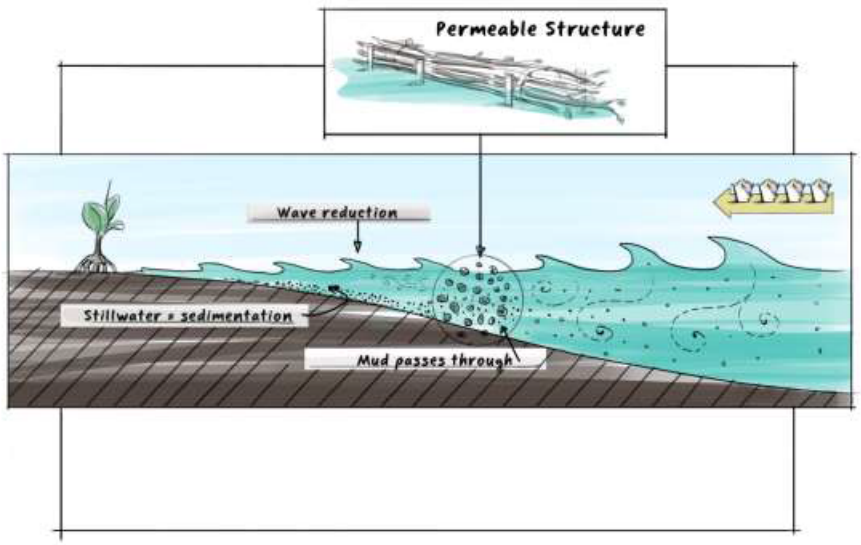

Figure 2.7: Functions of semi-permeable dams (courtesy of Ecoshape)

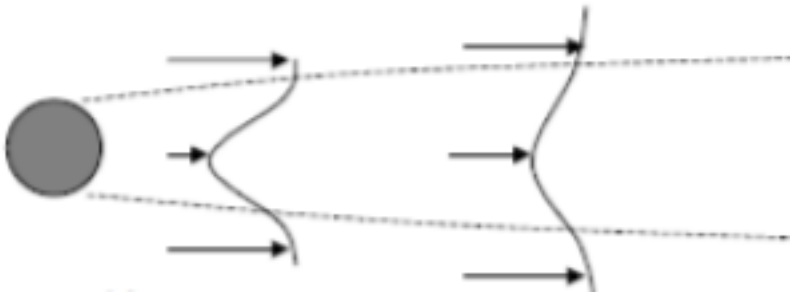

Figure 2.8: Flow field behind a single pile

2.4.1 Interaction with flow

Due to the interaction between the flow and the piles of the semi-permeable dams, waves are dissipated in a similar way as the wave attenuation by mangroves. Depending on the Reynolds number, the flow characteristics may differ. As water flows around a pile, it experiences drag from the pile and turbulent eddies may develop behind the pile (since water is a viscid fluid) that dissipate wave energy (Zhu, 2011). A wake flow develops in the vicinity of the pile, see figure 2.8, which implies that there are velocity gradients present in the flow field (Nieuwstadt, 1992). This gives rise to transfer of mass and momentum through turbulent mixing. Behind a row of multiple piles, the vortices caused by the individual piles will influence each other. The exact behaviour depends on multiple factors, such as the distance between the piles.

On a larger scale, the structures also interact with the flow. Cross-shore dams will decrease longshore currents and longshore dams will damp the incoming wave energy. For obliquely incident waves, diffraction around the dams may occur (Fleming, 1990). Moreover, the semi-permeable dams can cause eddy formation in their shadow zone, comparable to that of submerged breakwaters, or influence tidal and wave-induced currents like shore-normal dams. As the main type of wave breaking at a muddy coast is expected to be spilling breakers, the effects of such secondary flow are expected to be small.

2.4.2 Wave dissipation, reflection & transmission

Wave dissipation is characterised as the ability of a structure to damp wave action, which is directly linked to wave transmission and reflection, see figure 2.9. The interaction between waves and permeable structures such as brushwood dams is very strongly related to flow through porous media (Sayah, 2006). However, no specific formulation could be found that covers the effect of porosity on the interaction between brushwood dams and waves. Wave transmission by permeable breakwaters, on the other hand, has widely been studied in literature. Sayah (2006) discusses several researches on the effect of permeable breakwaters, constructed from granular materials, on incident waves.

Thornton & Calhoun (1972) proposed the following expression for energy dissipation:

$$K_D^2 + K_R^2 + K_T^2 = 1 \tag{2.2}$$

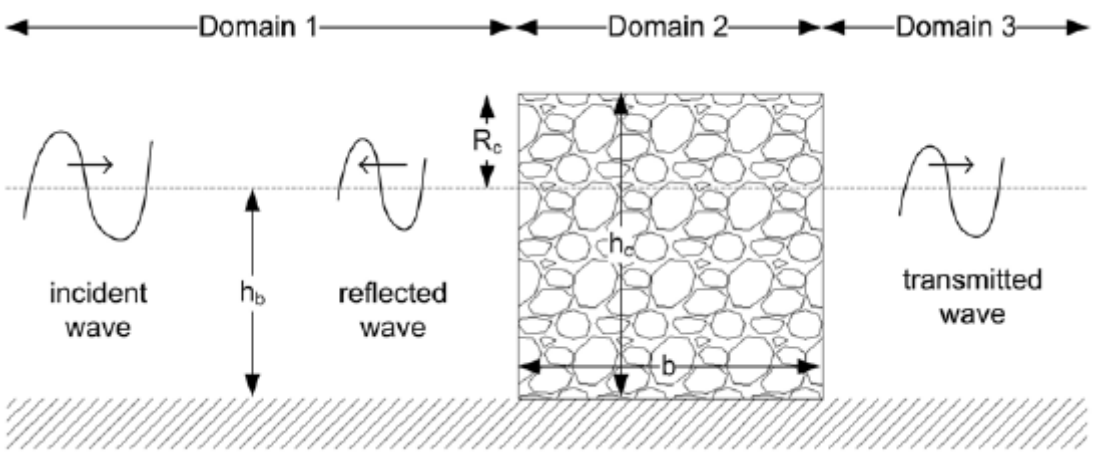

Figure 2.9: Schematisation of permeable breakwater by Losada *et al.* (1998)

where K_D is the dissipation coefficient of a porous structure, K_R is the reflection coefficient and K_T is the transmission coefficient. The reflection and transmission coefficients are determined as fractions of the incoming wave height. The rationale behind equation 2.2 is energy conservation: energy will be partitioned between reflection, dissipation and transmission. The wave energy is proportional to the square of the wave height, hence the squared proportionality of the coefficients.
In order to damp the waves and create a calm area in which sediment can settle, transmission should be prevented as much as possible. However, as brushwood fences are always permeable, wave transmission cannot completely be prevented. Moreover, wave reflection should also be limited as this could induce local scour, especially in muddy environments. In order to prevent erosion as much as possible, the dissipation term should therefore be as large as possible.

Mai *et al.* (1999) performed an experimental research using a full-scale prototype model to analyse the effect of water level variation on the transmission coefficient of a brushwood groyne, as well as changes of the transmitted mean wave period. The authors demonstrated that the wave damping of a brushwood groyne decreases significantly when water levels are above its crest height, but the wave period remains almost constant even after transmission.

Chapter 3

System analysis of Demak coastal zone

After treating the basic background theoretical concepts, the coastal system of Demak province is analysed in this chapter to obtain a thorough understanding of the system. First, the area of interest is introduced in section 3.1. In section 3.2 meteorological aspects influencing Demak coastal zone are treated. Next, the hydrodynamic conditions influencing flood risk and sediment transport are given in section 3.3, including the tide, waves and currents. Finally, in section 3.4 a morphological analysis of Demak coastal zone is performed, including the bed characteristics, sediment budget and potential sediment sources and sinks.

3.1 Area of interest

Figure 3.1 shows the location of the Java Sea, enclosed between the larger islands Sumatra (on the West), Kalimantan (on the North) en Java (on the South). It is a shallow and narrow shelf sea, where tide and tidal current play an important role. It also includes contour lines indicating depth in meters. The area of interest is Demak district, located on central Java (Indonesia) at the Java Sea coast. As explained in section 1.2, large parts of the Demak coastal zone currently suffer from severe erosion at an average rate of 100 m/year. In figure 3.2 the position of the Demak coastline is indicated in 1972, in 1994 and in 2013.

3.2 Meteorological characteristics

In this section, the meteorological aspects that are of importance for the coastal area of Demak are described. The area is subject to monsoons, which determine prevailing wind directions and rainfall intensities. In order to get a thorough understanding of the

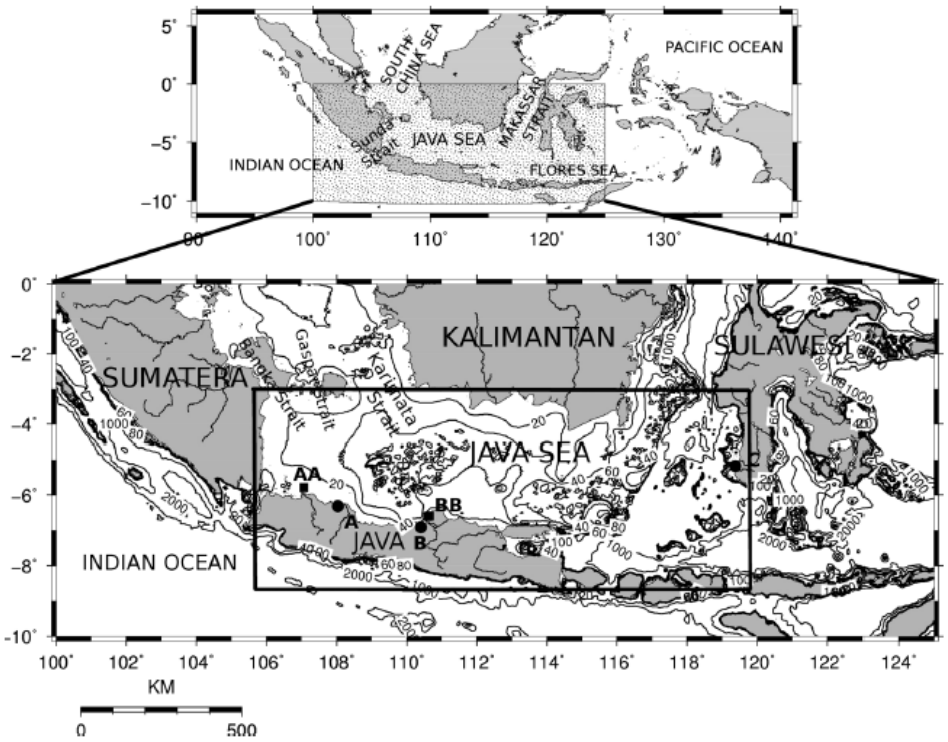

Figure 3.1: Indonesian waters (upper figure) and Java Sea (lower figure). Observation points of tide gauges are denoted by solid circles.

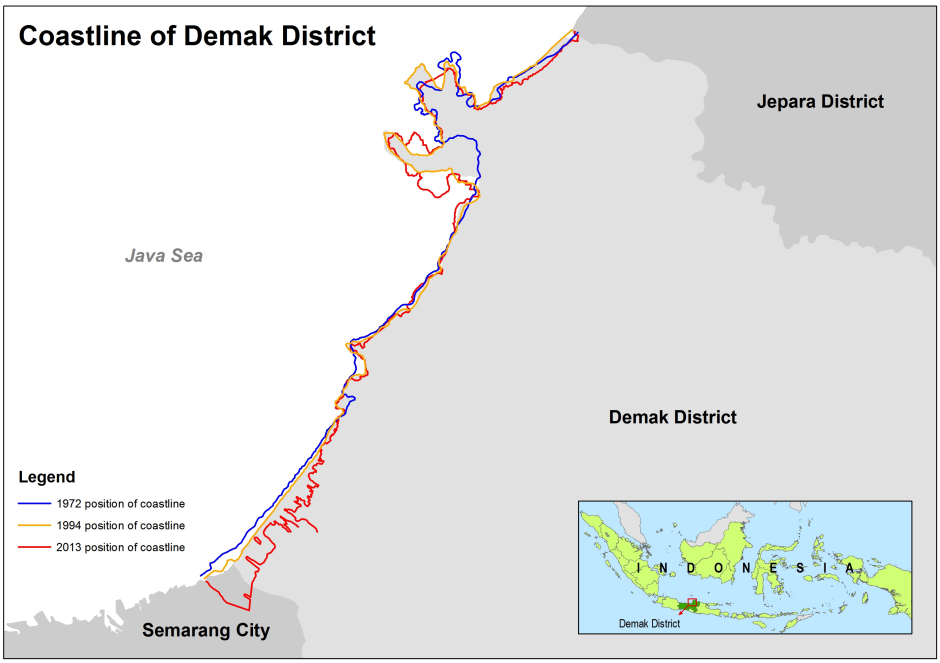

Figure 3.2: Historical development of Demak coastline between 1972 and 2013

meteorological system, first the monsoon is described for the somewhat larger region. Subsequently, site-specific information on rainfall and wind is given.

3.2.1 Monsoon

The equatorial pressure trough moves according to the position of the sun, crossing the equator twice a year. As a consequence, a monsoon develops between the high and the low pressure areas. Wyrtki (1961) described the effects of the monsoon on the circulation in Southeast Asia. The northwest monsoon occurs between November and April, with prevailing west winds over the Java Sea. The strongest winds occur in the months December, January and February. In May the system of northeast winds collapses and south winds prevail, thus reversing the monsoon. The southeast monsoon is fully developed in July and August and the circulation reaches its greatest strength. In October the equatorial trough begins to move rapidly southwards, indicating the second annual monsoon reversal. This results in the northwest monsoon again.

3.2.2 Wind

Due to the monsoon, the wind speed and direction have a strong seasonal character. In appendix C monthly wind roses are included. Figure 3.3 shows typical wind roses for the northeast monsoon period (December, January and February) and the southeast monsoon period (July and August), indicating wind speed and direction. The strongest winds occur for the northeast monsoon and are about 10-15 m/s.

3.2.3 Rainfall

The rainfall distribution can serve to estimate the distribution of fresh water flows from various rivers discharging into Demak coastal waters throughout the year. Figure 3.4 shows the rainfall distribution over the year in Semarang. In Java, the wet season is from November to April. December, January and February are the wettest months with an average rainfall of about 4 to 5 m/year. The dry season, on the other hand, is from May to October. June, July and August are the driest months with a rainfall of about 1 m/year (Bayong Tjasyono *et al.*, 2008). For this reason, the northwest monsoon is often referred to as 'the monsoon', whereas the southeast monsoon corresponds to the dry season.

3.3 Hydrodynamics

The hydrodynamic processes that were explained in section 2.1 can all influence sediment transport. Therefore the hydrodynamic conditions in Demak coastal zone are described qualitatively and quantitatively in this section.

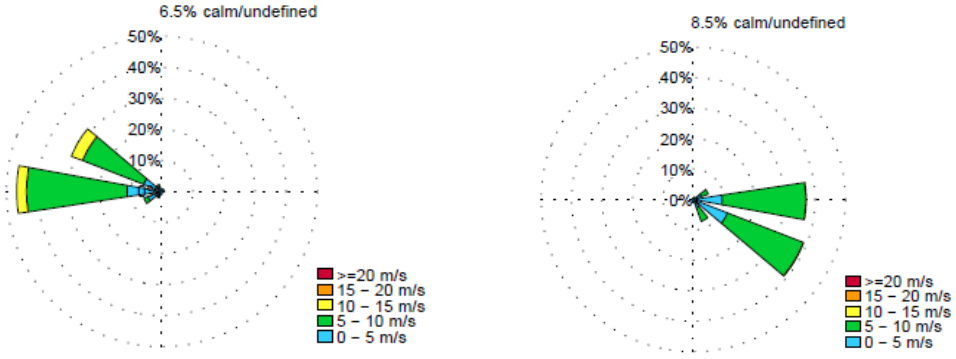

Figure 3.3: Typical offshore wind roses for northwest (left) and southeast (right) monsoon periods (courtesy of Boskalis)

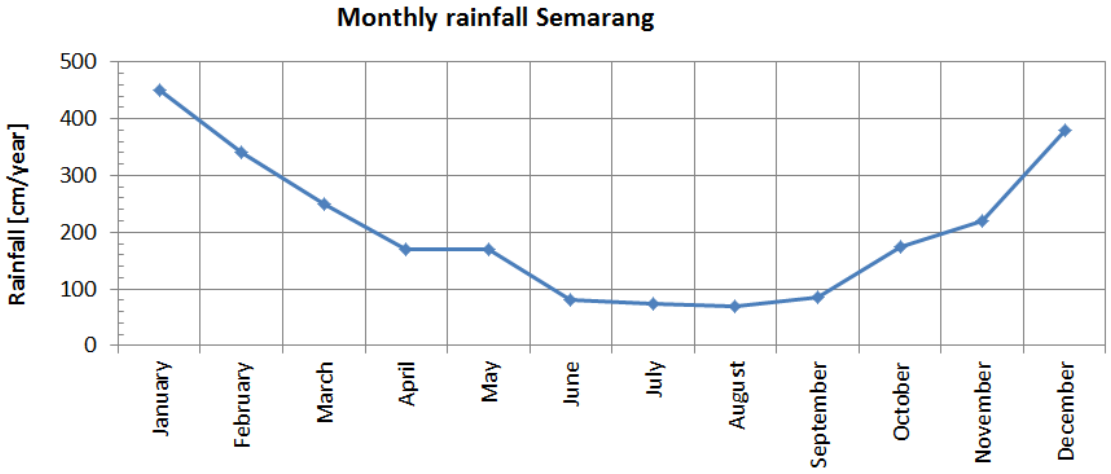

Figure 3.4: Rainfall distribution over the year in Semarang (Bayong Tjasyono *et al.*, 2008)

3.3.1 Tides

The phase of tides is well known to propagate counterclockwise in the northern hemisphere and clockwise in the southern hemisphere. The tidal propagation in the Java Sea, however, is quite complex, due to the geographical location, local bathymetry and surrounding land masses. The Java Sea forms the connection between the Indian Ocean (on the West) and the Pacific Ocean (on the East) and is surrounded by many large islands. The M_2 tidal wave is coming from the Indian Ocean through the Flores Sea, while the K_1 tidal wave is coming through the Makassar strait from the Pacific Ocean (Hatayama *et al.*, 1996). Together, they propagate westward in the Java Sea. Model results by Yusuf & Yanagi (2013) show that there is counterclockwise phase propagation of M_2 tidal wave in the Java sea, even though it is located in the southern hemisphere. The direction of the phase propagation is mainly goverened by the large amplitude part of the incoming wave from the Flores Sea through the Makassar Strait. The large amplitude part propagates along the northern boundary (southern coast of Kalimantan Island). It is clearly seen from co-tidal charts that the tidal wave propagates faster in the central southern part of the Java Sea (off the central Java island) rather than the central northern part of the Java Sea (off the Kalimantan island) due to the bottom topography of the Java Sea, where the southern part is deeper than the northern part.

The tidal constituents at Demak coast according to MMAF (2012) are given in table 3.1. Using the definition of equation 2.1 the form factor and corresponding category can be determined using table A.1 in the appendix. The corresponding form factor equals 2.4, indicating that the tide at Demak coast has a mixed tidal signal with mainly diurnal characteristics and small semi-diurnal components. The resulting variation in tidal water levels over time has a highly irregular periodicity, in which daily inequalities play a role, as well as the monthly variations of the spring-neap cycle.

Table 3.1: Overview of tidal constituents at Demak coast

Tidal constituent	Amplitude [cm]	Phase [deg]
S_0	95.44	-
M_2	7.57	541
S_2	5.93	124
N_2	2.03	440
K_2	1.36	124
K_1	21.41	-32
O_1	11.08	852
P_1	7.07	-32
M_4	0.6132	760
MS_4	1.40	321

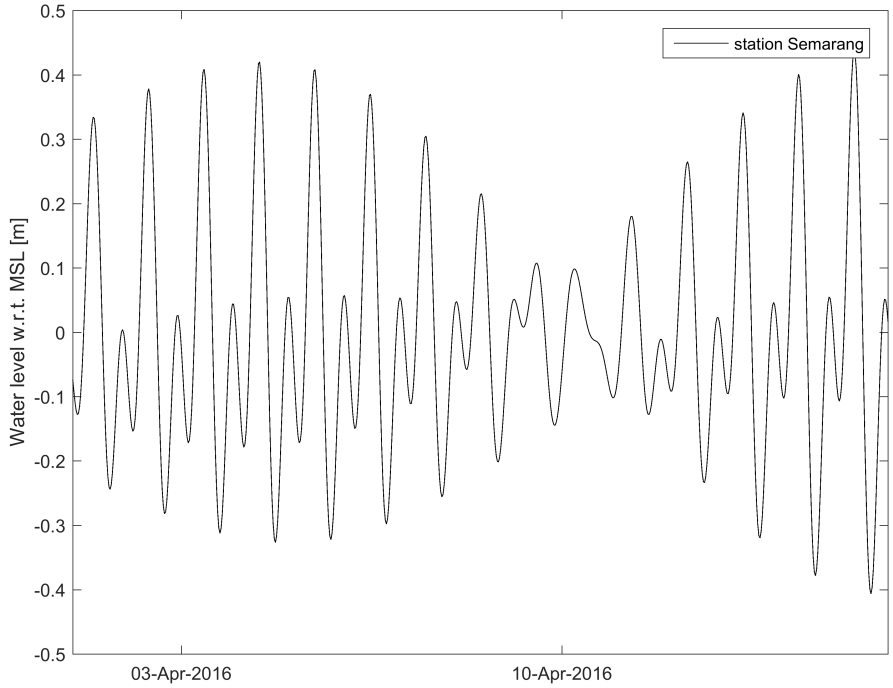

Figure 3.5: Water level measurement from a nearby tidal station in Semarang

The tidal range is approximately 0.60 m at spring tide and 0.40 m at neap tide. The spring tide can be a bit larger when semi-diurnal components synchronise with diurnal components. See figure 3.5 for an example measurement of tidal water levels at the nearby station in Semarang from April 2016.

3.3.2 Waves

In appendix D monthly wave roses are included, based on information from a wave buoy located just northwest of the area of interest (at $6.0°S$ and $110.50°E$). During the northwest monsoon, the largest waves develop. The predominant offshore wave direction is northwest with a maximum wave height of about 2.5 m. Figure 3.6 shows typical wave roses for the northeast monsoon period (December, January and February) and the southeast monsoon period (July and August), indicating wave height and direction.
The offshore waves are transformed as they propagate towards the coast, as explained in section 2.1.2. The relevant waves at Demak coast come from between north and west-northwest, with the majority of the waves from the north according to Winterwerp *et al.* (2014). The difference in wave direction between offshore and nearshore could be a result of wave transformation, although the influence of refraction is small due to the gentle bottom slope. Wave heights up to 1.8 m have been reported, whereas the maximum significant wave height amounts to about 1.5 m with a period of about 5.5 s. Based on fourteen years of wave data from a measuring station near Semarang, the mean wave height in the area equaled 0.46 m and maximum offshore wave height was between 2.6-3.0 m, although for the year 2009 much larger maximum waves were reported, presumably related to El Niño

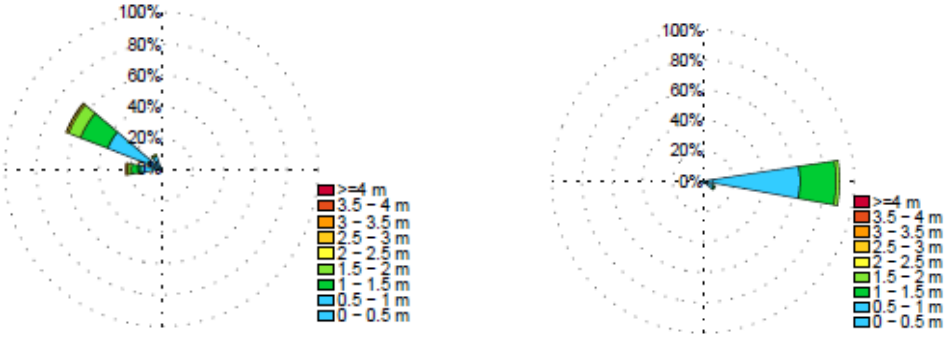

Figure 3.6: Typical wave roses for northwest (left) and southeast (right) monsoon periods (courtesy of Boskalis)

events. These waves had a significant wave height of about 2.2 m and a period of 8 s or larger.

3.3.3 Currents

Tidal currents in Sayung coastal waters vary, with maximum velocities of around 0.15 m/s, but the exact locations of these measurements is unknown (Bappenas & KOICA, 2012). The direction of the tidal current is also variable, because tidal propagation near the Demak coast is quite complex due to multiple nearby tidal nodes. The propagation of the main tidal components (K1 and M2) in the greater Java Sea is towards the West, as explained in section 3.3.1. From literature, however, little is known about the local propagation direction of the tidal current close to the coast. MMAF (2012) reported a predominant current direction between east and southeast, more or less perpendicular to the Demak coastline, due to the shallow foreshore. Based on tidal model outcomes, e.g. by Yusuf & Yanagi (2013), it is expected that the tidal current direction close to the coast varies over the spring-neap cycle.

Wave-induced currents are small, because there is low wave energy on mild slopes (see section 2.1.2). They flow toward northeast along the coastline, whereas in the open sea 5 km offshore the wave-induced current is directed toward the southwest. Bappenas & KOICA (2012) reported a wave-induced current of about 0.5 m/s when west-northwest waves propagate in Demak coastal area, but experts think the current velocity is an order of magnitude lower.

The larger oceanic circulation results from the large-scale wind-driven circulation. Due to the high constancy and regular appearance of the monsoon, the residual ocean currents along the north coast of Java show the same characteristics as the monsoon, reversing twice a year. From May to September, the southeast monsoon drives residual currents towards the west, whereas during the northwest monsoon and transitional months (from October to April) residual currents are directed towards the east (Wyrtki, 1961). Close to the coast, these currents are mainly directed from northeast to southwest, however these nearshore currents are small and therefore have little effect on sediment transport.

3.4 Morphology

In order to study the sediment transport in the Demak coastal zone, first the characteristics of the current bed are described, including bottom profile and sediment properties. Next information about the historical sediment budget and development of the coastline is given. Based on this information, potential sediment sources and sinks are identified.

3.4.1 Bed characteristics

The Demak coastal zone is very shallow, with slopes of about 1:600, although the original slope is expected to have been much gentler (1:1000 or even 1:1500). Further towards the shore, intertidal areas have bed slopes of about 1:1000, resulting in the convex-up profile that is typical for mud coasts. Close to the coast the substrate is extremely muddy, although the exact stratigraphy is unknown.
Stefan Verschure and Pak Sugeng performed depth measurements close to the coast, thus two sets of local bathymetry data were available. More information on the locations of the depth measurements is included in appendix F.
Just in front of the coast several *cheniers* are located on top of the muddy bed. Cheniers are thin, narrow lenses of sand that were originally located just in front of the mangrove greenbelt along some parts of the coast. Now these cheniers are fully exposed and cause waves to break, losing part of their energy. The sheltered parts of the coast behind the cheniers are therefore protected fairly well against wave impact, although it should be noted that the cheniers are now likely eroding due to the enhanced wave-induced shear stress. In figure 3.7 the cheniers in front of Timbulsloko can be seen as dark spots in the seawater.

3.4.2 Historical sediment budget

The historical development of human interferences with the sediment budget are described here. The original source of fine sediments in the foreshore is terrestrial, as weathered sediments are carried by numerous small rivers and creeks to the coastal zone. For centuries, those sediments were captured by the mangroves present in the coastal zone of Demak. However due to human interventions (i.e. the removal of mangrove forests), Ecoshape (2015) estimated that roughly half of the historic deposits have currently been lost to deeper water. This implies that the eroding coast cannot be restored entirely to its 2003 position.

Land use changes
Ecoshape (2015) described the changes in land use that have initiated erosion and associated the coastal retreat. In the 1980s the increased demand for shrimp, which was enhanced by the ban on fish trawling in 1984, caused a transformation of paddy field and mangrove forests into shrimp ponds. In the 1990s new ponds were opened, because of

Figure 3.7: Cheniers located in front of Timbusloko (drone image 14 September 2015)

frequent losses of shrimp harvests due to diseases. As a consequence, the once extensive mangrove forests in Demak coastal zone have virtually disappeared completely. This has reduced the resilience of the coast by initiating a self-accelerating erosion process, as Winterwerp *et al.* (2013) reasoned.
Nowadays, the Demak coastal zone is characterised by strong ocean-to-land environmental gradients, such as salinity gradients and flooding exposure. This can also be observed from vegetation in the area, as explained in Ecoshape (2015).

Land subsidence & sea level rise
According to Winterwerp *et al.* (2014), subsidence can occur when the floodplain is disconnected from river sediment input and drainage, and by peat oxidation. However, in Semarang land subsidence is mainly due to natural consolidation of alluvium soil and excessive groundwater withdrawal. In and around Semarang large volumes of ground water have been extracted from deep aquifers for the industry sector and by local villages and aquaculture from shallower wells. This has led to subsidence rates estimated up to 8 cm/yr based on satellite data (Lubis *et al.*, 2011), although no detailed data exists of the Demak coastal zone.
Marfai & King (2007) monitored land subsidence in Semarang, which is located directly south of the area of interest. Using Direct Elevation Model data accompanied by subsidence data, predictions were made for future subsidence. It is expected that that the area between 1.5 m up to 2.0 m below sea level will reach 275,000 m^2 in the year 2020. The contribution of subsidence to coastal retreat can be demonstrated by an overlay of coastal erosion and subsidence maps of the Semarang area, see figure 3.8.
Sea level rise along the coastline of Demak is estimated between 4.0 and 4.3 cm per year

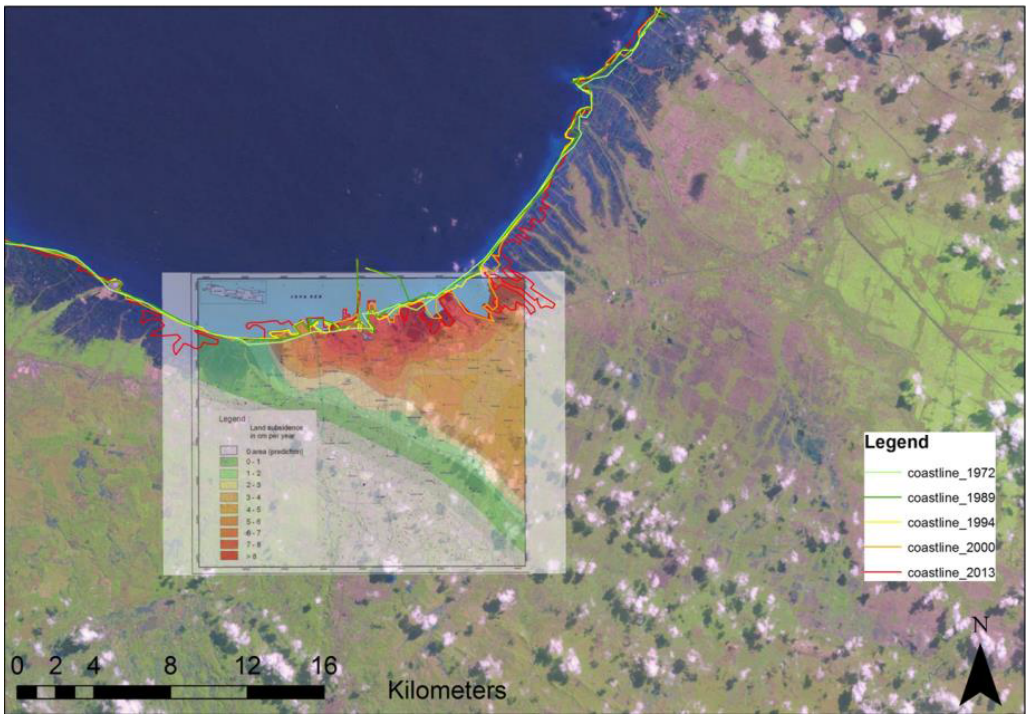

Figure 3.8: Subsidence map in and around Semarang (redder colours mean larger subsidence) with an overlay of coastal retreat since 1972 (Ecoshape, 2015)

(Bappenas & KOICA, 2012). The effects of land subsidence, in combination with (accelerated) sea level rise, make the Demak coastal system even more vulnerable to episodic events, which can cause large erosive forces in a brief period of time.

3.4.3 Sediment sources & sinks

During the northwest monsoon riverine fresh water plumes resulting from rainfall, which is largest during the northwest monsoon, are diverted to the east by wind and residual ocean currents, pushing them against the coastline. Along large parts of the coast this induces a gravitational circulation, keeping fine sediments close to the coast, thus forming a sediment source. During the southeast monsoon, fresh water is blown into the Java Sea. The effects of gravitational circulation are much more localised, so that no large-scale mechanism is active that keeps the fine sediments close to the coast (Winterwerp *et al.*, 2014). During this period fine sediments in Demak foreshore are lost to deeper water, thereby forming a sediment sink.
Most of the erosion occurs during northwest monsoon when winds are stronger, creating larger waves (sediment sink). However, fine sediment carried by rivers and fines from the foreshore are also mobilised in this season, leading to increased suspended sediment concentrations in the coastal zone, necessary for regenerating the coast (sediment source). So both gross sediment fluxes of erosion and sedimentation are larger during this season. Whether this results in coastal accretion or retreat depends on the magnitude of these fluxes.

Chapter 4

Design of semi-permeable dams

Semi-permeable dams were introduced in section 2.4, including some relevant theoretical information from literature. The most important design considerations for the semi-permeable structures are discussed in this chapter. Little is known about the spatial design, but experience with similar projects in muddy environments may be useful. Hence, first some reference projects are treated in section 4.1. Based on those reference projects, in combination with literature, design considerations for the new semi-permeable dams in Demak coastal zone are formulated in section 4.2.

4.1 Reference projects

In Suriname professor Sieuwnath Naipal from the Anton de Kom University is using semi-permeable dams for a mangrove recovery project to protect the coastal zone of Weg aan Zee. Allegedly, the pilot project has improved the knowledge of the local system and the dams successfully protect the coast from further erosion. Based on news articles the project has now been expanded, but unfortunately no scientific publications were available on this project yet. The remainder of this section therefore only treats projects of semi-permeable structures in very comparable muddy environments in Vietnam and Thailand.

4.1.1 Soc Trang & Kien Giang provinces (Vietnam)

Soc Trang province in the Mekong Delta of Vietnam is protected from erosion, storms and flooding by a narrow mangrove belt very similar to that in Demak. Here, too, the protective function is threatened by unsustainable land use and a site-specific approach has been put in place, including mangrove planting and rehabilitation. Schmitt *et al.* (2013) describes bamboo fences that were constructed for this purpose. Currents and waves are successfully damped, increasing the deposition rate of sediment.
The local conditions are as follows: fine sediment (mainly silt and clay); waves with significant wave height of about 0.65 m and a period between 5 and 6 s; a tidal range of 3.50

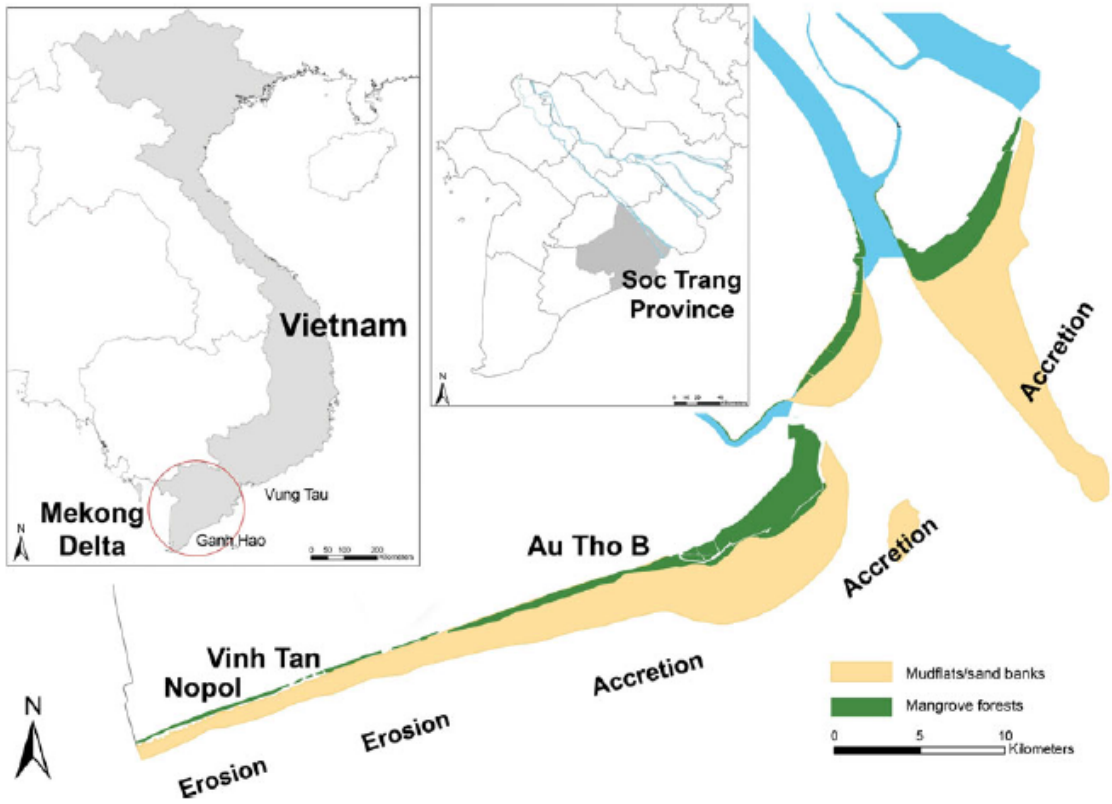

Figure 4.1: Location of pilot sites and accretion areas in Soc Trang province, Vietnam (Schmitt *et al.*, 2013)

m; a water depth at the structures of up to 2 m at high water. A schematisation of the area is given in figure 4.1. The accretion and erosion areas were determined by field work and reflect the situation in February 2013.
The design and construction of the wave-breaking structures ensures that coastal erosion is prevented as much as possible. Cross-shore and longshore fences are used to form a field of approximately 50 m x 50 m in size. The cross-shore fences decrease longshore currents and longshore fences damp incoming wave energy. The fences parallel to the shoreline have 20 m wide openings to secure the drainage of the fields. Using a physical model test and field testing, the dam dimensions were optimised for the wave transmission. The width of the constructed structures (or the distance between the bamboo piles) was about 0.30 m, as a result of the static design optimisation and for economic reasons. The top of the structures is designed at mean high water level. The field testing yielded very good results, mainly because of the strength, local availability and low costs of bamboo.

In the neighbouring Kien Giang province, erosion rates are up to 24 m/year due to mangrove loss. Past mangrove plantings were unsuccessful, mainly because of the lack of protection from wave action and seasonal sediment movement after planting. Van Cuong *et al.* (2015) describe three different designs of coastal protection fences that were tested

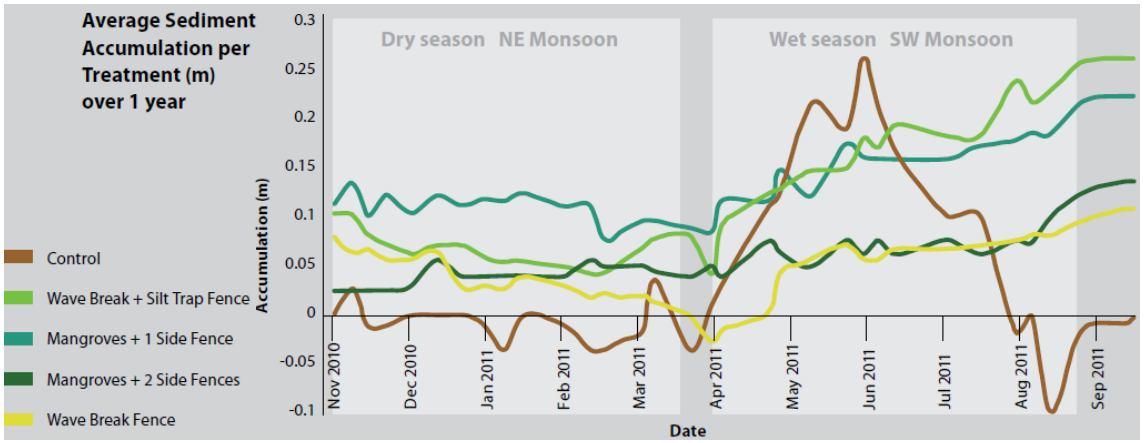

Figure 4.2: Observed changes in sediment elevation over time at treatment sites in Kien Giang province (Van Cuong *et al.*, 2015)

by the GIZ Conservation and Development of the Kien Giang Biosphere Reserve Project. The fences aim to reduce wave energy and prevent sediment deposited in the early wet season from being swept away through wave action when strong monsoon wind events occur in the second half of the wet season. The fences are constructed of melaleuca, a widely available inexpensive timber in the Mekong Delta.
The fences were found to reduce wave energy by up to 63%, retain up to 20 cm depth of sediment each year and up to 700 ton per hectare. Even in severe erosion sites, the fences protect planted or naturally recruited mangrove seedlings up to 100%. In figure 4.2 the sediment accumulation over one year can be seen. For the 'control' site, it is clearly visible that sediment was deposited in the first half of the wet season, but was eroded again in the second half. When applying fences, the initial deposition rate decreased slightly. However, deposition continued even in the second half of the wet season, resulting in more sediment accumulation over the entire year. It should be noted that the fences do not contain an opening to allow in- and outflow of sea water. Presumably, this causes the initial decrease in deposition rate compared to the control site, as the inflow of sediment is blocked.

4.1.2 Chachoengsao & Samut Sakhon provinces (Thailand)

In Chachoengsao province (near Bangkok, Thailand) three different coastal protection structures were surveyed: a low-crested revetment, a sand-filled geocontainer and a permeable bamboo structure. All these structures were tested in the field in combination with mangrove planting. According to Saengsupavanich (2013), unpublished documents from the provincial Office of Natural Resources and Environment reported that field research measuring the sediment deposition in the lee of the bamboo structures yielded a deposition rate of 20-25 cm per year. Loose sediment consolidated over time, becoming denser. Nevertheless, planted mangrove seedlings never survived due to uprooting by high waves during storms.

The standards for bamboo structures in Thailand require bamboo with a length of more than 6 m and a diameter of at least 7.5 cm, often obtained from farms. The construction method is relatively simple: the bamboo is brought to the site by boats and manually piled at least 2.5 m into the bed (for stability reasons). A few rows of smaller-sized bamboo of about 3 cm diameter is often placed in front of the main rows to filter drifted garbage and to prevent loose bamboo from hitting the main 7.5 cm piles. Approximately 27 main piles are used, along with 25 smaller piles, for each meter of shoreline. The cost of these bamboo structures is about USD 125 per meter. The sedimentation begins directly after installation of the bamboo structures. After about two years the deposited mud is consolidated enough to securely hold the roots of mangroves (Saengsupavanich, 2013).

Villagers of a fishing community in Kok Kham in the neighbouring Samut Sakhon province (also near Bangkok) built bamboo wave reduction barriers by submerging bamboo sticks of about 5 meters in triangle-shaped groups along two km of the 42 km long coast. The aim was to prevent big ripples from reaching the coast and to form a barrier by allowing mud and debris to collect on the fence. According to Russel & Michaels (2012), anecdotal evidence suggests that at some locations up to 1.5 meters of sediment deposited behind the fences within two years. However, at other locations, the fences lasted no more than 1 year (Naohiro *et al.*, 2012). According to Schmitt *et al.* (2013), on the other hand, experiences of over ten years of using similar permeable structures for erosion protection in Samut Sakhon province showed that bamboo used for wave-breaking structures lasts for five to seven years.

4.2 Design considerations

This section describes design considerations for the semi-permeable structures at the coast of Demak. Arentz & Van Wesenbeeck (2013) describe the design of semi-permeable dams for a pilot study of the same project. Based on their findings, literature from section 2.4 and the reference projects treated in section 4.1, the most important design considerations are specified. Dam dimensions, construction materials, orientation, planview shape and spatial arrangement are treated here consecutively.

4.2.1 Dimensions of dam

The transmission of the structures can be used as a design parameter to determine the dam dimensions. It can be altered by applying less or more material in the cross-section, thereby changing the permeability of the structure. The dams are constructed of two rows of poles that are put in the bottom vertically and filled with brushwood between the rows to create the semi-permeable character. The required pole length is determined from the water level, as they should not be overtopped by waves during high water levels. The poles should therefore have an elevation that is above the Maximum High Water, with some extra length to compensate for sea level rise and subsidence. A pole length of 4 meters

is recommended, including 30 cm extra length. The pole diameter can be linked to the pole length, using normalisation tables from the Dutch salt marsh works. The distance between the poles in a row should be 0.60 m (center-to-center) and the distance between the two rows of poles should be 0.30 m.

4.2.2 Construction materials

The use of local materials is preferred, which makes brushwood and bamboo suitable construction materials to create the semi-permeable character in southeast Asia. Besides the required dimensions, the quality of the wood should meet some requirements. The poles should be able to withstand wave forces and salt conditions for 7 to 10 years. Moreover, the poles should be able to endure the construction method. For this, the poles should have a sharp point (to enable driving the poles into the soil) and be able to withstand associated forces.
The brushwood should be fungus resistant and strong (to prevent leaching and breaking). It should have a good composition (variation between thick branches and smaller branches) to reduce maintenance and have sufficient permeability. The brushwood should be as long as possible to reduce maintenance, for which 2 to 4 m in length is recommended. The bundles of brushwood should have a diameter of around 30 cm to fit the distance between the two rows of poles. The filling needs to be maintained yearly, replenishing brushwood that has disappeared.

4.2.3 Orientation and planview of dams

The dams can be used to close off cells, in which sedimentation will take place. The orientation and planview shape of cells both affect the flow and thereby the deposition of sediment in the vicinity of the dam. To prevent wind wave generation within the sedimentation cells, the fetch length should not exceed a certain threshold. Based on Dutch standards a maximum value of 200 m could be suggested for the length of the dams. The dams that have currently been constructed for the pilot study, close off cells of approximately 50 to 100 meters length and width.
Each sedimentation cell should be constructed from the current coastline extending onto the mudflat in seaward direction. It should have a main drainage channel, which runs from the coast-parallel dam towards the back of the cell with a width of 2 to 3 meters and a depth of about 0.5 to 1 meter, in order to allow the seawater to enter the entire area. The seaward dam contains an opening in order to allow in- and outflow of sea water into the channel. These openings should be as small as possible to reduce wave impact, but large enough to let water in. For the width of these openings a value of around 5 to 7 meters is recommended. Two small perpendicular dams in the opening to prevent scouring due to gullies running parallel to the dams. For these small dams, a length of 4 to 5 meters is recommended, extending 2 m on either side.
Figure 4.3 shows a top view of the layout that was used for the pilot study, including an indication of the sizes.

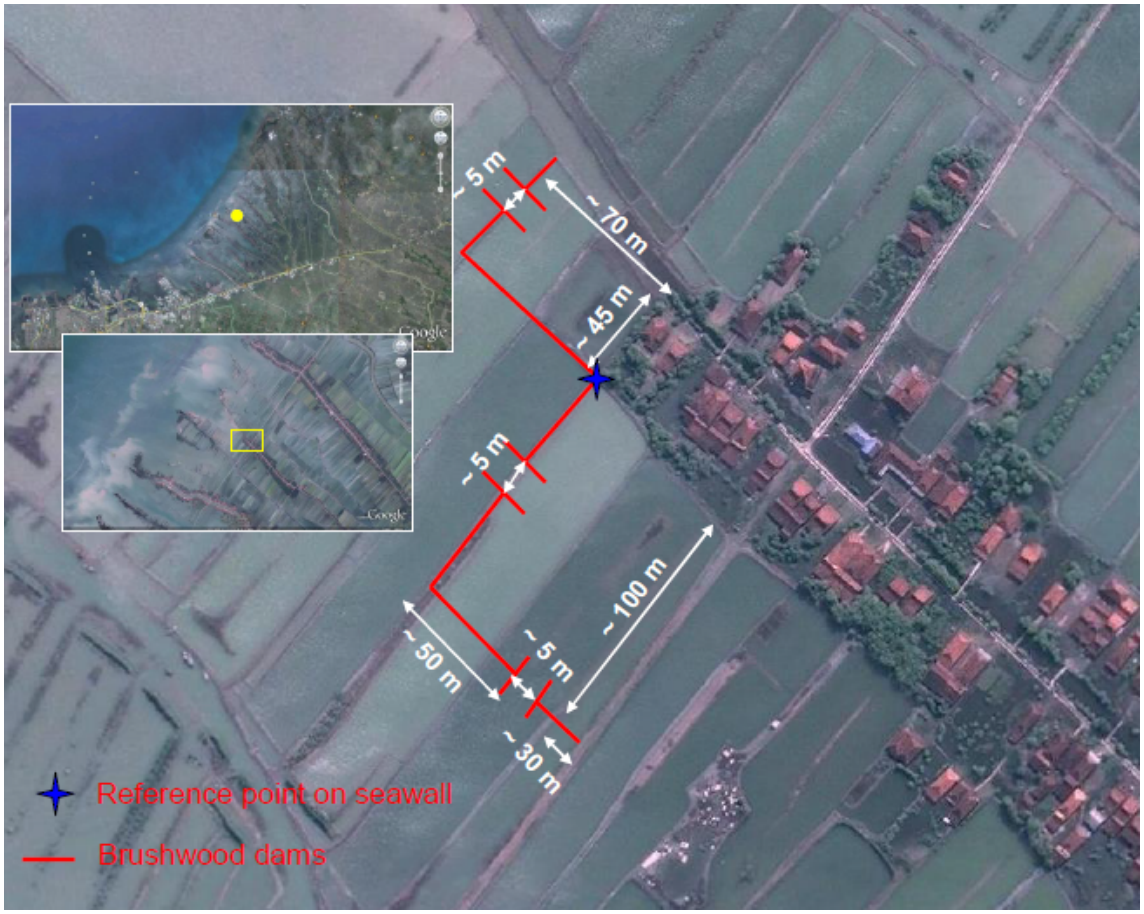

Figure 4.3: Planview of sedimentation cells that are closed of by semi-permeable dams (Arentz & Van Wesenbeeck, 2013)

4.2.4 Interaction between multiple dams

For large-scale application of the semi-permeable dams, the interaction between multiple dams is an important aspect. The spatial arrangement of the dams presumably has a large effect on the interaction, as this influences the flow and sediment transport. Currently, several dams have already been constructed. Ecoshape constructed the first dams for a pilot study near the villages Bedono and Bogorame. After this successful pilot the local Ministry of Marine Affairs and Fisheries (MMAF) constructed additional dams in front of the first dams. For 2016, the construction of a new batch of dams is planned to protect the village of Bedono. An overview of the dam configurations per construction batch is given in figure 4.4. Red lines indicate Ecoshape dams and orange lines indicate MMAF dams.

A numerical model will be used to assess the interaction between the dams that have currently been constructed. Based on the results, several scenarios will be tested with varying spatial arrangements in order to optimise the interaction. A detailed description of the numerical model and model set-up are given in chapter 5.

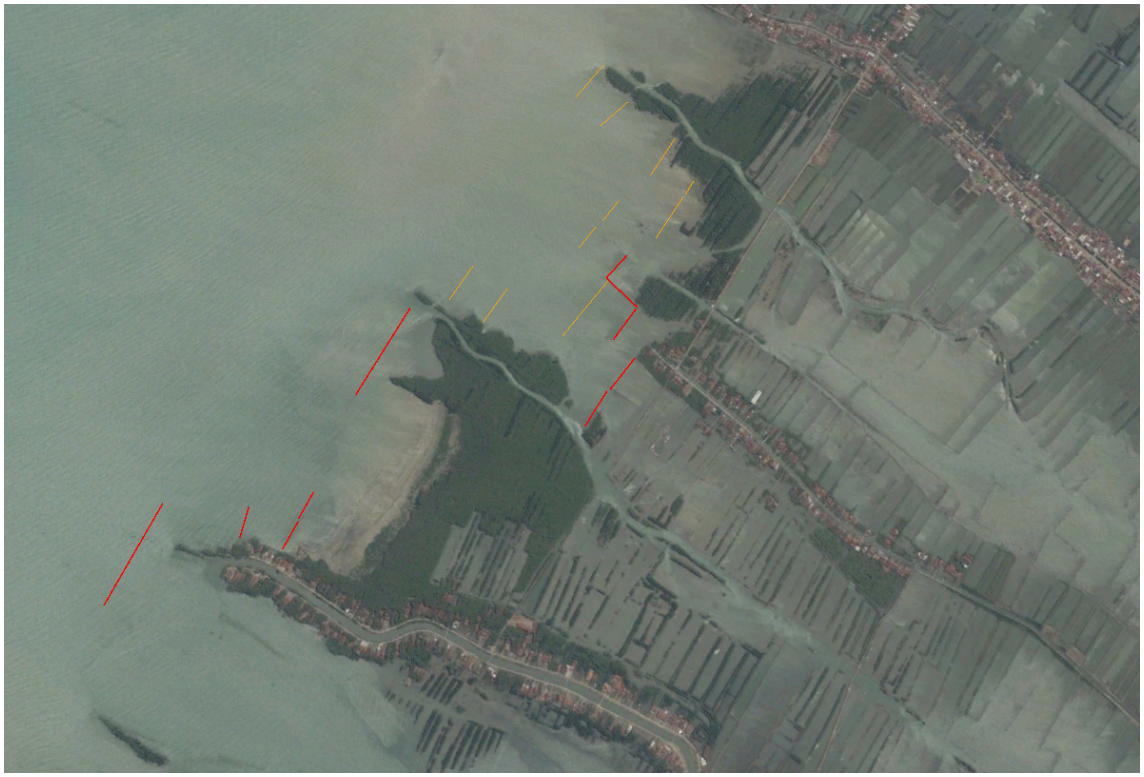

Figure 4.4: An overview of constructed dams for the pilot study by Ecoshape (shown in red) and MMAF (orange)

Chapter 5

Method

The main research method is the use of the numerical model Delft3D Flexible Mesh. This chapter describes the research method in detail. First, Delft3D Flexible Mesh is described in section 5.1. The model set-up is treated in detail in section 5.2. Section 5.3 describes my contributions to the testing and development of the sediment and morphology module. Finally, the model validation is described in section 5.4.

5.1 Model description

The Delft3D Flexible Mesh suite is the successor of the structured Delft3D 4.01 suite. It can carry out simulations of flows, waves, water quality and ecology. Sediment transport processes and morphological developments are still in development. Three modules were used for the model in this project: the flow module (D-Flow FM), the wave module (SWAN) and the sediment module. As the latter module was not yet operational during the course of this project, a beta version was used. Per module, some important aspects are elaborated in the remainder of this section. A more technical model description is given in appendix G, including the equations that are solved by the model. The information in this section is mainly based on the D-Flow FM user manual (Deltares, 2015).

5.1.1 Flow module

D-Flow Flexible Mesh (D-Flow FM) is the latest hydrodynamical simulation program that is used in Delft3D Flexible Mesh suite. It can perform simulations of non-steady flow and transport phenomena that result from tidal and meteorological forcing on structured and unstructured grids. The governing model equations of D-Flow FM are, equivalent to its predecessor Delft3D, the shallow water equations. These are derived from the Navier-Stokes equations for an incompressible fluid under the shallow water assumption (i.e. hydrostatic pressure) and the Boussinesq approximation (i.e. constant density), see section G.1 in appendix G.

The main development is the D-Flow Flexible Mesh engine for hydrodynamical simulations on unstructured grids, as opposed to the structured curvilinear grids that were previously required. This offers more flexibility in the grid resolution by combining curvilinear grids with unstructured grids composed of triangles, in order to increase the resolution locally. D-Flow FM implements a finite volume solver on a staggered grid. However, since there are no grid 'rows' or 'columns', it is not possible to use an ADI-solver. The continuity equation is solved implicitly for all points in a single combined system. Time integration is done explicitly for part of the advection term, resulting in a stability criterion for the time step. Based on the CFL condition (Courant number), a dynamic computational time step is applied, thereby ensuring numerical stability.

5.1.2 Wave module

Delft3D Flexible Mesh uses the SWAN wave model to simulate the evolution of random, short-crested, wind-generated waves. A brief model description of the SWAN model is given here. A more detailed, conceptual description can be found in SWAN (2000).
SWAN is a third generation numerical model that computes wave transformation from deep water to nearshore values based on a wave action balance. The model does not solve for individual waves, but transforms an offshore wave spectrum to a wave spectrum nearshore. These spectra are defined by a spectral shape, wave height, peak period and frequencies. Other input parameters that should be defined are the bottom level, initial water level, wind speed and wind direction.
The physical phenomena that are included in SWAN are generation of waves, quadruplet wave-wave interactions, triad wave-wave interactions, whitecapping, depth-induced breaking, friction and wave-setup. Based on algorithms, SWAN iterates the wave conditions for each grid cell, thereby generating output in any desired point within the grid.
The coupling between the flow and wave modules can be either offline or offline. For offline coupling, the entire hydrodynamic simulation is performed first. Based on the results of this first simulation, the wave simulation is executed separately. The wave simulation is thus determined by the hydrodynamic conditions. Next, the hydrodynamic simulation is performed again, with water level and velocity input from the wave simulation. There is no further interaction between the simulations. For many applications this is good modeling practice.
For online coupling, on the other hand, data is continuously exchanged between the simulations with a user-defined interval. In doing so, a direct feedback exists between the simulations and wave-induced effects, such as radiation stress and bed shear stresses, are included in the hydrodynamic computation.

5.1.3 Sediment module

During the course of this project, the implementation of sediment transport and morphological processes was not yet part of the standard release of Delft3D Flexible Mesh. The

software was still under development and being tested. Cohesive sediment applications – in particular – had not yet been tested. My contributions to the testing and development of the sediment and morphology module are described in section 5.3.
The sediment transport and morphology module supports both bed load and suspended load transport of non-cohesive sediments and suspended load of cohesive sediments. The focus here will be on cohesive sediments, which require different formulations than that of non-cohesive sediments. For example, settling velocity is an important parameter for cohesive sediments, where the hindered settling effect at high concentrations needs to be accounted for.
The input for the sediment module consists of initial and boundary conditions, as well as some physical parameters. The initial concentration can be given as uniform value or as spatially-varying concentration field. The boundary condition at the water surface is set at zero transport, whereas the exchange of material at the bed is computed as source and sink terms based on the Partheniades-Krone formulations (Partheniades, 1965), see section G.3 in appendix G. The calculated fluxes are also applied to the bed in order to update the bed level. This morphological update is performed for each computational time step, thus ensuring that the hydrodynamic computations are carried out using the correct bathymetry.
It should be noted that the present implementation of D-Flow FM has some limitations. Firstly, more advanced turbulence closure models (e.g. $k - \epsilon$ model) are available in D-Flow FM in order to account the effect that a vertical density gradient has on damping the amount of vertical turbulent mixing. However, for cohesive sediment the extra turbulent mixing due to waves is not yet included in the eddy diffusivity. Moreover, the effect of sediment on fluid density is not implemented in D-Flow FM yet. The influences of these limitations on the sediment transport and morphology are not expected to be large.

5.2 Model set-up

In this section, the model set-up is discussed. It discusses the processes that are included in the model and the input parameters, including the computational grid, the bathymetry, initial conditions and boundary conditions.

5.2.1 Computational grid

The model is in 2DH, so depth-averaged with two horizontal dimensions. Hence, 3D effects such as density currents and secondary circulations are neglected. The flow module and wave module use different computational grids, as can be seen in figure 5.1. The domain for the wave grid is somewhat larger - mainly in alongshore direction - in order to make sure that the shadow effect, which can occur near the boundaries of the wave grid, does not influence the outcomes of the flow module. As SWAN can only be used for rectangular or curvilinear grids, a nesting approach is applied for the wave module. For the outer domain a rectangular grid with constant cell size of about 250 m is used. The nested inner domain

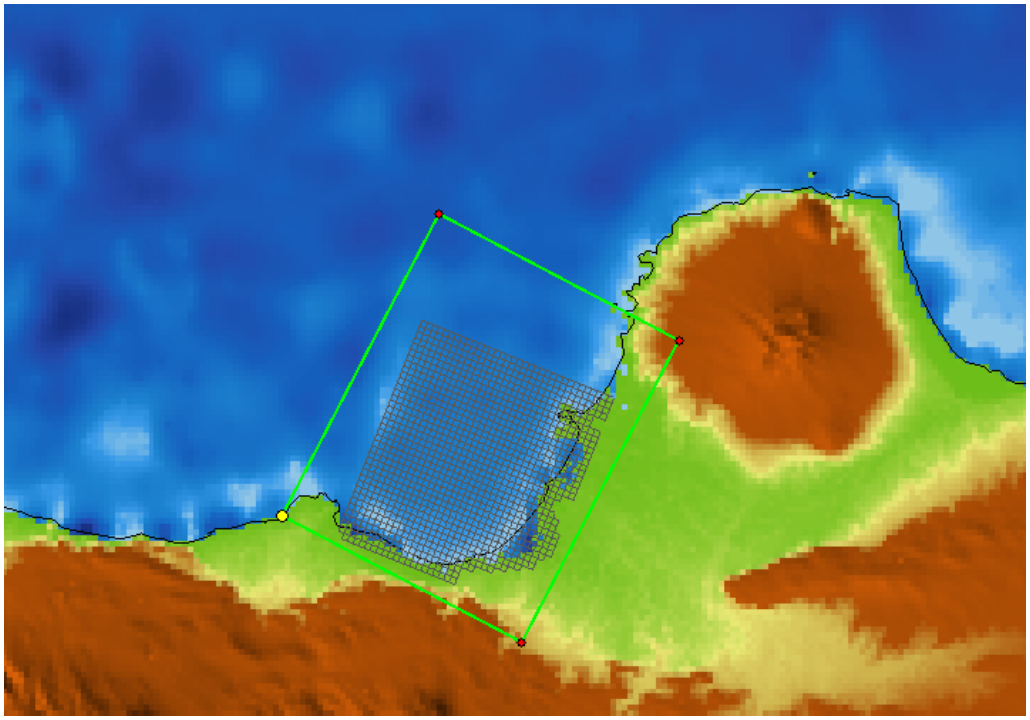

Figure 5.1: The extent of the wave grid indicated with the flow domain visualised inside of it

has a cell size of about 40 m.
The flow module can make use of the flexible mesh suite to perform computations on an unstructured grid. This feature was used to achieve a very high resolution locally at the Demak coast, where the cell size is approximately 16 m. Offshore, on the other hand, the resolution is much lower (with a cell size of about 1 km) to save computation time. For simplicity reasons, it was decided to use a predominantly rectangular grid in combination with triangular grid cells to achieve the local refinements. Another advantage of this approach is that it inherently results in optimal orthogonality - which is computationally favourable - without changing the smoothness. The computational grid that was used for the flow module can be seen in figure 5.2.

5.2.2 Bathymetry

Two sets of local bathymetry data were available from depth measurements as mentioned in section 3.4.1. This local nearshore bathymetry data is assumed to be representative for the entire coastline, as the bottom profile has a very gentle slope. For the depth in offshore grid cells an offshore bathymetry database by GEBCO was used. The final bathymetry that was used can be seen in figure 5.3. More information on the bathymetry datasets is given in appendix F.
The cheniers were not included in the depth measurements. They were artificially reproduced by increasing the bed level by 20 cm over a width of 30 m width at locations based on Google Earth images. In some simulations these cheniers were included to assess the

influence of the cheniers on the patterns of sedimentation and erosion.

5.2.3 Physical processes

In the wave module, the physical processes of depth-induced breaking, bed friction, wind growth, quadruplet wave-wave interactions, white capping, refraction and frequency shifting are all included. The wave module neglects wave setup, triad wave-wave interactions and diffraction. Diffraction can only be solved accurately when a detailed grid is applied (cell size about $1/10^{\text{th}}$ of the wave length). When diffraction is included for coarser grids, the SWAN computation can become unstable (SWAN, 2000). Wave setup and diffraction are accounted for in the flow module. Triad wave-wave interactions are neglected entirely. The JONSWAP formulation for bottom friction was used with a constant friction coefficient. The recommended value for smooth sea floors of 0.019 m^2/s^3 was applied.
In the flow module a Manning coefficient of 0.012 $s/m^{1/3}$ was used for bottom roughness. The water density was assumed to be 1025 km/m^3, which is the standard for sea water. All other possible effects of salinity and temperature (e.g. density differences and associated currents) were neglected. Tide generating forces were also neglected, as the research area is not large enough for a significant contribution of gravitational forces on the water motion. It is assumed that the tidal motion can be simulated accurately by imposing a water level boundary condition, see section 5.2.4. Uniform values of 1.0 m^2/s are used for the horizontal eddy viscosity and eddy diffusivity.
For the sediment module two cohesive mud fractions are used with constant settling velocities of of 0.1 and 0.5 mm/s. The dry bed density was 300 kg/m^3 for both fractions. The critical shear stress for erosion was set at 0.5 N/m^2 and the critical shear stress for sedimentation was set at a very large value of 1000 N/m^2 in order to allow unlimited sedimentation. For the erosion parameter from the Krone-Partheniades formulation a value of $5 * 10^{-5}$ $kg/m^2/s$ was used. A uniform initial concentration of 0.1 g/L was applied.

5.2.4 Boundary conditions

The boundary condition of the flow module is a water level boundary, created from tidal constituents. This tidal boundary was obtained using the Indian Ocean Tidal Model Driver. The sediment concentration at the open inflow boundaries was varied between zero (no sediment inflow) or 0.1 g/L.
For the wind and wave parameters, three scenarios were set up. The scenario 'monsoon' is for the northwest monsoon period (December upto February) and the scenario 'non-monsoon' is representative for the rest of the year. Moreover, a 'storm' scenario was set up that has representative conditions for a storm of two days. Based on the data analysis of appendix E, representative values were determined for the wave and wind parameters, as listed per scenario in table 5.1. The varying wind parameters are wind speed and direction, whereas for waves the wave height, wave period, wave direction and spreading were varied per scenario. A JONSWAP spectrum was used with a peak enhancement factor of 3.3 in all scenarios.

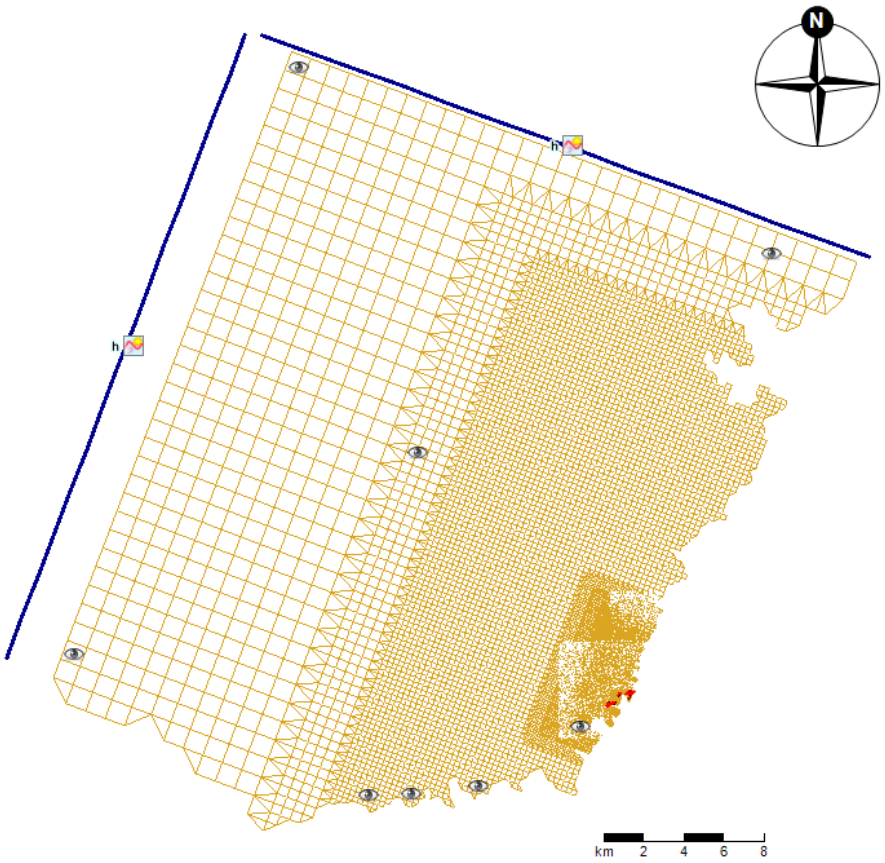

Figure 5.2: The unstructured computational grid that was used for the flow module

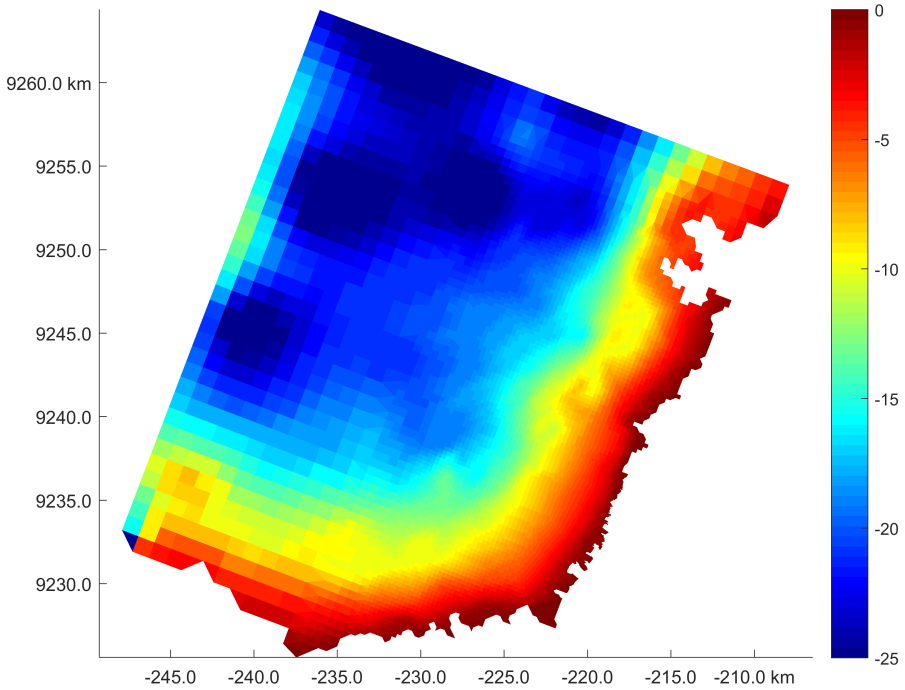

Figure 5.3: The final bathymetry that was used for the flow module

Table 5.1: Wind and wave parameters per scenario

	Wind		Waves			
Scenario	speed	direction	H_s	T_{mean}	direction	spreading
	[m/s]	[-]	[m]	[s]	[-]	[deg]
Monsoon	4.4	W-NW	0.7	4.75	NW	15
Non-monsoon	3.0	E-SE	0.4	4.3	E	10
Storm	11.0	NW	2.1	5.9	NW	10

5.2.5 Dams

In the flow module, the dams could only be included as so-called 'thin dams'. These close off a cell face, preventing any flow through that cell face. Hence, thin dams are impermeable. A thin dam is modeled with an infinite height, i.e. no water overflows a thin dam. The fact that the dams are impermeable in the flow module is not expected to be of big influence on the model outcomes, as the majority of the sediment presumably flows in through the gaps.
In the wave module, it was possible to apply the dams as obstacles through which waves are partly transmitted and partly reflected. Reflections can be switched on or off and the obstacle height is user defined. For all dams in the wave module a height of 2.0 m above mean sea level was used and reflections were switched off.

5.3 Model development

As mentioned in section 5.1.3, the sediment module was still under development and being tested during the course of this project. This section describes my contributions to the testing and development of the sediment and morphology module.
The behaviour of cohesive sediment transport and morphological updating of the bed level was tested for Delft3D Flexible Mesh. Two test cases were developed: in the first case only tidal flow was used (D-Flow FM standalone) and in the second case tidal flow was combined with waves. The results obtained with FM were compared to results of the validated Delft3D model (D3D).
Some bugs were encountered, that could be identified by testing several parameter settings. At first, no sedimentation occurred at all. Moreover, the bed shear stresses were not computed correctly in presence of waves, because the code was not using the correct roughness heights in the computations.
Finally, once all bugs were fixed, Delft3D Flexible Mesh gave reasonable results that show similar sedimentation and erosion as the Delft3D simulations (both in magnitude and in spatial patterns). Additional research is necessary to further improve the results. The final results of the tests were reported to the software developers in an internal memo, which is included in appendix H. The test cases were approved and added to the Delft3D Flexible Mesh test bank.

5.4 Model validation

As the availability of observation data in the model area is very limited, it is not possible to completely validate the model with data. Model validation will therefore be partially based on expert judgement by supervisors.
In order to validate the tidal boundary conditions, tidal prediction data of IHO station Semarang was used. Two different tidal models were used to obtain tidal constituents at the boundaries. The Indian Ocean Tidal Model Driver (IO TMD) was obtained from OTIS website and has a resolution of 1/12°, which is about 1 km. Through Delft Dashboard conditions for the TOPEX/Poseidon (TPXO 6.2) model were obtained with a resolution of 2 km. Figure 5.4 shows resulting water levels for both models compared to the tidal station in Semarang. Both models show good correspondence, although the transition from semi-diurnal to diurnal tides gives some issues. The IO model performs somewhat better than the TPXO model and is therefore used to generate tidal conditions. It should be noted that the exact conditions at the Semarang station are unknown, which could be influencing the water level signal.
As explained in section 3.3.3, little is known about the tidal current direction close to the coast. The tidal currents are quite variable and could therefore not be validated.
No quantitative data is available about the morphological development of the area. Nevertheless, it is known that the area suffers from erosion if no measures are taken. Moreover the dams are expected to capture sediment based on the pilot study. Expert judgement and these qualitative observations were used as guideline for the sediment and morphology outcomes of the model simulations. The sediment parameters that were used for calibration are the erosion parameter, the critical shear stress for erosion and the settling velocity.

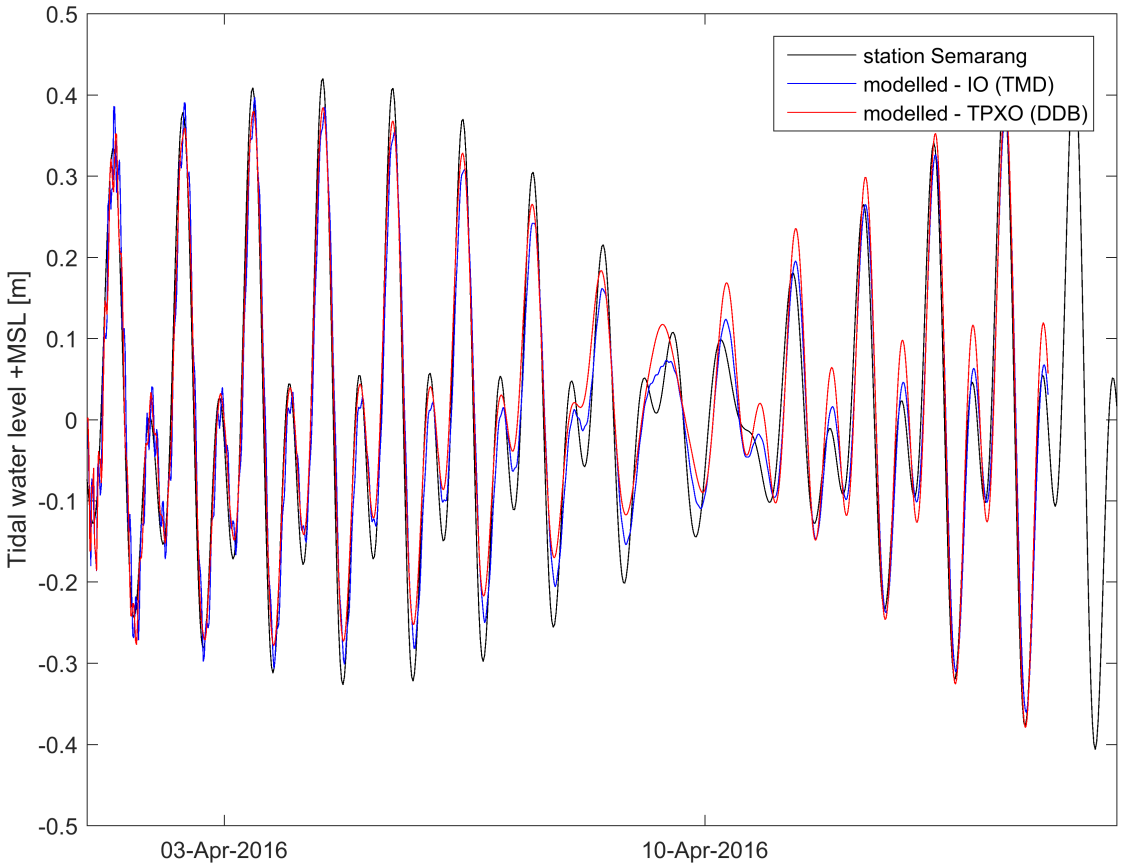

Figure 5.4: Tidal validation of Indian Ocean and TOPEX/Poseidon tidal models compared to a tidal station Semarang

Chapter 6

Results

This chapter describes the results of the model simulations. First section 6.1 describes a general understanding of the system. In this context, the results of the model simulations are presented in section 6.2. It introduces the dam configurations that were tested and describes the outcomes of the simulations per case. The sensitivity of model results to the value of the model parameters is assessed in section 6.3. An interpretation of the results is given in chapter 7.

6.1 General system understanding

The system analysis in chapter 3 helps to get a general understanding of the large-scale morphodynamics of the Demak coastal zone. The area is subject to a seasonal monsoon climate. The strongest winds occur during the northwest monsoon in the months December, January and February. The southeast monsoon reaches its greatest strength in July and August. The largest waves also occur during the northwest monsoon. During the southeast monsoon very few waves reach the Demak coast, mainly because then the waves are predominantly coming from the West. As the coastal slope is very gentle, waves are approaching the coast mostly perpendicularly and wave-induced currents are small.
The tide in the area is quite complex, due to its geographical location, local bathymetry and surrounding land masses. The tidal signal at Demak coast is mixed with mainly diurnal characteristics and small semi-diurnal components. Based on literature, the direction of the tidal current could not yet be determined, but tidal current velocities are expected to be larger than current velocities induced by waves. Hence, the flow pattern will be dominated by the tide.
Waves dominate erosion of the seabed, as explained in section 2.2.3, and thereby the availability of suspended sediment. After waves have stirred up sediment on the foreshore, currents transport sediments towards shore. Therefore, both erosion and sedimentation are largest during the months December, January and February when the wave height is largest. During the rest of the year, the amounts of erosion and sedimentation are much smaller.

6.2 Test cases

First a simulation was performed without any dams, in order to improve the system understanding. The results of this reference simulation are described in section 6.2.1. Subsequently, simulations were performed with Ecoshape and MMAF dams (as indicated in figure 4.4) to assess the influence of the dam configuration on flow patterns and on sedimentation and erosion patterns. The results are described in sections 6.2.2 and 6.2.3 respectively. The effect of closing off cells using side dams is tested in section 6.2.4. By placing a new dam in one of two possible locations, the effect of dam spacing was tested in section 6.2.5. In order to optimise the design, the model was used to research the interaction between multiple dams. The results are included in section 6.2.6. Finally, section 6.2.7 describes the results of simulations with southwest monsoon and storm scenarios. For brevity, not all figures are included in the main report. In appendix I additional figures are given.

6.2.1 No dams (reference)

For the reference case (a simulation without any interventions), the time-averaged flow pattern is given in figure 6.1. Figure 6.2 shows the flow pattern near the location of the dams. It can be seen that overall the flow enters the domain in the southwest and flows out through the northeast boundary. At the location of the dams the tidal current flows southwards along the coast. Note that the flow pattern depends on the tidal phase and that velocity magnitude and direction vary accordingly.
The resulting wave field is shown in figure 6.3. It can be seen that the significant wave height equals 0.7 m at the boundary and grows to a maximum of about 0.8 m throughout the domain. Closer to the coast, the largest waves start to break, causing a decrease in significant wave height. Near the location of the dams, the significant wave height is about 0.20-0.25 m, see figure 6.4. Figures 6.5 and 6.6 show the bed shear stresses averaged over the simulation period, respectively for the entire domain and zoomed in at the location of the dams. It can be seen that the bed shear stress is largest in a small strip along the coast, which is where the waves break. Closer to the coast, the shear stress decreases again. Near the location of the dams the time-averaged bed shear stress is about 0.5-0.6 Pa.
Figures I.1 and I.2 show the resulting bed level after one monsoon period. In figure 6.7 the corresponding cumulative erosion and sedimentation is indicated with red colours representing sedimentation and blue colours for erosion areas. It can be seen that hardly any bed changes were found throughout large parts of the domain. Only close to the coast morphologic development occurred. Figure 6.8 shows the cumulative erosion and sedimentation near the location of the dams. It indicates about 50 cm of erosion around the location where the waves break and shear stresses are large. Sedimentation occurred mostly just landward and just seaward of the erosion locations. Just in front of the location where the dams would be, 10-15 cm of sedimentation was found (even without any dams included in the simulation yet).

Time-averaged figures of the mud concentration show that most suspended sediment is located in the same area where the shear stresses are large and erosion is found. There, the mean concentration of the mud fraction with settling velocity of 0.1 mm/s is between 0.15 and 0.25 g/L (see figures I.3 and I.4). The mean concentration of the mud fraction with settling velocity of 0.5 mm/s is about 0.03-0.05 g/L in these areas (see figures I.5 and I.6).

In order to check the sediment balance, the total amounts of erosion and sedimentation were computed. Over the entire domain, 1.37 Mton sediment was deposited, whereas only 0.22 Mton sediment eroded. The difference of 1.15 Mton sediment originates from the initial concentration. By comparing the final concentration to the initial concentration, it is concluded that 1.45 Mton sediment disappeared from the water column. This sums to a total of 0.3 Mton less sediment at the final timestep. The same computation was performed for the smallest cells, which are located close to the coast. There, 64.8 kton sediment was deposited, whereas 42.5 kton sediment eroded. The difference in concentration accounts for about 1 kton of additional sediment that was deposited. In total 21 kton extra sediment was found in the smallest grid cells at the final timestep.

6.2.2 Ecoshape dams

For a simulation of one monsoon period with Ecoshape dams, the wave height throughout the domain corresponds largely to that of the reference case. The most important differences in wave height are found near the location of the dams, which is shown in figure 6.9. The significant wave height behind the dams was found to be only zero to 0.10 meters, instead of the 0.20-0.25 meters in surrounding areas. The bed shear stresses, which are shown averaged over the simulation period in figure 6.10, were also lower behind the dams (0.10-0.20 Pa) compared to surrounding areas (about 0.50 Pa). Here, the magenta lines indicate the locations of the dams.
The resulting bed level also corresponds to that of the reference case in the majority of the domain. A zoom of the resulting bed level near the location of the dams is shown in figure I.7. Figure 6.11 shows the corresponding cumulative erosion and sedimentation around the dams. It can be seen that deposition is found behind the dams. The amount of deposition varies from about 7 cm for the dams near Bogorame upto 35 cm for the dams near Bedono. Compared to the reference case, some additional erosion (known as scour) occurred alongside the dams and between them.

6.2.3 MMAF dams

For a simulation of one monsoon period with the MMAF dams and Ecoshape dams, again the wave height and bed shear stresses were found to be lower behind the dams. The resulting bed level is given in figure I.8. Figure 6.12 shows the cumulative erosion and sedimentation over the entire monsoon period. The magenta lines indicate the locations of the newly introduced MMAF dams, whereas the Ecoshape dams are indicated in black.

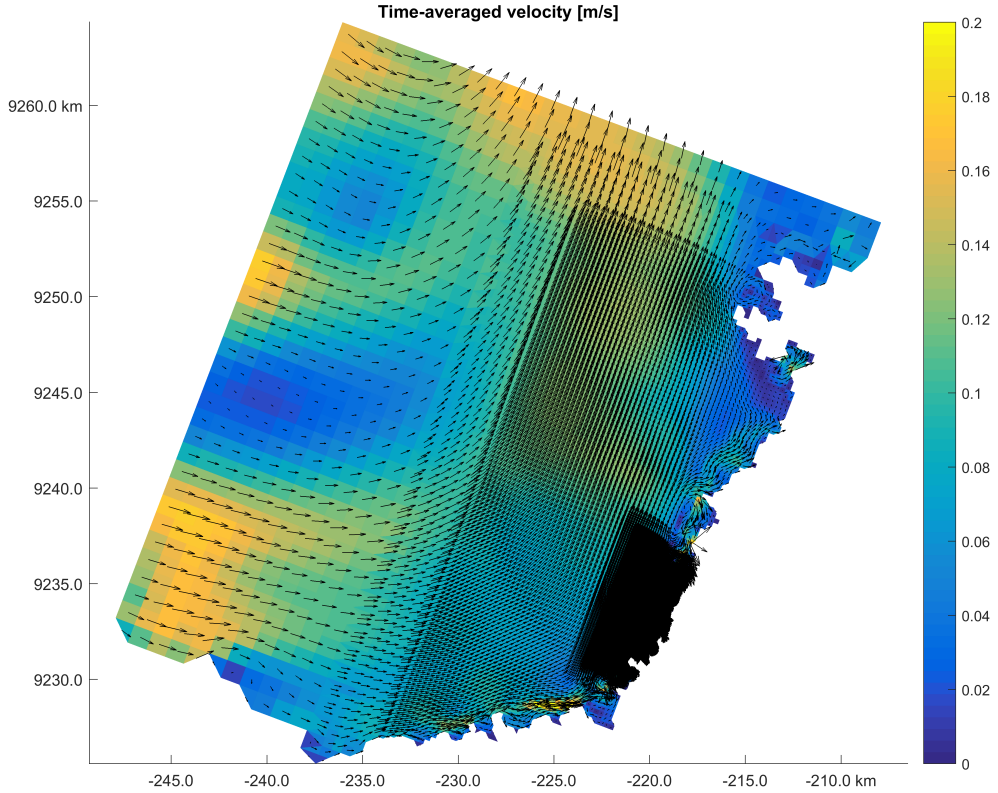

Figure 6.1: Time-averaged velocity [m/s] for a simulation period of three months with the monsoon scenario (domain). Colours indicate velocity magnitude and arrows indicate velocity vectors.

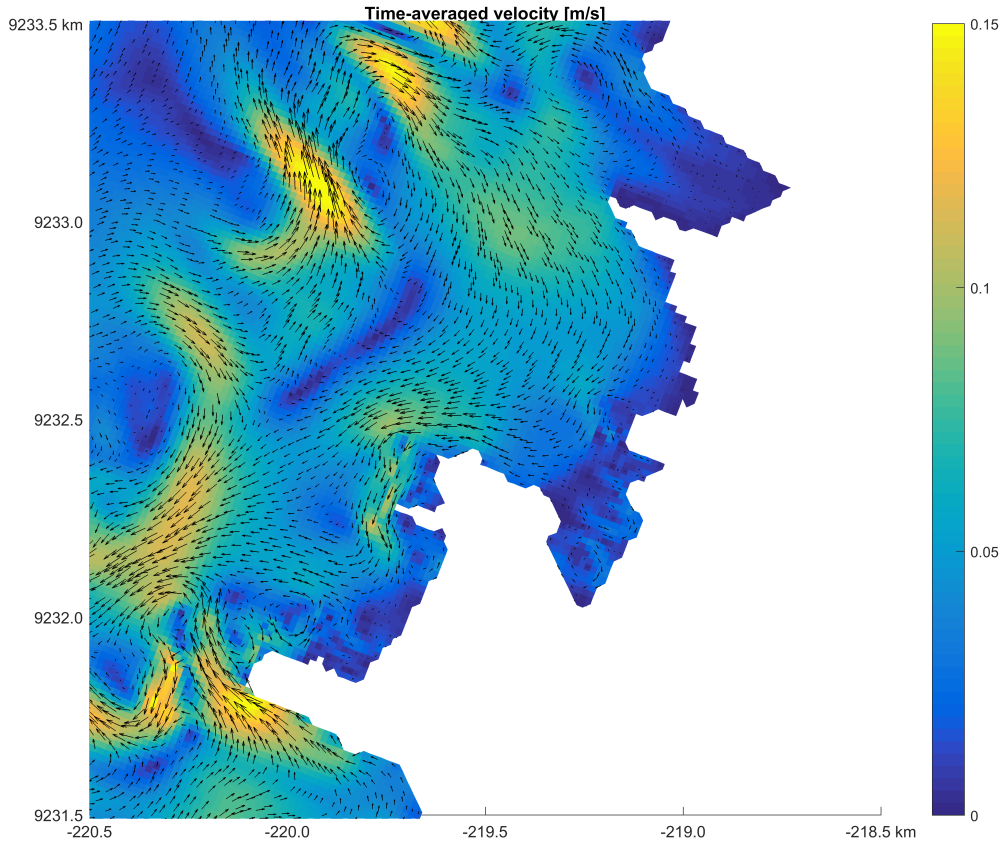

Figure 6.2: Zoom of time-averaged velocity [m/s] for a simulation with the monsoon scenario without dams

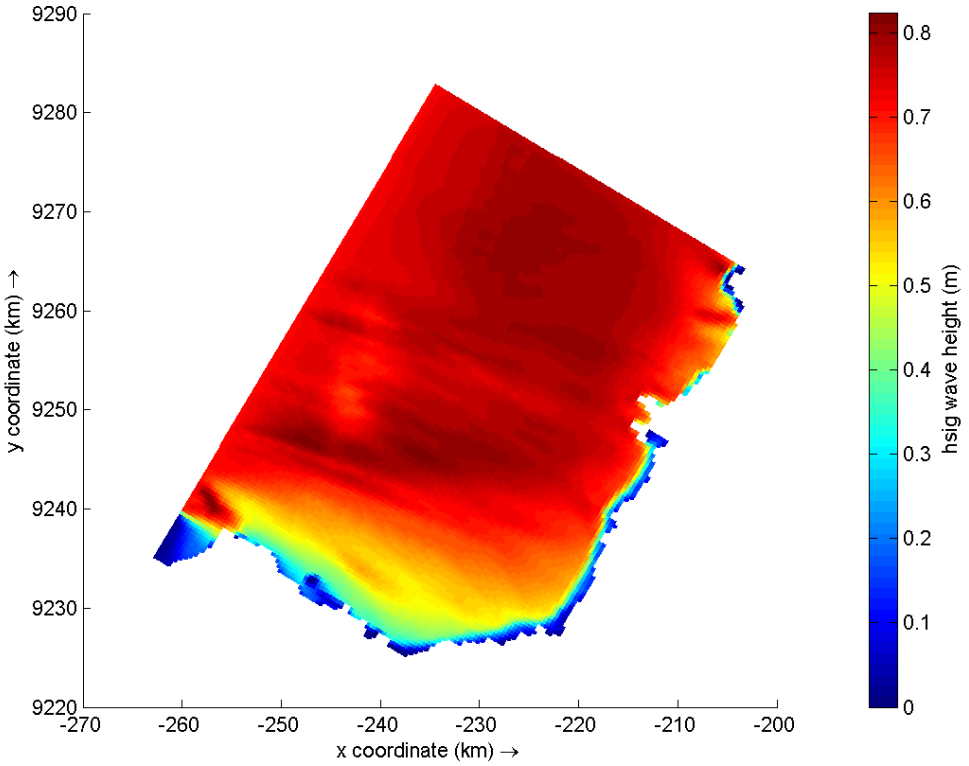

Figure 6.3: Significant wave height [m] at last time step of the monsoon scenario (domain)

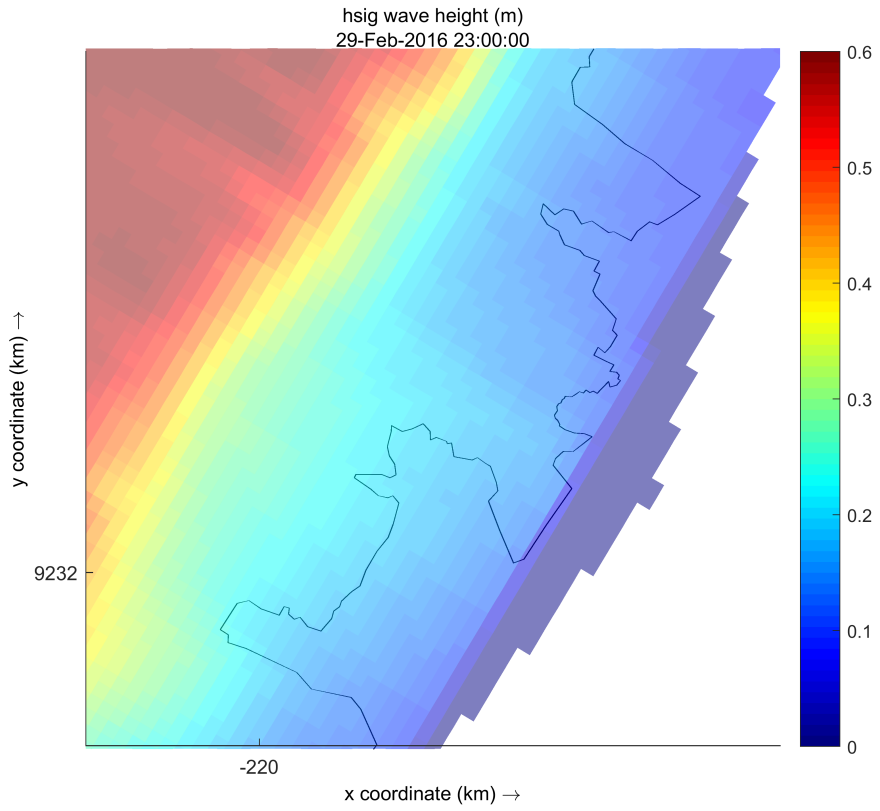

Figure 6.4: Zoom of significant wave height [m] at the last time step of the monsoon scenario without dams

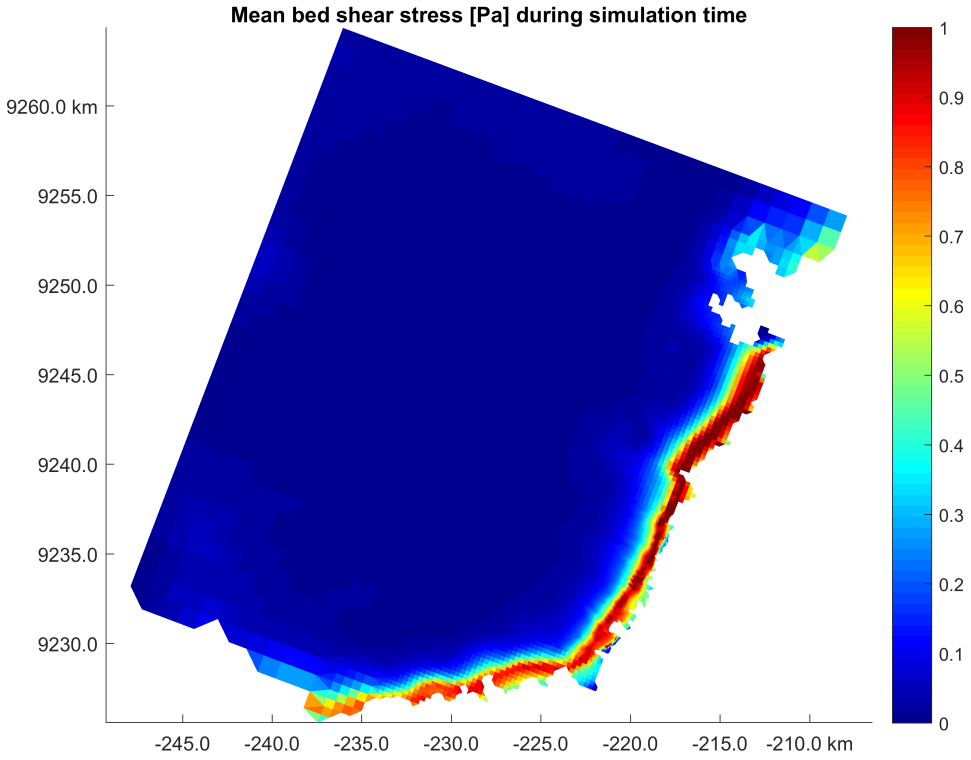

Figure 6.5: Time-averaged bed shear stress for a simulation period of three months with the monsoon scenario (domain)

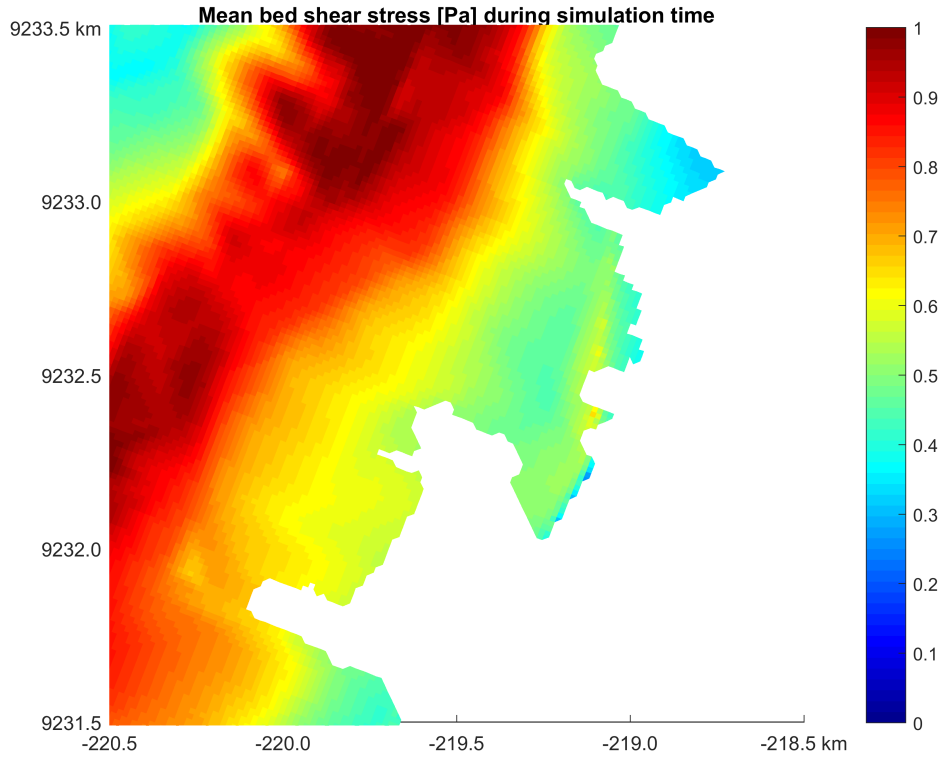

Figure 6.6: Zoom of time-averaged bed shear stress for a simulation with the monsoon scenario without dams

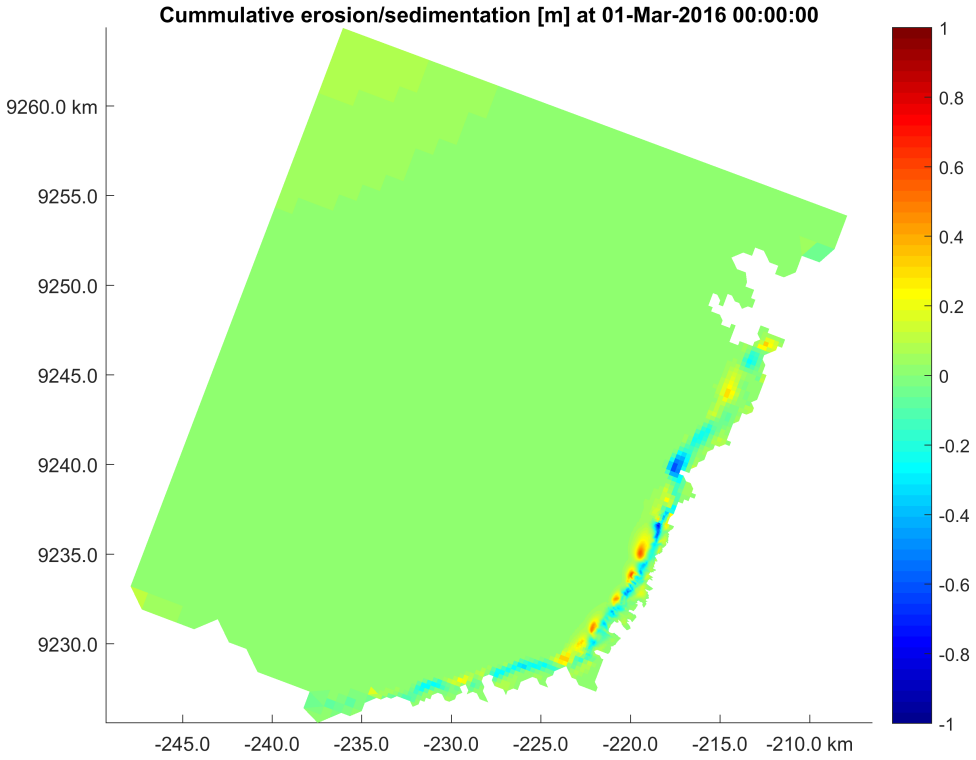

Figure 6.7: Cumulative erosion and sedimentation for a simulation period of three months with the monsoon scenario (domain)

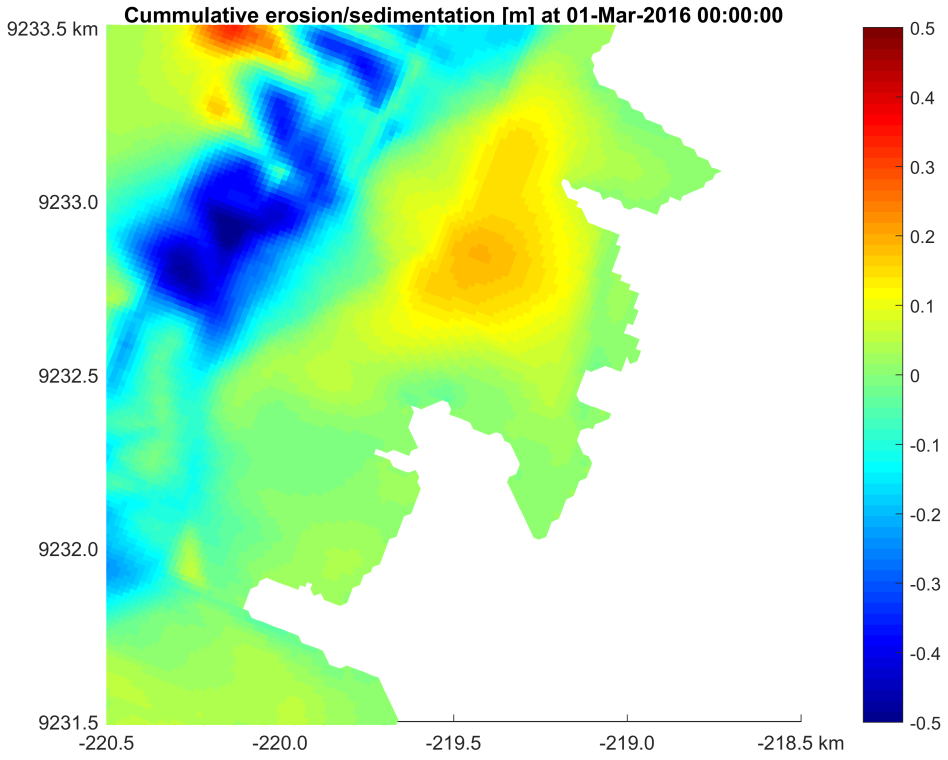

Figure 6.8: Zoom of cumulative erosion and sedimentation for a simulation with the monsoon scenario without dams

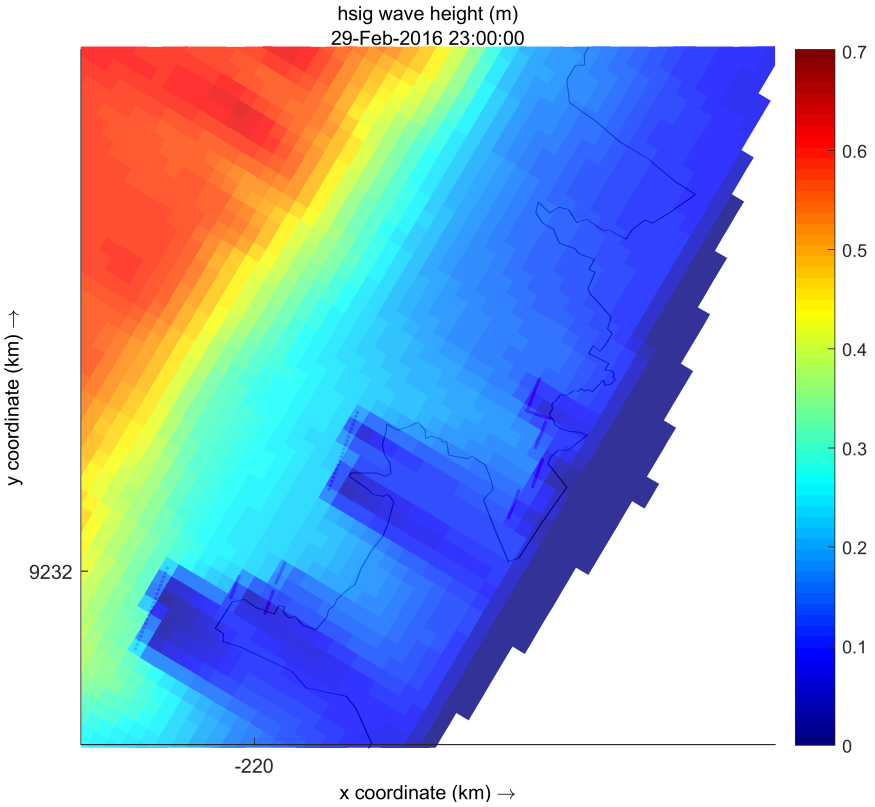

Figure 6.9: Zoom of significant wave height [m] at the last time step of the monsoon scenario with Ecoshape dams

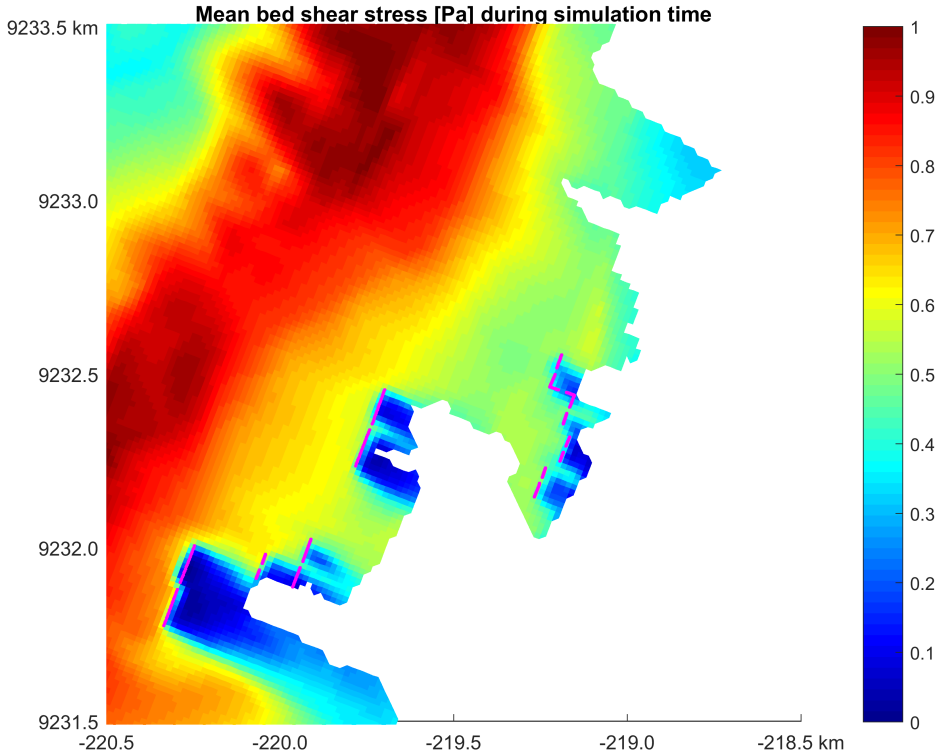

Figure 6.10: Zoom of time-averaged bed shear stress for a simulation with the monsoon scenario with Ecoshape dams

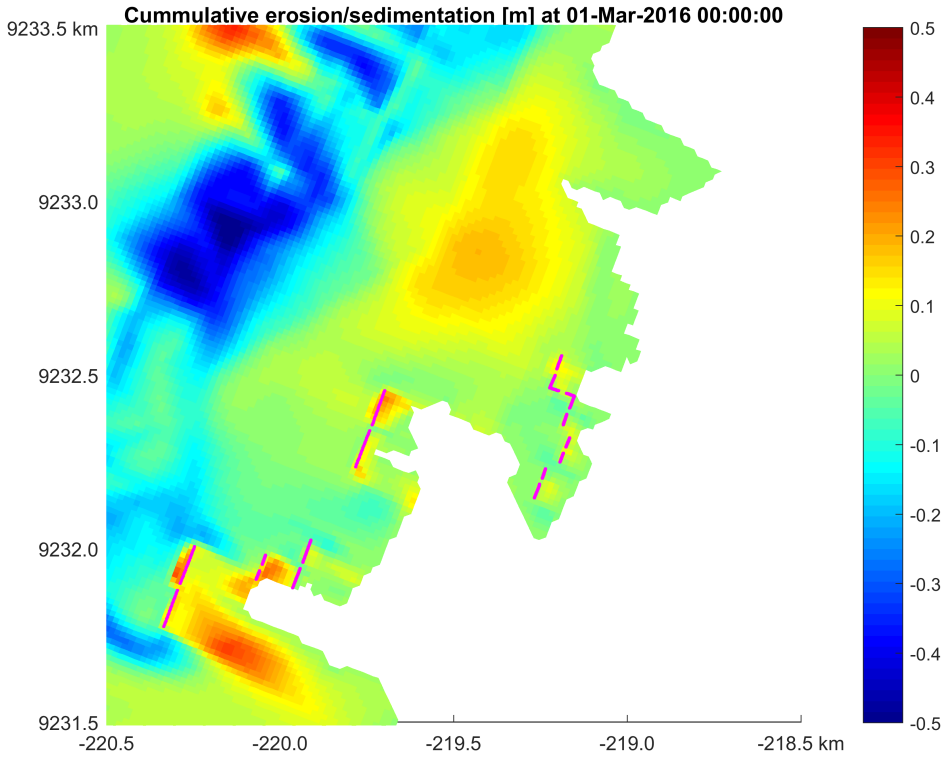

Figure 6.11: Zoom of cumulative erosion and sedimentation for a simulation with the monsoon scenario with Ecoshape dams

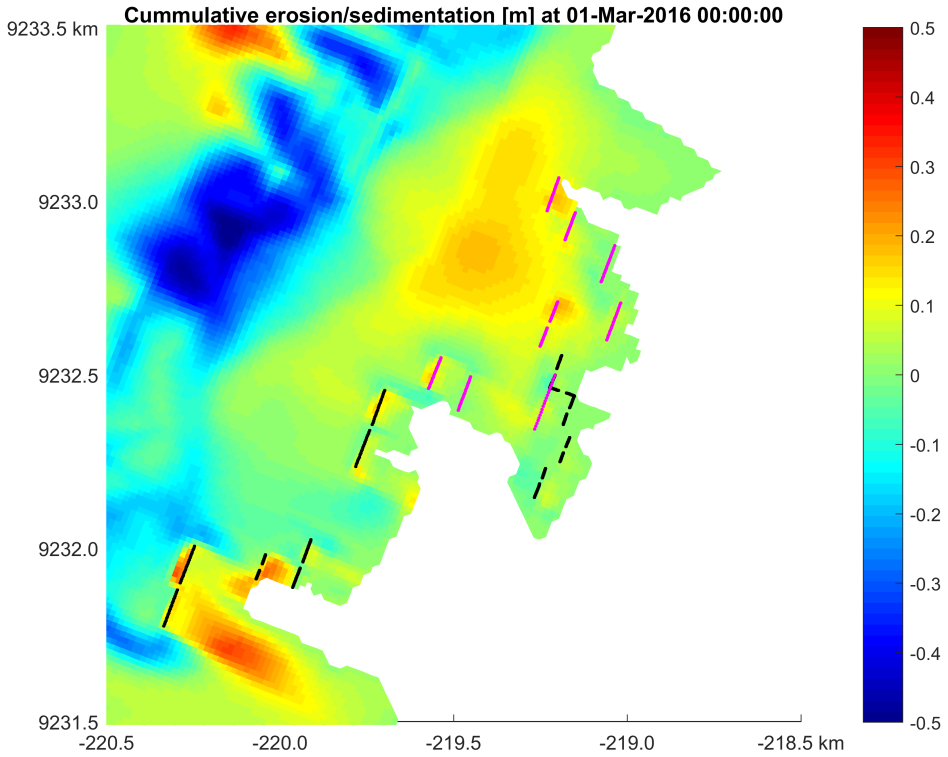

Figure 6.12: Zoom of cumulative erosion and sedimentation for a simulation with the monsoon scenario with MMAF dams

It can be seen that deposition is found behind the MMAF dams. Moreover, the rate of sedimentation behind the Ecoshape dams decreases slightly. This can be illustrated by looking at the accumulation behind the dams as a function of time. In figure I.9 it can be seen that sediment is captured behind the MMAF dams, where previously erosion was found. Figure I.10, however, indicates that the total accumulation behind the first pilot dam by Ecoshape at Bogorame decreased by about 50%.

6.2.4 Side dams

The dams that were constructed for the first pilot study had coast-parallel dams, as well as coast-perpendicular dams to close off cells, as explained in section 4.2.3. Later, only coast-parallel dams were constructed, hypothesising that this would enable more inflow of sediment. Two simulations were performed to test this hypothesis. In the first simulation the coast-perpendicular dam that was constructed by Ecoshape was left out to see the effect on the amount of sediment captured behind the remaining dams. In the second simulation another coast-perpendicular dam was added at dam 6.
The resulting bed level for a simulation without side dams is given in figure I.11. Figure I.12 shows the cumulative erosion and sedimentation over the entire monsoon period. It can be seen that about 10-15 cm sediment is deposited behind dam Ecoshape 1, compared to 5-10 cm with side dam in section 6.2.2. By comparing the resulting bed level without side dams to the bed level of the original Ecoshape case with side dam, the differences can be visualised. In figure 6.13 the difference in bed level is plotted, so that red colours indicate a higher resulting bed level for case without side dams and blue colours indicate a lower resulting bed level.
The resulting bed level for a simulation with an extra side dam is given in figure I.13. Figure I.12 shows the corresponding cumulative erosion and sedimentation. The deposition behind the side dam varies mostly between 5 and 10 cm, compared to about 15 cm without the side dam in section 6.2.2. Again, the differences in bed level were computed, see figure 6.14.
Finally, figures I.15 and I.16 show graphs of the accumulation over time behind the removed side dam and behind the extra side dam respectively. In both graphs, it can be seen that more sediment is deposited if no side dam is used.

6.2.5 Dam spacing

In order to assess the effect of dam spacing on the sedimentation rate, two possible locations for a new dam near Bedono were compared. First, the new dam was placed about 100 meters from the coast. Next, the dam was placed 150 meters from the coast. In order to simplify and prevent influence by surrounding dams, the other dams were not included in the simulation.
Figure I.17 gives the resulting bed level for the case with a dam 100 m from the coast. The corresponding cumulative erosion and sedimentation over one entire monsoon period

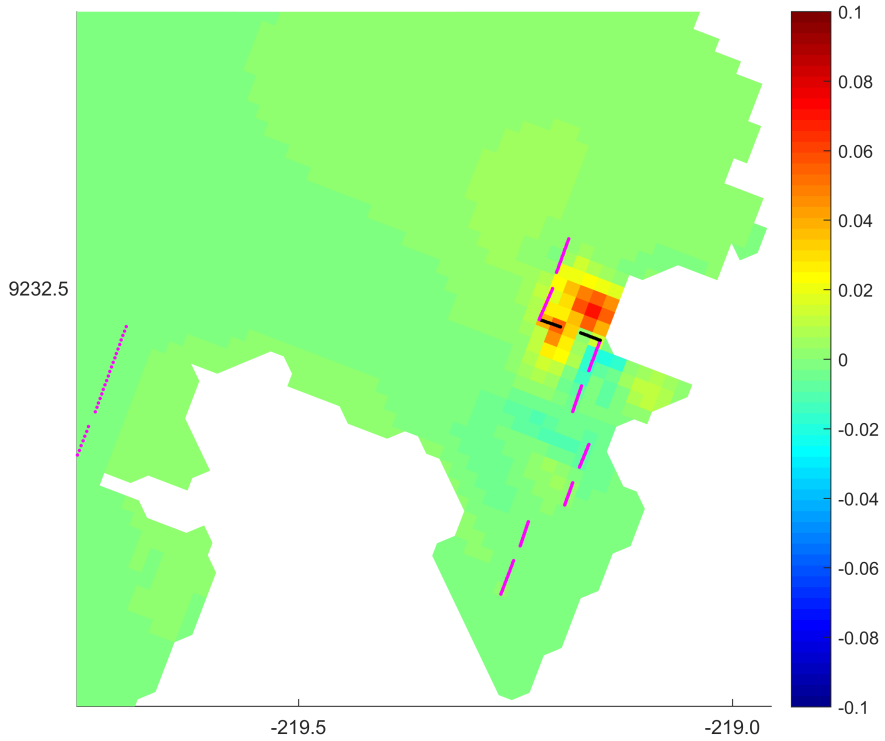

Figure 6.13: Differences in bed level [m] for the case without side dams compared to the original Ecoshape case after a simulation of three months with the monsoon scenario

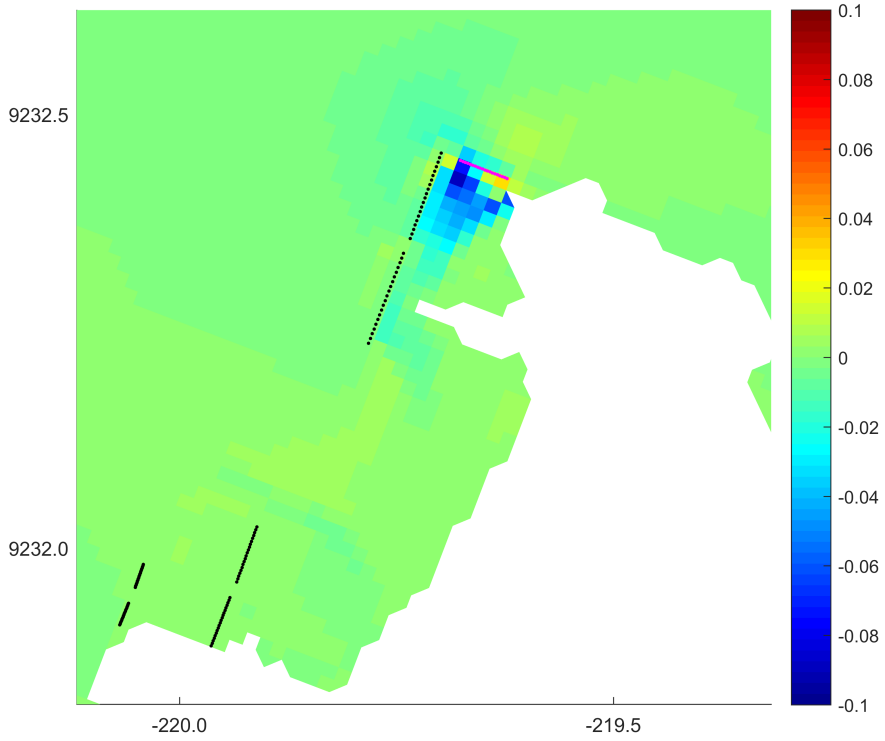

Figure 6.14: Differences in bed level [m] for the case with an extra side dam compared to the original Ecoshape case after a simulation of three months with the monsoon scenario

is shown in figure I.18. Behind the dam about 7 cm is deposited on average, with upto 15 cm deposition in some cells. Figures I.19 and I.20 contain the same information for the case with a dam 150 m from the coast. Here, per cell about 4 cm of deposition is found on average throughout the area behind the dam, which is a larger area. Again the maximum deposition is about 15 cm.
In observation points 150 m from the coast, of course more sediment is deposited when a dam is placed seaward of it, see figure I.21. Figure I.22, on the other hand, shows that about 100 m from the coast more sediment accumulates if the dam is placed 100 m from the coast, than if the dam is located 150 m from the coast. Figure 6.15 shows the accumulation in two locations closer to the coast, with the solid and dotted lines each indicating a separate observation point around 50 m from the coast. The blue lines indicate the results with the dam located at 100 m from the shore and the red lines indicate the same observation points when the dam is located further offshore (150 m). It can be seen that close to the coast more sediment accumulates if the dam is located further offshore. Finally, by comparing the resulting bed level with a dam located 150 m from the coast to the bed level with a dam located 100 m from the coast, the difference in bed level is visualised in figure 6.16.

6.2.6 Interaction between multiple dams

The influence of a new dam on the sedimentation rate behind surrounding dams was investigated by altering the dam configurations. First, the MMAF dams that are located most outward were removed, to see the effect on the dams right behind.
Figure I.23 shows the cumulative erosion and sedimentation for this altered MMAF case over the entire monsoon period. In figure 6.17 the bed level of this altered MMAF case is compared to the original MMAF case. It can be seen that 3-7 cm less sediment is captured behind the dams that were removed. However, some of the dams that are located behind the removed dams, now capture about 8 cm extra sediment, depending on which dam is considered.
Two graphs are included that show the accumulation over time behind one of the removed dams (figure I.24) and behind the dam that is located behind a removed dam (figure I.25). In these graphs it can also be seen that the dams behind benefit from the removal of the forward located dams.

Instead of putting dams in front of each other, dams can also be placed besides each other. By adding the new dam from section 6.2.5 next to the dams at Bedono in one of two possible locations, the effect on the surrounding dams was investigated. For the dam at 100 m from the coast, the cumulative erosion and sedimentation is shown in figure I.26 and the differences in bed level compared to the original Ecoshape case are shown in figure I.27. Figures I.28 and I.29 contain the same information for the 150 m dam. In both cases, it can be seen that the new dam captures sediment. However, less sediment is deposited behind the surrounding dams if a dam is added. Additionally, it can be seen that the dam 150 m from the coast has a worse effect on surrounding dams, than the

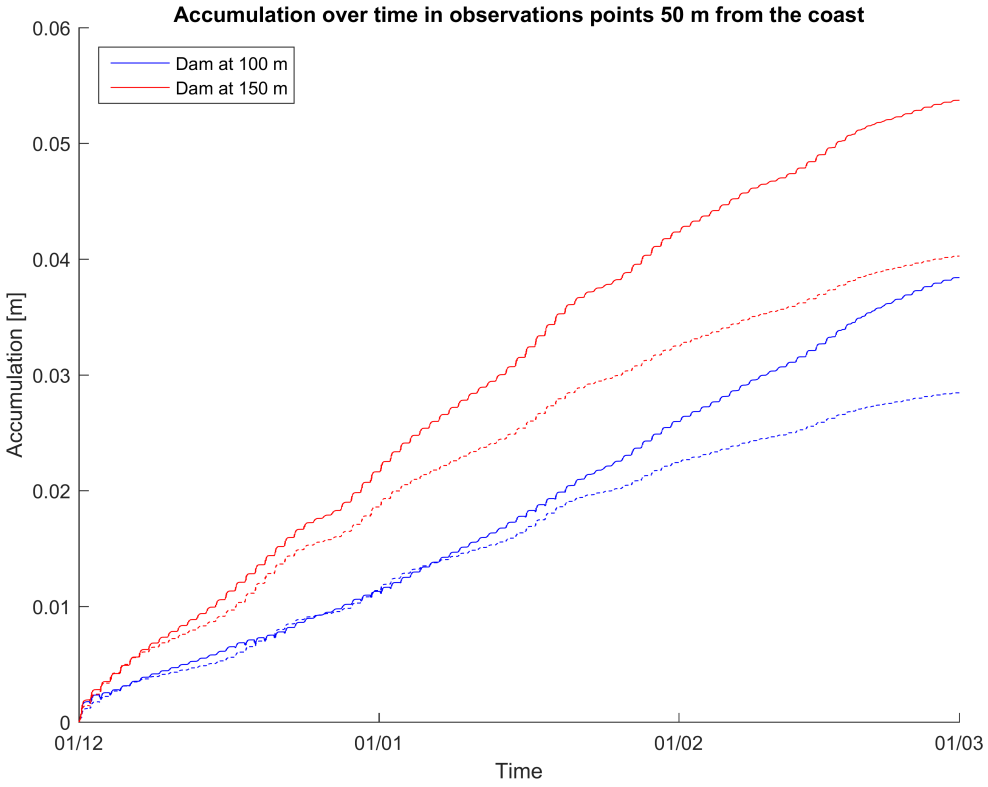

Figure 6.15: Accumulation over time for a simulation of three months with the monsoon scenario at a location 50 m from the coast

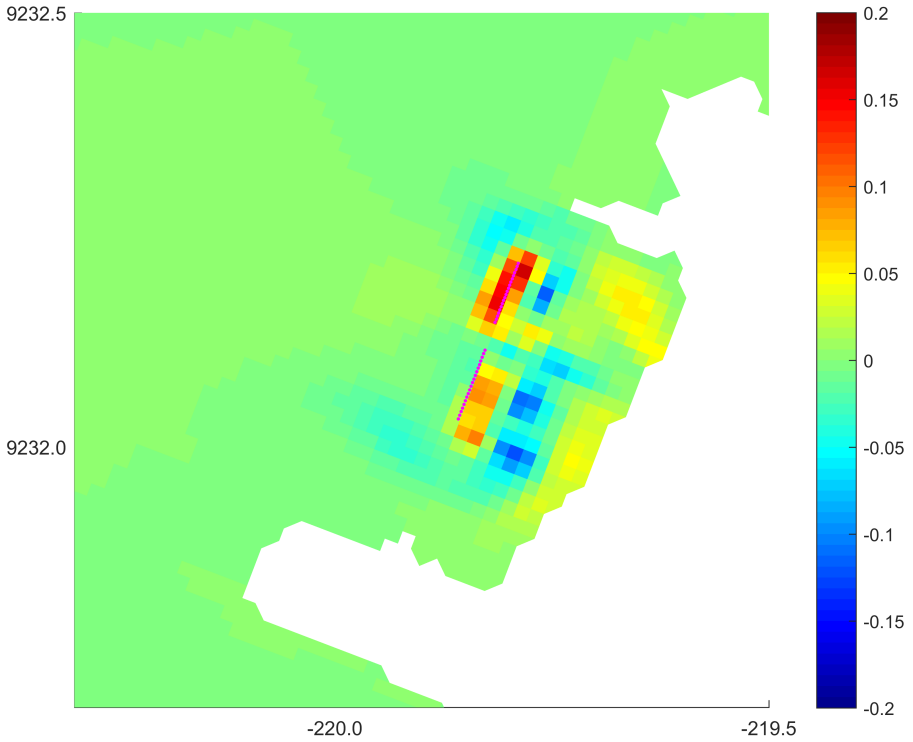

Figure 6.16: Differences in bed level [m] for the 150 m dam compared to the 100 m dam after a simulation of three months with the monsoon scenario

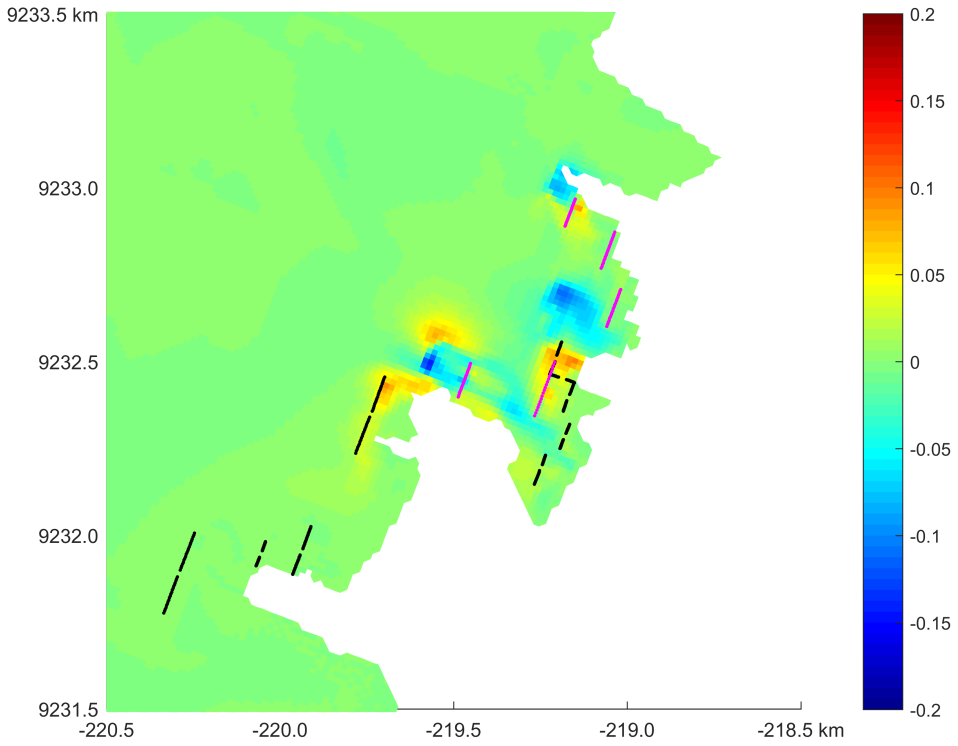

Figure 6.17: Differences in bed level without front dams compared to the original MMAF case

dam 100 m from the coast. This is most clearly visible in figures I.30 and I.31 that show the accumulation behind the neighbouring dams (respectively the dams northward and southward) over time.

6.2.7 Meteorological scenarios

Simulations were also performed for the southeast monsoon scenario and for a storm scenario. During the southeast monsoon no bed change occurred near the location of the dams. Apparently, waves coming from the East cannot reach the area within the model domain. Therefore, a simulation was performed with waves coming from the North, which may be the local situation at the model boundary. Figure I.32 shows the cumulative erosion and sedimentation after three months with incoming waves from the North. It can be seen that for such waves, some dams do capture sediment.
For the storm scenario, the model became unstable after 2 days because the bed gradients became too large. Nevertheless, as the storm duration will be about one or two days, the results of the first day are considered. The cumulative erosion and sedimentation of the storm scenario after one day is shown in figure I.33. The patterns of sedimentation and erosion are quite different from the monsoon scenario. Overall, much more erosion occurred. A zoom of the area around the dams is shown in figure I.34. The erosion

occurs further offshore and is about 1 cm within one day. The sedimentation also occurs somewhat further offshore and is somewhat less (about 0.7 cm). Behind the dams about 0.2 cm sediment was deposited, although the dams in deeper water capture somewhat more (about 0.5 cm).

6.3 Sensitivity analysis

The sensitivity of the model results to the input parameters was researched to obtain information about the accuracy of the results. It may also help to determine which parameters to focus on for data collection. Here only the most important results of the sensitivity analysis are included. Figures can be found in appendix J.
External forcings that were taken into account for the sensitivity analysis are offshore wave height, wind speed and sediment concentration on the boundary. Calibration parameters that were included in the analysis are diffusivity, viscosity, roughness, wave bottom friction, critical shear stress for erosion and the erosion parameter (M) from the Krone-Partheniades formulation.

A simulation was performed with an offshore significant wave height of 1.0 m. In figures J.1 and J.2 comparisons are made to the resulting bed level of the reference case. For an offshore significant wave height of 1.0 m, the waves break further offshore, which causes a difference in spatial erosion and sedimentation patterns. Moreover, the wave-induced shear stress will be larger, which causes an increase in erosion. The sediment is then transported towards shore in suspension, which could potentially lead to more deposition behind the dams.
The influence of wind on the wave transformation is mainly the generation of wave energy. If no wind had been included in the model, the morphologic development of the coastline would hardly be affected. The amounts of sedimentation and erosion are the same, although the spatial patterns are slightly different. The influence of the wind speed on the model results is therefore very small.
If 0.1 g/L sediment concentration is imposed on the boundaries, more sediment would flow into the domain. However, only the area close to the boundary itself would be affected by the incoming sediment. Deposition of sediment was found close to the boundary, but the morphologic development in the area of interest remains the same.

The sensitivity to diffusivity and to viscosity is simultaneously tested in order to keep the Prandtl number equal to 1, which is standard for sediment transport. When diffusivity and viscosity are both 0.5, the results are hardly affected.
A simulation was performed with a larger Manning friction factor of 0.015 $s/m^{1/3}$. The resulting bed level is compared to that of the reference case in figures J.3 and J.4. It can be seen that stronger bed change effects occur for a larger friction factor. As the same forcing would lead to larger bed shear stresses, more erosion occurs. Consequently, more suspended sediment is transported towards the shore, increasing the amount of sedimen-

tation. As both the amounts of erosion and sedimentation increase, bed gradients become larger. The locations of sedimentation and erosion are largely unaffected.
The critical shear stress for erosion is a threshold value beyond which the bed starts to erode. The influence of the critical shear stress is researched by performing simulations with critical shear stress values of 0.25 Pa and 0.50 Pa. The corresponding cumulative erosion and sedimentation are shown in figures J.5 and J.6 respectively. It can be seen that about two times as much erosion and sedimentation occur for the case with lower critical shear stress. Additionally, erosion and sedimentation occur in larger areas.
The erosion parameter determines how much erosion occurs once the critical shear stress has been reached. For values of M twice as large, the amount of erosion and sedimentation would also be about doubled. The spatial patterns would remain unaffected.

Chapter 7

Discussion

This chapter discusses the results of the model simulations. First, the general system understanding is reconsidered in section 7.1. In section 7.2 the results of the model simulations are discussed for each test case. Finally, section 7.3 contains the most important findings from the sensitivity analysis.

7.1 General system understanding

As the flow pattern is hardly affected when waves are included in the simulation, the flow pattern is mainly dominated by the tide, which corresponds to expectations. This is because the waves are so small that wave-induced currents are an order of magnitude smaller than tidal currents. Both the TOPEX/Poseidon and Indian Ocean tidal model boundaries resulted in the same flow pattern entering the domain in the southwest and flowing out through the northeast boundary. In order to double-check this flow pattern, a very simple tidal model was set up of a larger area (from Cirebon to Rembang). This resulted in the same flow direction in front of the coast near Semarang. Closer to the coast, currents are mainly directed from northeast to southwest. To give an overview of all hydrodynamic forcings, figure 7.1 shows a schematisation of the area.

The sediment transport and bed change patterns found in the model simulations correspond to findings by Winterwerp *et al.* (2005), as explained in section 2.2.3. Waves dominate erosion of the sea bed, by enhancing bed shear stresses inside the breaker zone. Thus, fine sediments are stirred up from the bed. After waves have mobilised sediments, the sediments are transported in suspension. This local erosion of the foreshore is a more important source of sediment than inflow of suspended sediment from offshore. The availability of sediment for suspended transport is thus dominated by waves. Therefore, in order to get deposition behind the dams, the system is dependent on locally eroded sediment.
During the northwest monsoon period, the waves are largest and sediments are mobilised. During the southeast monsoon, on the other hand, hardly any large waves reach the coast,

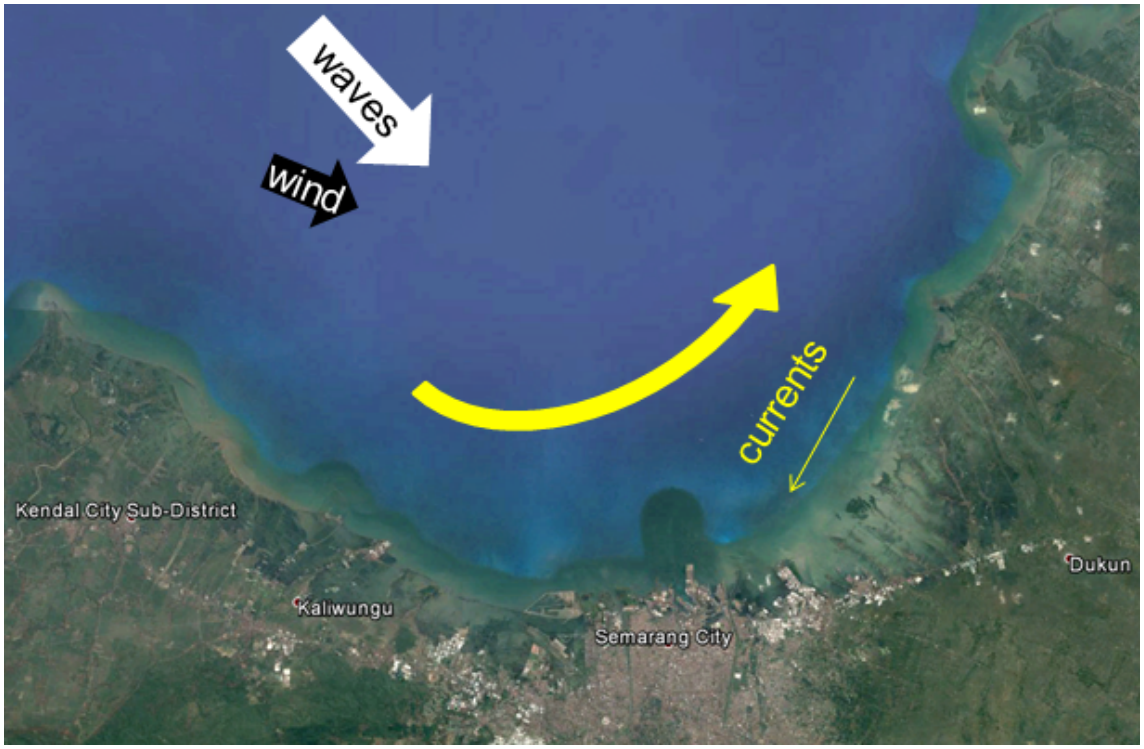

Figure 7.1: Overview of all hydrodynamic forcings

so little sediment is available. Therefore, the most sediment can potentially be captured during the months December, January and February.
It is expected that about half the sediment that is eroded from the coast remains in the area between the shore and the cheniers. The rest of the sediments are permanently lost to locations further offshore and cannot be captured by the dams. Therefore, it will not be possible to fully restore the coastline to it's initial position.

7.2 Test cases

In this section the results of the test cases from section 6.2 are discussed in corresponding subsections. But first some general remarks are made regarding the model.
It was decided to work with the new Delft3D Flexible Mesh software, because this offered much better computation times for the purpose of this project. Instead of having to use a very high resolution in the entire flow domain or having to apply a nesting approach, the D-Flow Flexible Mesh engine offered the possibility to locally increase the resolution. On the other hand, the use of Delft3D Flexible Mesh for the purpose of this study was a limiting factor, as the sediment and morphology module was still under development during the course of this thesis, as explained in section 5.3. Moreover, some additional features are still under development that may improve the results.
The model is 2DH (depth-averaged), neglecting any 3D effects. Therefore secondary circu-

lations, such as the undertow that may keep sediments close to shore during the northwest monsoon, are not included. This may lead to an overestimation of the amount of sediment that is lost to locations offshore, although this effect is expected to be small.
Additionally, the semi-permeable character of the dams was not taken into account in the model, as explained in section 5.2.5. Hence, water and sediment particles cannot pass through the dams in the model, whereas in reality they can. Two potential implications for the model results are that part of the wave energy may be reflected and that the amount of sediment deposited behind the dam may be underestimated. The reflection of wave energy is not an issue, as wave reflection by the dams is switched off in SWAN. This can also be seen from the results, as the wave height does not increase in front of the dams. Regarding the sediment, the amount entering through the gaps between two dams is expected to be much larger than the amount passing through the dam itself. Therefore, it is a reasonable approximation to neglect the small amount of extra sediment passing through the dam.
Finally, the cheniers were not included in the final simulations. As explained in section 5.2.2, the initial bed level was manually adjusted at the location of the cheniers. However, in test runs these cells eroded within a few time steps, creating an extra source of sediment. Using the critical shear stress for erosion, this erosion can potentially be prevented, but unfortunately it is not yet possible to apply a spatially-varying critical shear stress in Delft3D Flexible Mesh. As this behaviour of the cheniers does not seem realistic and would form an extra source of sediment, it was decided to leave the cheniers out of the final simulations. This may lead to an overestimation of the waves that else would break due to the presence of the cheniers. Moreover, some additional sediments may be stirred up at the location of the cheniers, because the local sediment properties are not represented in the model.

7.2.1 No dams (reference)

In the reference case, the largest waves occur during the northwest monsoon period, when the significant wave height is about 0.7 m from the northwest direction. The wave height decreases where the depth starts to influence the wave transformation, due to dissipation and breaking. Hence, the wave height at the location of the dams is much smaller. The bed shear stresses are mainly affected by waves, as the time-averaged bed shear stress is very small in the majority of the domain. Nearshore the largest bed shear stresses are found, due to wave breaking. However, even in this breaker zone the bed shear stresses are quite small (about 1 Pa), as the bottom profile is very gentle and smooth.

In the model simulations, hardly any bed changes were found in the majority of the domain. Patterns of sedimentation and erosion only occurred close to the coast, where waves break. Between the coastline and the location of the cheniers quite some deposition was found, even without including any dams. This could not be confirmed as no exact data is available on the bed change in that location. It should be noted that the simulation does not lead to an equilibrium profile. Nevertheless, the outcomes of simulations with dams

can be compared to this reference case to assess the influence of the dams.
The mud concentration is also large nearshore as sediments are stirred up by waves and transported in suspension, mainly by tidal currents. If erosion occurs during flood, sediments will be transported towards shore. If instead erosion occurs during ebb, sediments will be transported offshore from the breaking zone. Once in suspension sediments start to settle and are eventually deposited again on the bed. As the sedimentation areas are located close to the erosion areas and suspended sediment is concentrated in the same locations, it is likely that the deposited sediments originated from locally eroded bed.

The model can be used to perform computations to check the sediment balance and to analyse dominant sediment sources and sinks. For the reference case, such computations resulted in 0.3 Mton sediment that was missing in the entire domain. This sediment was presumably lost by flow of suspended sediment out of the domain. The extra 21 kton sediment that was found in the smallest grid cells may have originated from other eroding cells in the domain. However, this does not correspond to the expectation of a nett sediment loss from the area between the shore and the cheniers. It should be noted, though, that the smallest grid cells contain that area, as well as some cells that are located offshore of the cheniers, due to the unstructured character of the grid. Moreover, coastal erosion of land cells is not taken into account by the model.

7.2.2 Ecoshape dams

By comparing the resulting significant wave height and bed shear stresses to those of the reference case in figures 6.4 and 6.6 respectively, it can be concluded that the dams successfully attenuate waves. Consequently, the local bed shear stresses are lower and sediment is deposited behind the dams. The rate of sedimentation depends mostly on the availability of sediment and on the water depth. It is hypothesised that the deposited sediment originates from the local foreshore, where erosion was found, but this cannot be confirmed.
Only one observation could be used to check the rate of sedimentation behind the dams. Behind the first dams that were constructed to close off the cell near Bogorame about 50 cm of sediment was deposited after one monsoon period. That is significantly more than the 10-12 cm that was found in the model results. Nevertheless, it was decided not to change the model calibration merely based on one measurement.
Even though the permeability of the dams could not be modelled, no wave reflection occurred and no scour was found in front of the dams. The scour that was found alongside the dams and in the gaps is a known problem that can be prevented by constructing small perpendicular dams of about 4-5 m in length on the edges of the dams, as explained in section 4.2.3.

7.2.3 MMAF dams

In the simulation with Ecoshape and MMAF dams, sediment is captured behind more dams, which leads to a total increase in sedimentation. However, less sediment is captured by the Ecoshape dams. The MMAF dams, located in front of the Ecoshape dams, thus hamper the sedimentation behind the further backward located Ecoshape dams. In some locations upto 10 cm extra deposition would be achieved if no MMAF dams are put in front of the Ecoshape dams.

7.2.4 Side dams

In both simulations performed to test the effect of side dams, the deposition behind the dam was smaller when a side dam was applied. This corresponds to the hypothesis that side dams block part of sediment inflow. It should be noted, however, that this conclusion only holds for very specific areas with small variation in incoming wave direction and where longshore currents are small, typical for mangrove-mud coasts. In the Netherlands, for example, side dams are necessary to decrease longshore currents in order to capture sediment.

7.2.5 Dam spacing

In the simulations with only one new dam located at either 100 m or 150 m from the coast, the most deposition is always found right behind the dam. It was hypothesised that waves could be regenerated further behind the dam, leading to resuspension of sediment. However, on the contrary, more sediment deposited close to the coast for the simulation with a dam at 150 m from the coast than with a dam at 100 m from the coast. Apparently, a dam spacing of 150 is sufficiently small not to regenerate waves and still capture sediments. The most important effect of a larger dam spacing seems to be the spreading of sediment over a larger area.

7.2.6 Interaction between multiple dams

Section 7.2.3 already describes the effect of 'backward hampering': if two dams are placed in front of each other at the same time, the dam in front may hamper the deposition of the dam that is located behind. This hypothesis is confirmed by removing the MMAF dams that are located farthest offshore. More sediment is then captured by the dams behind.
The alternative to add a new dam besides already existing dams also influences the sedimentation behind the original dams. Again, less sediment is captured by dams adjacent to the new dam. This effect is called 'sideways hampering'. If the new dam is located somewhat behind the existing dam, less sideways hampering occurs, but the new dam itself will capture less sediment.
A potential way to capture more sediment would be constructing dams close to the shore

first and place the farther seaward located dams at a later stage. The most important consideration for this 'construction phasing' is the rate of sedimentation behind the dams, which should be large enough to establish an area above mean sea level, but small enough not to smother the mangrove seedlings. Another consideration would be the design lifetime of the dams, which is around five to seven years, as explained in section 4.1.

7.2.7 Meteorological scenarios

The model was unable to fully refract waves coming in from the East. Instead, the southeast monsoon was simulated with waves coming from the North. This leads to some erosion and sedimentation near the dams. However, it is unclear from what direction the waves are coming in reality. The actual bed changes during the southeast monsoon are expected to be small. During a storm, on the other hand, severe erosion occurs. This instantly causes a small increase in the sedimentation rate behind the dams. Moreover, it brings sediments in suspension, which could lead to additional deposition behind the dams at a later stage.

7.3 Sensitivity analysis

The results of the simulations described in section 6.3 lead to conclusions on the sensitivity of the model to these parameters.
When a different offshore wave height is used the sedimentation and erosion patterns are quite different. As explained in section 2.2.3, waves cause erosion of sediment. Whereas small waves only erode the coast, large waves 'give and take' as they erode the foreshore, after which the sediments are brought to shore by tidal currents. Therefore waves are the dominating forcing that determine the sediment balance. Small changes in the offshore wave height or wave transformation would therefore have a significant effect on the model results. The influence of wind speed and incoming sediment concentration on the model outcomes are negligible.
The model results are not very sensitive to the viscosity and diffusivity. An important calibration parameter is the bottom roughness, which largely determines flow velocities and amounts of erosion and sedimentation in the simulations, although it does not affect the locations of erosion and sedimentation. For lower critical shear stress values erosion occurs more often, but also in more cells, as this critical shear stress value is exceeded more often. Thus, for a lower critical shear stress erosion would occur at more locations and the amount of erosion would also increase. The sensitivity of the model results to the erosion parameter is almost linear: if the erosion parameter is increased by a certain factor, the amount of erosion and sedimentation respond with about the same factor. Patterns remain the same.

Chapter 8

Conclusions & recommendations

This chapter contains the final conclusions and recommendations of this study. Section 8.1 describes the conclusions and answers the research questions that were formulated in section 1.3. Recommendations for further research are given in section 8.2.

8.1 Conclusions

This study aims to optimise the design of semi-permeable dams to capture sediment in order to encourage mangrove re-establishment in Demak coastal zone. First, in order to get a better understanding of the large-scale morphodynamics of the area, a system analysis was performed. It was concluded that waves dominate erosion of the seabed and thereby the availability of sediment. Both erosion and sedimentation are largest during the months December, January and February, in which the area is subject to the northwest monsoon and the wave height is largest. During the rest of the year, the erosion and sedimentation are much smaller, mainly because the waves are coming from the West.
After waves have stirred up sediment on the foreshore, currents transport sediments towards shore. Wave-induced currents are much smaller than tidal currents, which dominate the flow pattern and thereby the transport of suspended sediment.
The effect of sediment inflow from the boundary on the sediment transport and morphologic development of the coastline is negligible, as the amount of sediment that enters the domain in suspension is much less than the amount of sediment that is locally eroded. Therefore, in order to capture sediment, the system is dependent on locally eroded sediment.

In order to simulate the morphodynamic development of the coast a site-specific model was set up in the new Delft3D Flexible Mesh software, including flow, waves and sediment transport. It should be noted that the sediment module of Delft3D Flexible Mesh was still under development during the course of this thesis. My contribution to this development consisted of testing the behaviour of cohesive sediment transport and morphological updating of the bed level for Delft3D Flexible Mesh. After improvements the software can

now be used for this purpose.
As Demak coastal zone is a data poor environment, the model validation was largely based on qualitative observations and expert judgement. Nevertheless, the outcomes could be used for the purpose of this study. The model helped to determine the tidal flow pattern, which could not be determined based on literature. Incoming waves dissipate and break on the gentle coastal slope, causing large bed shear stresses and thereby erosion of the foreshore. After waves have mobilised sediments, the sediments are transported in suspension, corresponding to expectations based on literature and knowledge on the local system. Using the model outcomes, the sediment balance was checked. It was concluded that part of the sediment was lost from the domain by suspended transport. As the model simulations did not give a morphodynamic equilibrium, the results were used for comparison analyses rather than to forecast exact deposition rates.
The model outcomes were shown to be barely sensitive to a variation of the forcing by wind and to the inflow of sediment, nor to the calibration parameters viscosity and diffusivity. The most important external forcing is the offshore wave height, which confirms that waves dominate the availability of sediment in Demak coastal zone. Calibration parameters that have a considerable influence on the outcomes are the Manning friction factor, critical shear stress for erosion and erosion parameter. These can be used for further improvement of the model, if more data would become available.

Next, the design of semi-permeable dams was optimised in order to capture sediment. Important design aspects were studied for different meteorological scenarios to formulate more generic guidelines for the design of such structures. Even though the permeability of the dams could not be taken into account, the influence of these dams was successfully simulated, i.e. behind the dams waves were attenuated, leading to a decrease in bed shear stresses and, consequently, to deposition of sediment behind the dams.
It was concluded that side dams have a negative influence on the amount of sediment that is captured behind the coast-parallel dam, presumably due to smaller inflow of sediment. Therefore the use of dams to close off cells, as was done in the first pilot project, is not advisable for comparable mangrove-mud coasts. As no regeneration of waves occurred for dam spacings of 100 to 150 m based on the model results, the most important effect of increasing the dam spacing is the spreading of sediment over a larger area. This conclusion depends largely on the local physical environment and does not necessarily hold for all mangrove-mud coasts.
Moreover, it was concluded that new dams influence the deposition behind surrounding dams. Dams constructed in front of or next to other dams hamper the deposition of dams that are located farther backward or sidewards. Therefore, it is advised to apply construction phasing for the planning of new dams in Demak or other mangrove-mud coasts.

To conclude, this study has helped to gain insights in the hydrodynamics and sediment transport in Demak coastal zone. It was concluded that waves are the most important physical factor that influences the availability of sediment. Local erosion of the foreshore was found to be the main source of sediment. Deposition patterns were simulated behind

the pilot dam that has been constructed in the field. Moreover, several design aspects were considered for the optimisation of semi-permeable dams to capture sediment on the Demak coast. The findings from this study may be useful for eroding mangrove-mud coasts elsewhere, but as the results mainly depend on site-specific conditions a thorough understanding of the local physical environment remains indispensable.

8.2 Recommendations

There are several recommendations for further research. First general recommendations about the study are given, including research questions that are interesting to follow up on. Next, recommendations are given to improve the site-specific model that is used to study semi-permeable dams for mangrove rehabilitation.

The results of this study can be used to improve the design of new dam configurations. Moreover, it is recommended to use the model to test these new dam configurations before construction. Additionally, other dam design aspects can be considered than those studied here. The model can be used to analyse the dam orientation and gap width. In this study the dams were all modeled at the same angle perpendicularly to the incoming wave angle and with the same gap width. Using the fact that the computational grid is unstructured, the optimal dam orientation and gap width could be researched. Another aspect that can potentially be studied is the sedimentation pattern behind the dams. Lastly, the formation of meandering creeks could be stimulated by making staggered dam configurations.
The conclusions with respect to the dam optimisation are strongly linked to site-specific physical factors. For the application of semi-permeable dams on mangrove-mud coasts elsewhere, the conclusions from this study should be interpreted carefully in the context of the local physical environment, such as the source of sediment on which the system depends. For example the optimal dam configuration could be quite different, if such a site depends on riverine sediment, instead of locally eroded sediment from the foreshore. In order to draw more general conclusions, semi-permeable dams should be carefully monitored and studied on multiple mangrove-mud coasts.
It should be noted that this study only considered physical phenomena that influence sediment transport in the Demak coastal zone, hence the final conclusions only include abiotic factors. Based on ecological research, these conditions should be favourable for mangrove regrowth. Furthermore, the focus of this study was on the interaction between multiple dams on sediment transport and sedimentation patterns. Findings should be combined with research on individual dam design.

The site-specific model that was used for this study can be further improved. First of all, it could not yet fully be validated, due to lack of data. It is recommended to carefully monitor the pilot study and to deploy a tidal gauge for comparison to the model results. Moreover, more detailed sediment and bathymetry data could improve the model input. It is therefore recommended to do measurements of sediment properties (such as the siltation rate, suspended sediment concentration, settling velocity and dry bed density) and to do

more accurate depth measurements.
Secondly, expected developments of the Delft3D Flexible Mesh software may create new possibilities to improve the site-specific model. For example, the semi-permeable dams were included in the model as 'thin dams', which have an infinite height and are impermeable. In former Delft3D models 'porous plates' could be used with a user-defined height and porosity. For Delft3D Flexible Mesh, this porous plates application is still under development. Additionally, the effects of consolidation were not included in the model, thus ignoring the compaction and increased strength of the soil behind the dams. In order to include the effects of consolidation into the model, a consolidation model could be implemented. For Delft3D Flexible Mesh, such a consolidation module is also under development. It is recommended to implement the porous plates application and consolidation module into the current model at a later stage.
The use of SWAN to compute the wave transformation may be questionable, as SWAN gives a poor approximation of the redistribution of wave energy through triad wave-wave interactions on mud flats. In the current model the triad wave-wave interactions were neglected entirely. It would be interesting to compare the outcomes of SWAN to those of another wave model. Potentially, a future application of X-Beach as wave module for Delft3D Flexible Mesh may be used.
Finally, in the current model no land cells were included in order to simplify the model area. In reality, intertidal areas behind the coastline are flooded during the tidal cycle, thereby increasing the tidal prism. Moreover, rivers may bring in terrestial sediments forming a potential source of sediment. By applying an inundation model, these intertidal areas and rivers could be included in the simulations.

Bibliography

Anthony, E., & Gratiot, N. (2012). Coastal engineering and large-scale mangrove destruction in Guyana, South America: averting an environmental catastrophe in the making. *Ecological Engineering*, *47*, 268–273.

Arentz, L., & Van Wesenbeeck, B. (2013). Design for test with permeable dams near Timbul Sloko (Indonesia). Memo.

Ariathurai, C., & Arulanandan, K. (1978). Erosion rates of cohesive soils. *ASCE, Journal of the Hydraulics Division*, *104(2)*, 279–282.

Balke, T., Bouma, T. J., Horstman, E. M., Webb, E. L., Erftemeijer, P. L., & Herman, P. M. (2011). Windows of opportunity: thresholds to mangrove seedling establishment on tidal flats. *Marine Ecology Progress Series*, *440*, 1–9.

Bao, T. (2011). Effect of mangrove forest structures on wave attenuation in coastal vietnam. *Oceanologia*, *53*, 807–818.

Bappenas, & KOICA (2012). Coastal protection and management policy adressing climate change impact in Indonesia. Tech. rep.

Batchelor, G. (1960). *The theory of homogeneous turbulence*, vol. 4. Cambridge University Pressl.

Battjes, J. (1974). Surf similarity. In *The 14th International Conference on Coastal Engineering*, vol. 1, (pp. 466–480).

Bayong Tjasyono, H., Gernowo, R., Sri Woro, B., & Ina, J. (2008). The character of rainfall in the Indonesian monsoon. Presented at the International Symposium on Equatorial Monsoon System, Yogyakarta, Indonesia.

Bosboom, J., & Stive, M. (2013). *Coastal Dynamics I: lecture notes CIE4305*. Delft Academic Press, 0.4 ed.

Bradshaw, A. (1987). *Restoration ecology: A synthetic approach to ecological research. The reclamation of derelict land and the ecology of ecosystems*. Cambridge University Press.

Cahoon, D., Hensel, P., Spencer, T., Reed, D., McKee, K., & Saintilan, N. (2006). Coastal wetland vulnerability to relative sea-level rise: wetland elevation trends and process controls. *Wetlands and Natural Resource Management*, *190*, 271 – 292.

Cahoon, D., & Lynch, J. (1997). Vertical accretion and shallow subsidence in a mangrove forest of southwestern florida. *U.S.A. Mangroves and Salt Marshes*, *1*, 173–186.

Dankers, P., & Winterwerp, J. (2007). Hindered settling of mud flocs: theory and validation. *Continental shelf research*, *27(14)*, 1893–1907.

Deltares (2015). D-Flow Flexible Mesh user manual. Tech. Rep. 1.1.148, Deltares.

Ecoshape (2015). Building with nature Indonesia (securing eroding delta coastlines): Design and engineering plan. Tech. rep., Ecoshape.

Ellison, A. (2000). Mangrove restoration: Do we know enough? *Restoration Ecology*, *8(3)*, 219–229.

Fleming, C. (1990). Groynes in coastal engineering: data on performance of existing groyne systems. Tech. rep., CIRIA. Technical Note (No. 135).

Hatayama, T., Awaji, T., & Akitomo, K. (1996). Tidal currents in the Indonesian Seas and their effect on transport and mixing. *Journal of Geophysical Research: Oceans*, *101(C5)*, 12353–12373.

Hinze, J. (1975). *Turbulence*. McGraw-Hill, 2nd ed.

Holthuijsen, L. (2007). *Waves in oceanic and coastal waters*. Cambridge University Press.

Hutchison, J., Spalding, M., & zu Ermgassen, P. (2014). The role of mangroves in fisheries enhancement. Tech. rep., The Nature Conservancy and Wetlands International.

Ippen, A. (1966). *Estuary and coastline hydrodynamics*. McGraw-Hill.

Kandiah, A. (1974). *Fundamental aspects of surface erosion of cohesive soils*. Ph.D. thesis, University of California.

Lewis III, R. (2005). Ecological engineering for successful management and restoration of mangrove forests. *Ecological Engineering*, *24*, 403–418.

Lewis III, R. (2009). *Methods and criteria for successful mangrove forest restoration*. Elsevier.

Lighthill, J. (1978). *Waves in fluids*. Cambridge University Press.

Longuet-Higgins, M. (1953). Mass transport in water waves. *Phil. Trans. R. Soc. Lon. A.*, *245*, 535–581.

Longuet-Higgins, M., & Stewart, R. (1962). Radiation stress and mass transport in gravity waves, with applications to 'surf beats'. *J. Fluid Mech.*, *13*, 481–504.

Losada, I., Dalrymple, R., & Losada, M. (1998). Wave-induced mean flows in verticle rubble mound structures. *Coastal Engineering*, *35*, 251–281.

Lubis, A. M., Sato, T., Tomiyama, N., Isezaki, N., & Yamanokuchi, T. (2011). Ground subsidence in Semarang (Indonesia) investigated by ALOS–PALSAR satellite SAR interferometry. *Journal of Asian Earth Sciences*, *40(5)*, 1079–1088.

Mai, S., Von Lieberman, N., & Zimmermann, C. (1999). Interaction of foreland structures with waves. In *Proceedings of the XXVIII IAHR congress*.

Major, J. J. (2003). *Sedimentology*, chap. Hindered settling, (pp. 578–582). Dordrecht: Springer Netherlands.
URL `http://dx.doi.org/10.1007/978-1-4020-3609-5_110`

Mangor, K. (2004). Shoreline management guidelines. Tech. rep., DHI.

Marfai, M., & King, L. (2007). Monitoring land subsidence in Semarang, Indonesia. *Environmental Geology*, *53*, 651–659.

Mazda, Y., Wolanski, E., King, B., Sase, A., Ohtsuka, D., & Magi, M. (1997). Drag force due to vegetation in mangrove swamps. *Mangroves and Salt Marshes*, *1*, 193–199.

McIvor, A., Möller, I., Spencer, T., & Spalding, M. (2012). Reduction of wind and swell waves by mangroves. natural coastal protection series: Report 1. Tech. rep., The Nature Conservancy and Wetlands International.

McIvor, A., Spencer, T., Möller, I., & Spalding, M. (2013). Response of mangrove soil surface elevation to sea level rise. natural coastal protection series: Report 3. Tech. rep., The Nature Conservancy and Wetlands International.

McKee, K., & Faulkner, P. (2000). Restoration of biogeochemical function in mangrove forests. *Restoration Ecology*, *8(3)*, 247–259.

Mehta, A., Hayter, E., Parker, W., Krone, R., & Teeter, A. (1989). Cohesive sediment transport. i: Process description. *Journal of Hydraulic Engineering*, *115(8)*, 1076–1093.

Miche, M. (1944). Mouvements ondulatoires de la mer en profondeur constante ou decroissant. *Annales des Ponts et Caussees*, *114*, 25–87.

MMAF (2012). Oceanography condition in coastal of Sayung sub-district, district of Demak (province of Central Java). Tech. rep., LGF team in Demak, Ministry of Marine Affairs and Fisheries, Republic of Indonesia.

Naohiro, M., Putth, S., & Keiyo, M. (2012). Mangrove rehabilitation on highly eroded coastal shorelines at Samut Sakhon, Thailand. *International Journal of Ecology*.

Nieuwstadt, F. (1992). *Turbulentie: inleiding in de theorie en toepassingen van tubulente stromingen*, vol. 24. Epsilon Uitgaven.

Partheniades, E. (1965). Erosion and deposition of cohesive soils. *Journal of the Hydraulics Division*, *ASCE 91 (HY 1)*, 105–139.

Penney, W. G., & Price, A. (1952). The diffraction theory of sea waves and the shelter afforded by breakwaters. *Phil. Trans. Roy. Soc. London*, *A, 244)*, 236–253.

Quartel, S., Kroon, A., Augustinus, P., Van Santen, P., & Tri, N. (2007). Wave attenuation in coastal mangroves in the Red River delta, Vietnam. *Journal of Asian Earth Sciences*, *29(4)*, 576–584.

Russel, M., & Michaels, K. (2012). Effectiveness of melaleuca. Tech. rep., GIZ.

Saengsupavanich, C. (2013). Erosion protection options of a muddy coastline in Thailand: stakeholders' shared responsibilities. *Ocean & Coastal Management*, *83*, 81–90.

Sayah, S. (2006). Efficiency of brushwood fences in shore protection against wind-wave induced erosion. Tech. rep., Laboratoire de Constructions Hydrauliques, Ecole Polytechnique Fédérale de Lausanne.

Schmitt, K., Albers, T., Pham, T., & Dinh, S. (2013). Site-specific and integrated adaptation to climate change in the coastal mangrove zone of Soc Trang province, Vietnam. *J. Coast Conserv.*.

Scoffin, T. (1970). The trapping and binding of subtidal carbonate sediments by marine vegetation in Bimini Lagoon, Bahamas. *Journal of Sedimentary Petrology*, *40(1)*, 249–273.

Svendsen, I. (2006). *Introduction to nearshore hydrodynamics*, vol. 24. World Scientific.

SWAN (2000). Swan cycle iii version 40.11 user manual. Tech. rep., Delft University of Technology.

Thornton, E., & Calhoun, R. (1972). Spectral resolution of breakwater reflected waves. *Journal of Waterway, Harbour and Coastal Engineering division*, *98(4)*, 443–446.

Tomlinson, P. (1986). *The botany of mangroves*. Cambridge University Press.

Van Cuong, C., Brown, S., To, H., & Hockings, M. (2015). Using melaleuca fences as soft coastal engineering for mangrove restoration in Kien Giang (Vietnam). *Ecological Engineering*, *81*, 256–265.

Van Kessel, T., J.C., W., Van Prooijen, B., Van Ledden, M., & Borst, W. (2011). Modeling the seasonal dynamics of SPM with a simple algorithm for the buffering of fines in a sandy seabed. *Cont. Shelf Res.*, *31(10)*.

Van Prooijen, B., & Winterwerp, J. (2010). A stochastic formulation for erosion of cohesive sediments. *Journal of Geophysical Research: Oceans*, *115(C1)*.

Van Wesenbeeck, B., Balke, T., Van Eijk, P., Tonneijck, F., Siry, H., Rudianto, M., & Winterwerp, J. (2015). Aquaculture induced erosion of tropical coastlines throws coastal communities back into poverty. *Ocean & Coastal Management*, *116*, 466–469.

Wells, J., & Roberts, H. (1980). Fluid mud dynamics and shoreline stabilization: Louisiana chenier plain. In *Proceedings of the 17th International Conference on Coastal Engineering (Sydney). Part II: Coastal Sediment Problems*, vol. 1, (pp. 1382–1401).

Winterwerp, J., Borst, W., & De Vries, M. (2005). Pilot study on the erosion and rehabilitation of a mangrove mud coast. *Journal of Coastal Research*, *21(2)*, 223–231.

Winterwerp, J., Erftemeijer, P., Suryadiputra, N., Van Eijk, P., & Zhang, L. (2013). Defining eco-morphodynamic requirements for rehabilitating eroding mangrove-mud coasts. *Wetlands*, *33*, 515–526.

Winterwerp, J., & Van Kesteren, W. (2004). *Introduction to the physics of cohesive sediments in the marine environment*. Elsevier, 56 ed.

Winterwerp, J., Van Weesenbeeck, B., Van Dalfsen, J., Tonneijck, F., Astra, A., Verschure, S., & Van Eijk, P. (2014). Sustainable solution massive erosion central java. Tech. rep., Deltares & Wetlands International.

Wood, A., & Fleming, C. (1981). *Coastal hydraulics*. John Wiley, 2nd ed.

Wyrtki, K. (1961). Physical oceanography of the Southeast Asian water, naga report. Tech. rep., Scripps Institute of Oceanography, University of California.

Yusuf, M., & Yanagi, T. (2013). Numerical modelling of tidal dynamics in the Java Sea. *Coastal Marine Science*, *36(1)*, 1–12.

Zhu, D. (2011). Hydrodynamic characteristics of a single-row pile breakwater. *Coastal Engineering*, *58*, 446–451.

List of Figures

List of Tables

Appendices

Appendix A

Form factor categories

Table A.1 shows an overview of form factor categories. Figure A.1 shows examples of tidal curves per category.

Table A.1: The tidal character expressed by the form factor F

Category	Value of F
Semi-diurnal	0-0.25
Mixed, mainly semi-diurnal	0.25-1.5
Mixed, mainly diurnal	1.5-3
Diurnal	>3

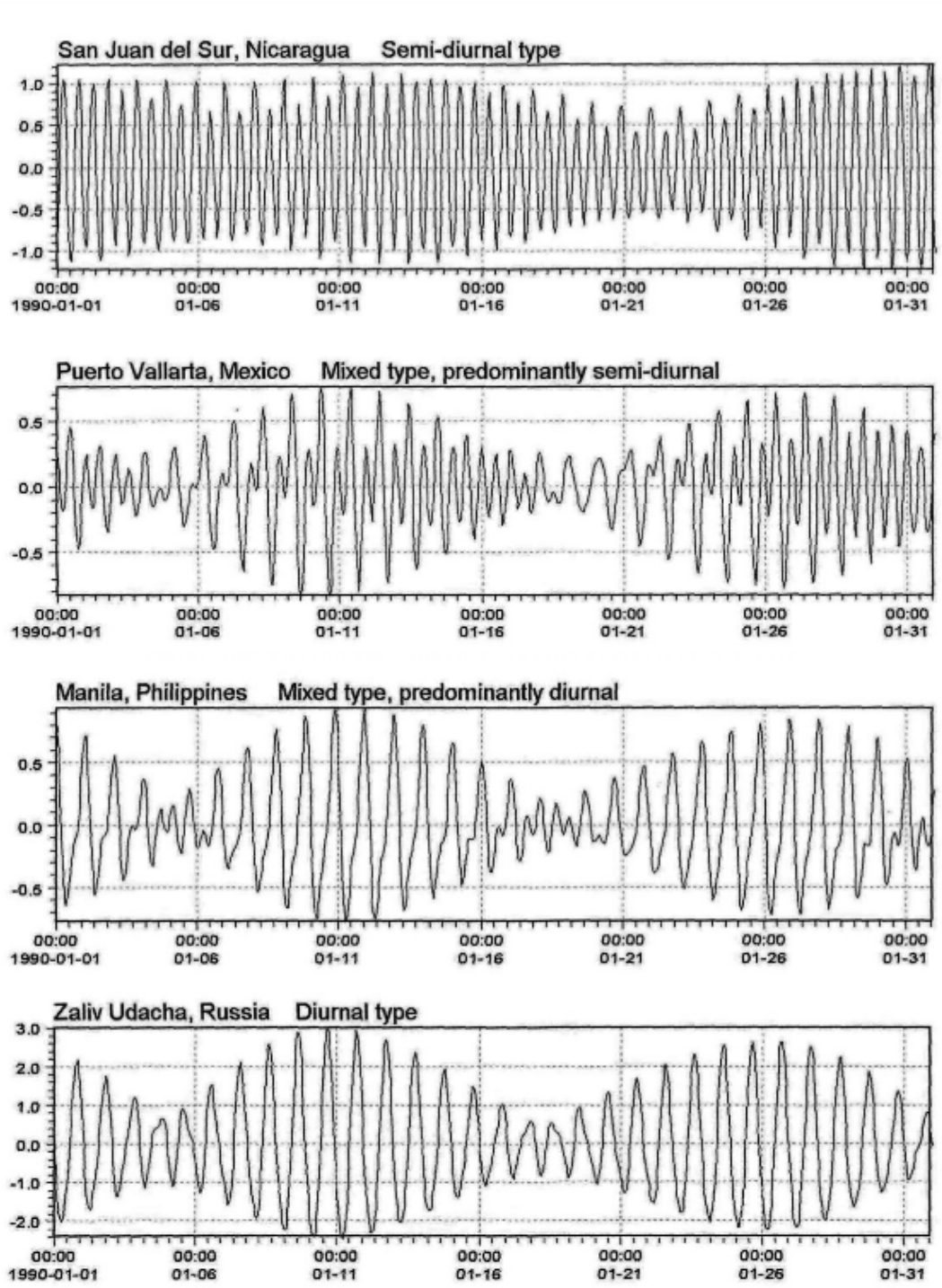

Figure A.1: Examples of tidal curves showing each of the four tidal characters (Mangor, 2004)

Appendix B

Wave breaking

Miche (1944) expressed the limiting wave steepness based on Stokes wave theory (a non-linear expansion of the linear Airy theory that describes steeper waves):

$$\frac{H}{L}_{max} = 0.142 \tanh(kh) \tag{B.1}$$

which in shallow water becomes $\frac{H}{L}_{max} = 0.142\frac{2\pi h}{L} = 0.88\frac{h}{L}$. This implies a breaker index ($\gamma = \frac{H_b}{h_b}$) of 0.88, which is close to the value $\gamma = 0.78$ found using solitary wave theory (a non-linear wave theory valid for shallow water). The maximum wave height H_{max} in a wave record is equal to $2H_s$ using a Rayleigh distribution. Hence, $H_s/h = 0.4 - 0.5$ based on the Miche criterion.

However, the breaker index also depends on the bottom slope. The Iribarren number relates the slope of the bottom (α) to the slope of the waves ($\frac{H_0}{L_0}$) and creates categories for different breaker types (Battjes, 1974):

$$\xi = \frac{tan(\alpha)}{\sqrt{H_0/L_0}} \tag{B.2}$$

A distinction is made between spilling, plunging and surging breakers depending on the value of ξ, see figure B.1. Along flat beaches, as is the case in this report, spilling breakers are usually found ($\xi < 0.5$). According to Bosboom & Stive (2013), a combination of experimental research and theoretical considerations suggest that waves will break at smaller water depths for steeper bottom slopes. For spilling breakers a range of $0.6 - 0.8$ is given for the breaker index.

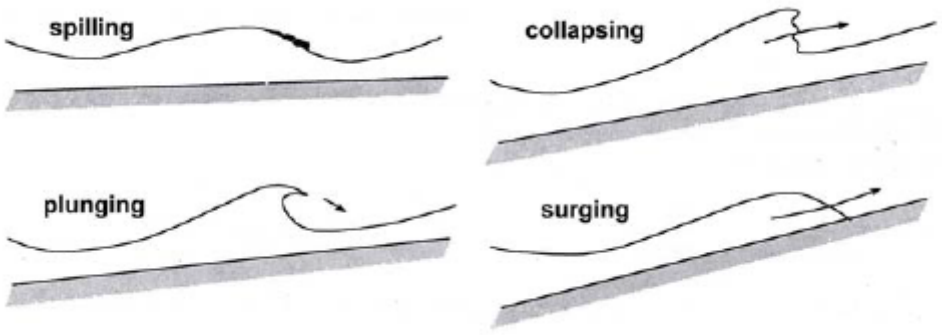

Figure B.1: Types of breakers (Wood & Fleming, 1981)

Appendix C

Wind data

Offshore wind roses and workability

Coordinate: *6.0°S 110.50°E*

Depth: *56m*

Samples: *24836 samples (1997.1.1−2013.12.31)*

Database: *WorldWaves offshore database (February 2015)*

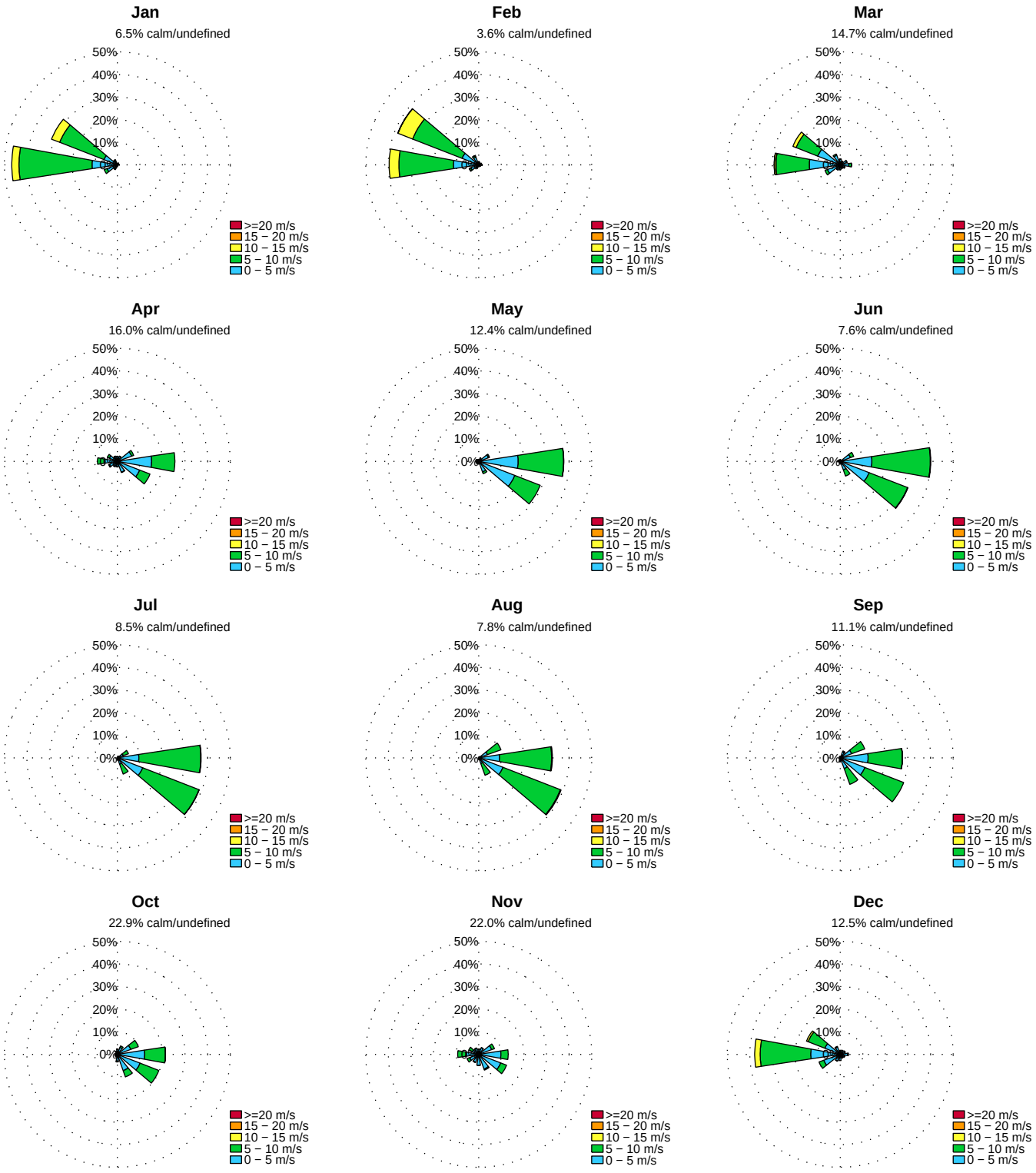

Workability [%]

	Jan	Feb	Mar	Apr.	May	Jun	Jul	Aug	Sep	Oct	Nov	Dec	year
U<1.6m/s (<=Bft.1)	10	9	24	28	20	11	10	9	14	30	35	22	18
U<3.4m/s (<=Bft.2)	20	23	48	55	38	23	17	16	25	49	63	45	35
U<5.5m/s (<=Bft.3)	44	44	74	86	74	60	48	46	62	81	90	67	65
U<8.0m/s (<=Bft.4)	76	70	92	98	98	95	92	93	96	99	99	89	91
U<10.8m/s (<=Bft.5)	96	93	99	100	100	100	100	100	100	100	100	98	99
U<13.9m/s (<=Bft.6)	100	99	100	100	100	100	100	100	100	100	100	100	100
U<17.2m/s (<=Bft.7)	100	100	100	100	100	100	100	100	100	100	100	100	100
U<20.8m/s (<=Bft.8)	100	100	100	100	100	100	100	100	100	100	100	100	100

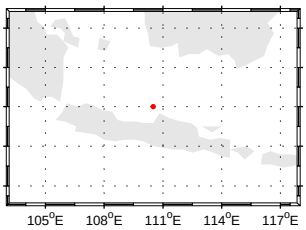

− Input time series: *g:\WERKBAARHEID\Worldwaves\data\offshore_points\2015\wave\world\Dat_files\ww15_offshore_06.0S_110.5E.dat*

− m−file: *G:\matlab\GSAL\Matlab\MetOcean_MATLAB_20150422\Plot_wave_wind_roses\plot_wave_wind_roses_2014_v2.m*

− print date: *29−Apr−2015 18:07:36*

Appendix D

Wave data

hydronamic

Offshore wave roses and workability

Boskalis

Offshore wave roses and workability for total wave height (sea and swell)

Coordinate: *6.0°S 110.50°E*
Depth: *56m*
Samples: *24836 samples (1997.1.1−2013.12.31)*
Database: *WorldWaves offshore database (February 2015)*

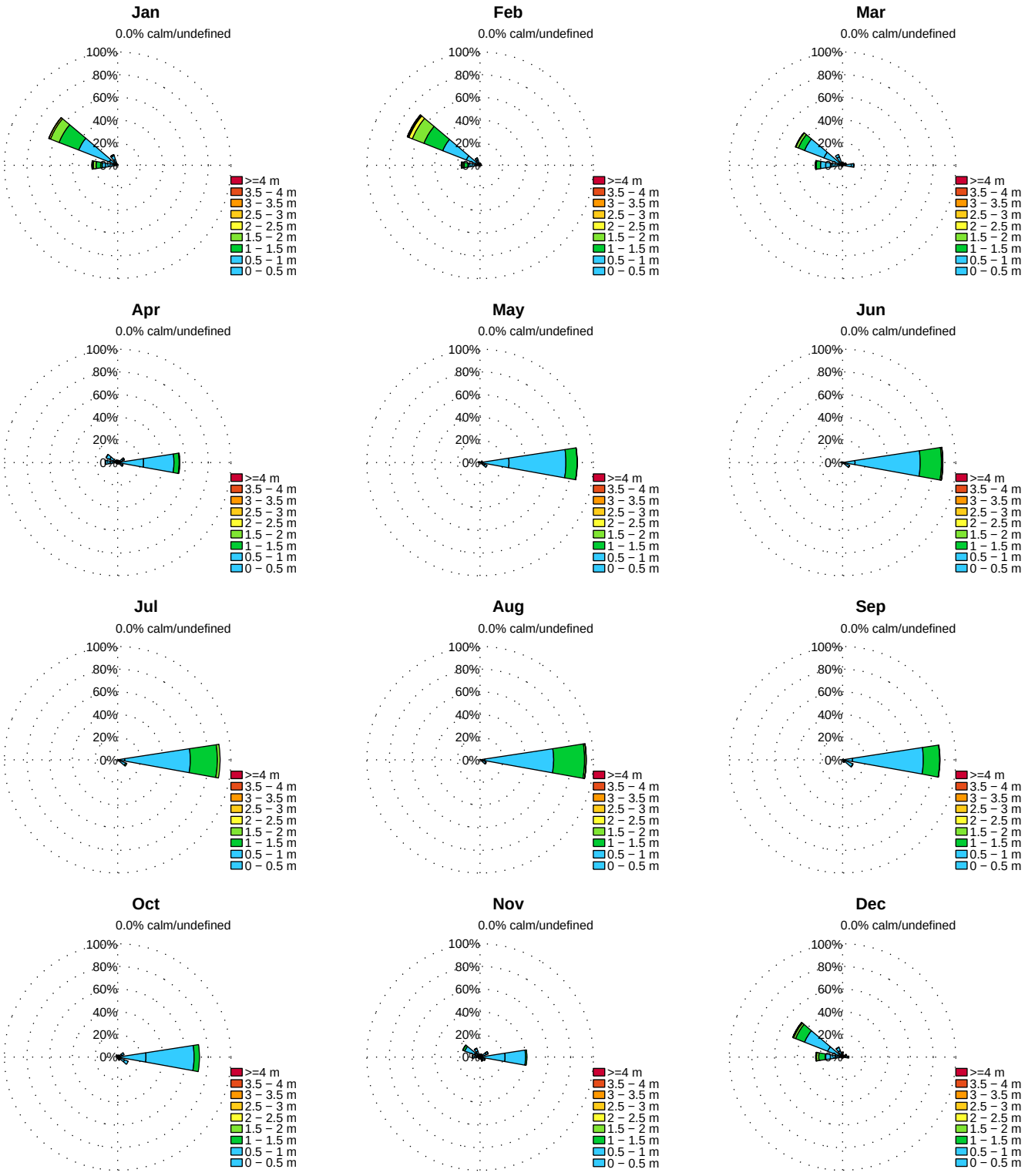

Workability [%]

	Jan	Feb	Mar	Apr.	May	Jun	Jul	Aug	Sep	Oct	Nov	Dec	year
H_s=0.50m	19	29	54	58	38	16	8	5	14	45	62	44	33
H_s=0.75m	41	45	75	84	69	50	37	32	53	80	88	65	60
H_s=1.00m	62	60	87	94	90	80	73	72	85	95	96	80	81
H_s=1.50m	86	82	97	99	100	99	98	99	100	100	100	95	96
H_s=2.00m	97	95	100	100	100	100	100	100	100	100	100	99	99
H_s=2.50m	99	98	100	100	100	100	100	100	100	100	100	100	100
H_s=3.00m	100	99	100	100	100	100	100	100	100	100	100	100	100
H_s=3.50m	100	100	100	100	100	100	100	100	100	100	100	100	100

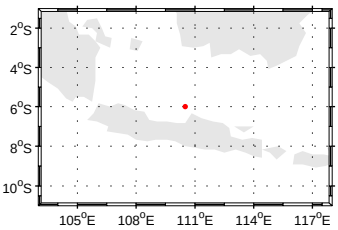

− Input time series: *g:\WERKBAARHEID\Worldwaves\data\offshore_points\2015\wave\world\extracted\Dat_files\ww15_offshore_06.0S_110.5E.dat*
− m−file: *G:\matlab\GSAL\Matlab\MetOcean_MATLAB_20150422\Plot_wave_wind_roses\plot_wave_wind_roses_2014_v2.m*
− print date: *24−Apr−2015 18:54:11*

Appendix E

Analysis wave & wind data

This appendix describes a data analysis of the wind and wave data given in appendices C and D. The dataset that was used for this analysis was obtained from Boskalis. It is not measured data from a wave buoy, but composed out of local data collected from several observation points. The dataset spans from 1997 until 2013 and is representative for location 6.5° South, 110.0° East. A data analysis was performed in order to obtain representative wind and wave conditions for the model.

From the wind data it can clearly be seen that the dataset is bimodal, as two distinct peaks can be observed in the histogram of wind directions (see figure E.1). The peaks correspond to the directions of the monsoon, as explained in section 3.2.1. When separating the dataset based on the northwest monsoon period (December, January and February) and the southeast monsoon period (March until November), the representative wind directions can be determined per period. Figures E.2 and E.3 give the histograms of wind direction probability for the northwest monsoon and the southeast monsoon respectively.
Moreover, storms were identified by selecting the 5% largest wind speed and wave height values for the northwest monsoon period.

Once the data was categorised per monsoon period, representative values to be used in the model were determined for the wind speed, wave height and wave period. It was assumed that the median value is a good representation of these parameters, when it is imposed continuously throughout the monsoon period. Figures E.4 and E.5 give the histograms of wind speed probability for the northwest monsoon and the southeast monsoon respectively. The representative wind speeds are 4.4 m/s for the northwest monsoon period and 3.0 m/s for the southeast monsoon period. The histograms for wave height probability are shown in figures E.6 and E.7. The representative significant wave heights are 0.7 m and 0.4 m respectively. Corresponding wave periods were selected based on the relation between wave height and wave period.
For the storms, the mean value of the parameters was used as representative storm condition throughout two days. The storm wind speed is 11.0 m/s and the significant wave height is 2.1 m.

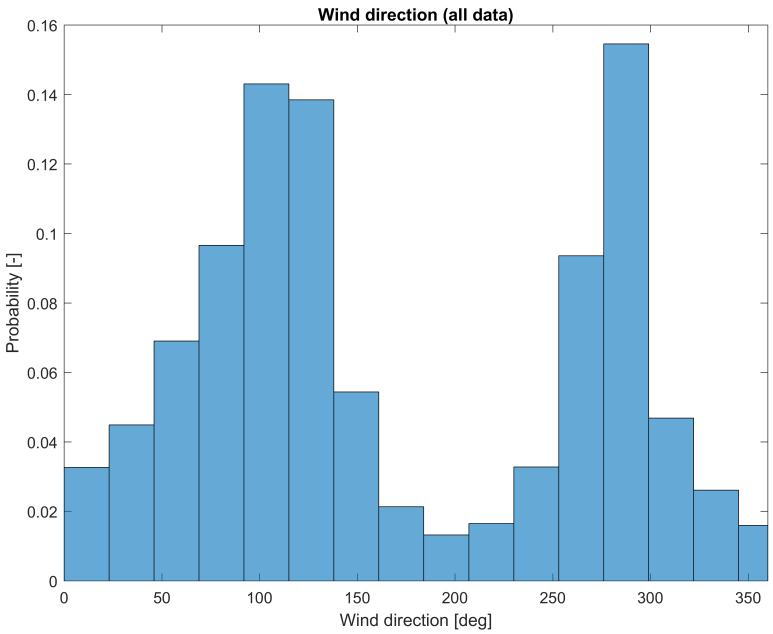

Figure E.1: Histogram of wind direction probability for entire dataset

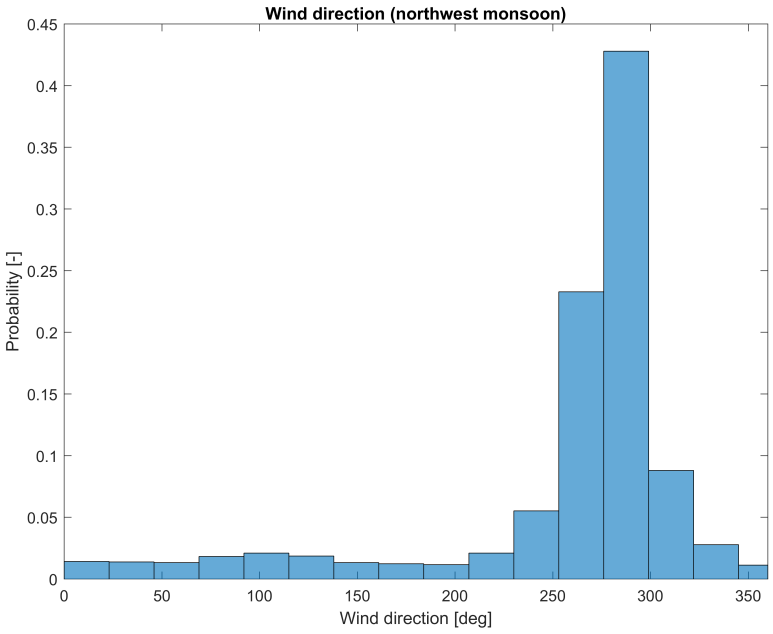

Figure E.2: Histogram of wind direction probability for northwest monsoon period

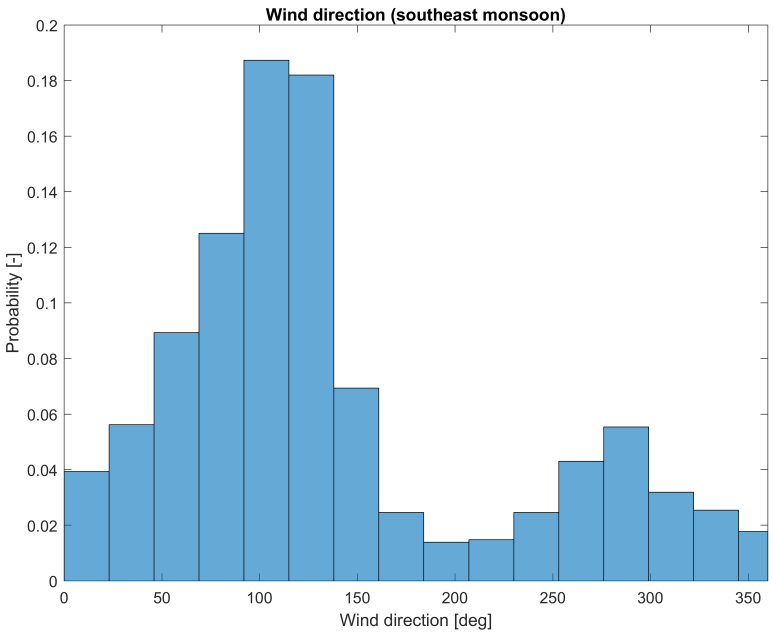

Figure E.3: Histogram of wind direction probability for southeast monsoon period

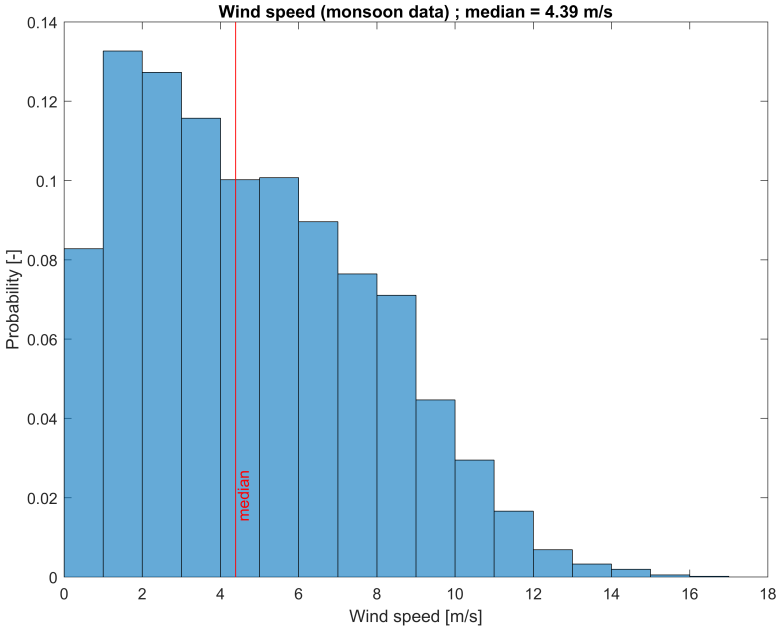

Figure E.4: Histogram of wind speed probability for northwest monsoon period

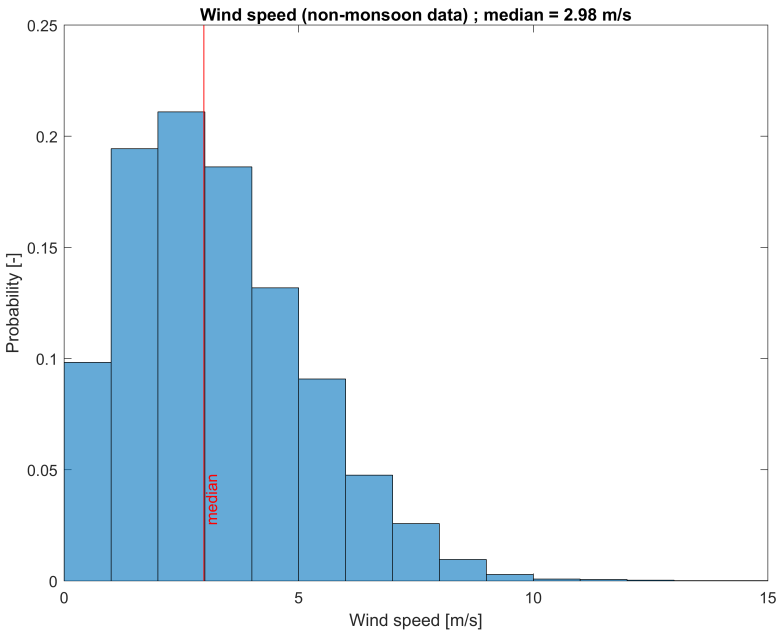

Figure E.5: Histogram of wind speed probability for southeast monsoon period

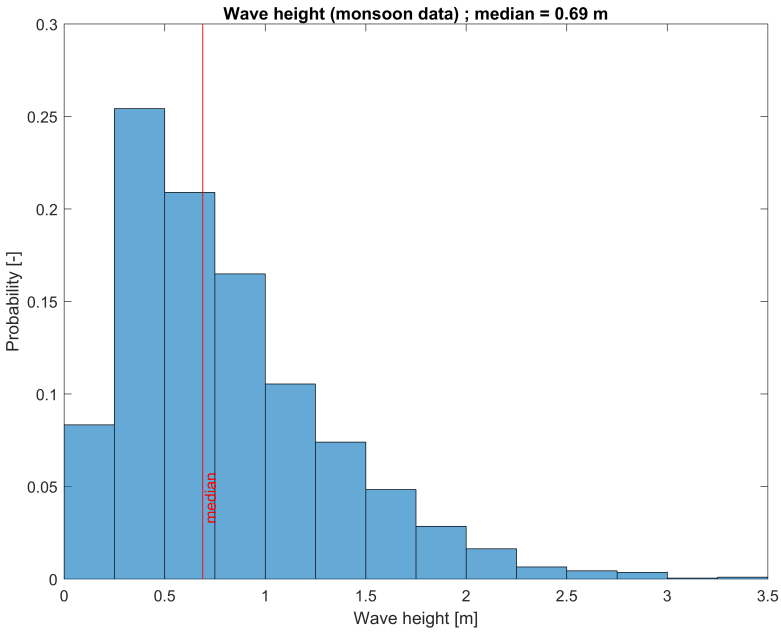

Figure E.6: Histogram of wave height probability for northwest monsoon period

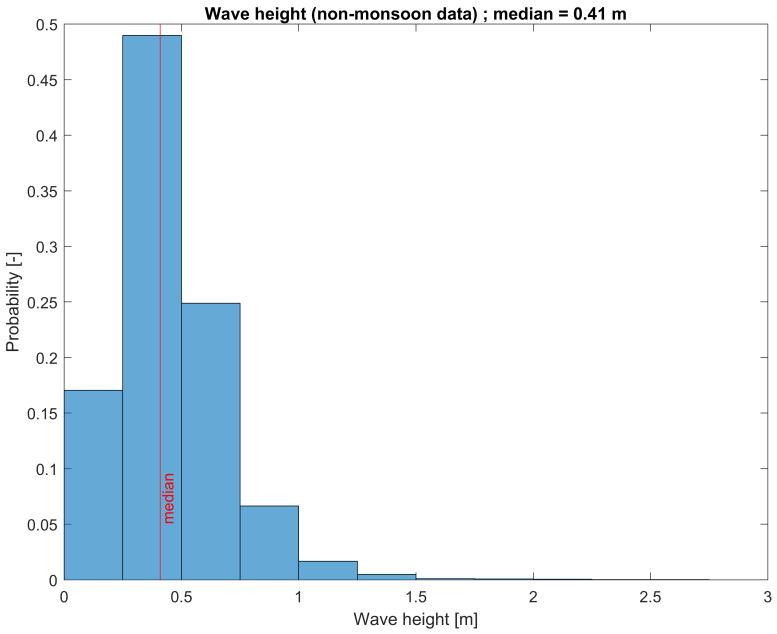

Figure E.7: Histogram of wave height probability for southeast monsoon period

Appendix F

Bathymetry data

In this appendix the bathymetry sets are described. GEBCO data was used for the offshore bathymetry in the model. Some background information about GEBCO is given in section F.1. Moreover, section F.2 describes two sets of bathymetry data that were available from depth measurements.

F.1 GEBCO database

The offshore bathymetry was taken from General Bathymetric Chart of the Oceans (GEBCO), which was founded by an international group of experts. Their work amounts to a range of bathymetric data sets and data products, including gridded bathymetric data sets. The dataset that was used was GEBCO'08, a global bathymetric grid with one arc-minute spacing (about 1 km) that was originally based on the bathymetric contours contained within the Centenary Edition of the GEBCO Digital Atlas, in many regions (particularly shallow water areas and semi-enclosed seas) extended with additional control contours and sounding point data. It is a continuous digital terrain model for ocean and land, with land elevations derived from the Global Land One-km Base Elevation (GLOBE) database. For more information about the development and limitations of the grid, please see the data set documentation hosted on the British Oceanographic Data Centre (BODC) web site.

F.2 Depth measurements

Stefan Verschure performed depth measurements around the cheniers near Timbulsloko and in the area behind them, where the coast has eroded. The locations where Stefan took the depth measurements are indicated in figure F.1. In figure F.2 the location of the depth measurements by Pak Sugeng are indicated with green markers. The locations of the measurements by Stefan Verschure are also indicated for reference.

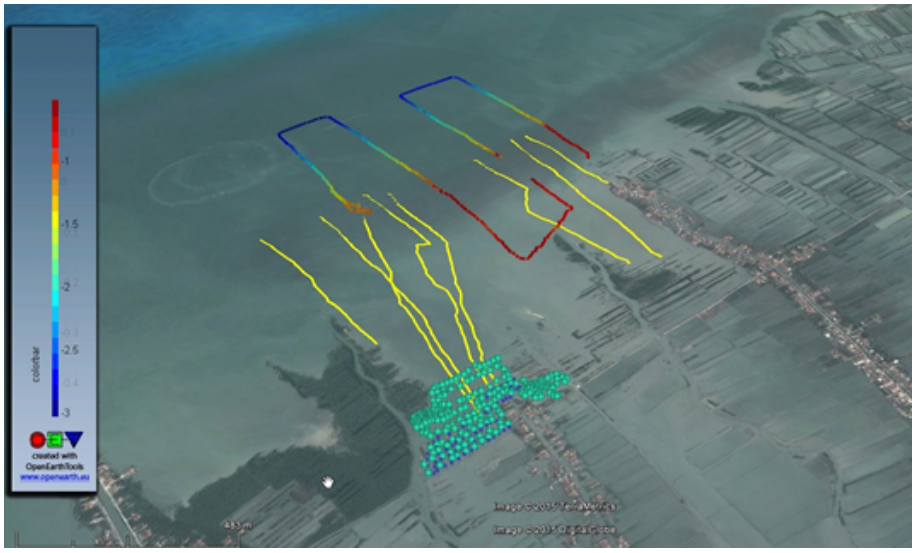

Figure F.1: Locations of depth measurements performed by Stefan Verschure

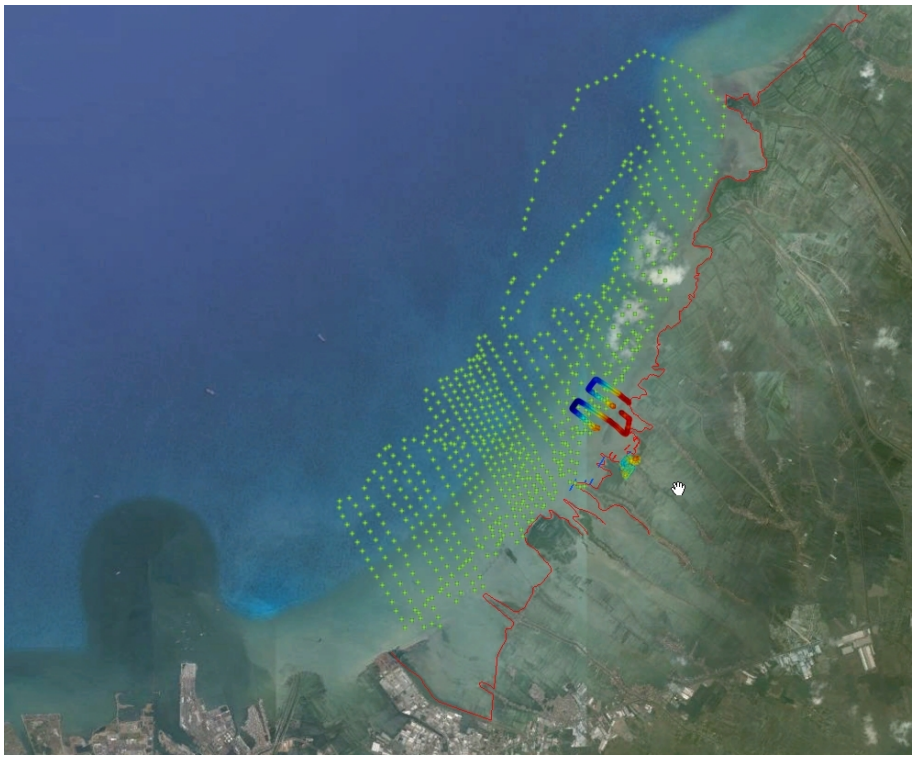

Figure F.2: Locations of depth measurements performed by Pak Sugeng (Google Earth)

As can be seen from the figures, the depth measurements give quite a detailed local bathymetry set. However, in the rest of the modeled area, only GEBCO information was available with relatively low resolution. As the bottom profile has a very gentle slope, depth contours will be mostly parallel. Therefore the local nearshore bathymetry data is assumed to be representative for the entire coastline. Depth samples were manually added to reproduce the parallel depth contours.

Appendix G

Technical model description

In this appendix a technical model description of the Delft3D Flexible Mesh model is given. Section G.1 describes the equations implemented in the flow module. In section G.2 the numerical implementation of the wave formulations is discussed. Finally, the equations used to compute cohesive sediment transport are given in section G.3.

G.1 Flow module

D-Flow FM solves the Navier-Stokes equations for an incompressible fluid under the shallow water assumption (i.e. hydrostatic pressure) and the Boussinesq approximation (i.e. constant density). For relatively long, weakly non-linear waves these are valid assumptions. The Navier-Stokes equations are given by:

$$\frac{\partial u}{\partial t} + u\frac{\partial u}{\partial x} + v\frac{\partial u}{\partial y} + w\frac{\partial u}{\partial z} = -\frac{1}{\rho_0}\frac{\partial p}{\partial x} + \nu\Delta u - f_x \tag{G.1}$$

$$\frac{\partial v}{\partial t} + u\frac{\partial v}{\partial x} + v\frac{\partial v}{\partial y} + w\frac{\partial v}{\partial z} = -\frac{1}{\rho_0}\frac{\partial p}{\partial y} + \nu\Delta v - f_y \tag{G.2}$$

$$\frac{\partial w}{\partial t} + u\frac{\partial w}{\partial x} + v\frac{\partial w}{\partial y} + w\frac{\partial w}{\partial z} = -\frac{1}{\rho_0}\frac{\partial p}{\partial z} + \nu\Delta w - f_z - \frac{\rho}{\rho_0}g \tag{G.3}$$

where u, v and w denote the velocity components in x-, y- and z-direction respectively, ρ the density, ρ_0 the initial density, p the pressure, ν the kinematic viscosity and f_x, f_y and f_z represent the components of the Coriolis force. The equations can be recognised by the momentum balance equations on the left hand side and the forcing on the right hand side. These can be derived based on conservation of momentum under the assumption of an incompressible fluid.
Similarly, the continuity equation can be derived under the assumption of mass conservation:

$$\frac{\partial u}{\partial x} + \frac{\partial v}{\partial y} + \frac{\partial w}{\partial z} = 0 \tag{G.4}$$

In the 2DH approach, it is assumed that the vertical accelerations are small enough to be neglected. The rate of change in the vertical, as described by equation G.3, then reduces to the hydrostatic pressure distribution over the vertical:

$$\frac{\partial p}{\partial z} = -\rho g \tag{G.5}$$

Elaborating the viscous stresses in equations G.1 and G.2 and substituting equation G.5 yields:

$$\frac{\partial \zeta}{\partial t} + \frac{\partial hu}{\partial x} + \frac{\partial hu}{\partial y} = 0 \tag{G.6}$$

$$\frac{\partial u}{\partial t} + u\frac{\partial u}{\partial x} + v\frac{\partial u}{\partial y} + g\frac{\partial \zeta}{\partial x} - fv + \frac{1}{\rho_0}\left(\frac{\partial \tau_{xx}}{\partial x} + \frac{\partial \tau_{xy}}{\partial y} + \frac{\partial \tau_{bx}}{h}\right) = 0 \tag{G.7}$$

$$\frac{\partial v}{\partial t} + u\frac{\partial v}{\partial x} + v\frac{\partial v}{\partial y} + g\frac{\partial \zeta}{\partial y} - fu + \frac{1}{\rho_0}\left(\frac{\partial \tau_{yx}}{\partial x} + \frac{\partial \tau_{yy}}{\partial y} + \frac{\partial \tau_{by}}{h}\right) = 0 \tag{G.8}$$

These are the equations that are implemented in D-Flow FM. The only three remaining unknows are the water level ζ and the velocities u and v, which are approximated numerically.

G.2 Wave module

The wave formulations implemented in D-Flow FM are based on the Delft3D formulations. The main differences are the method of integration and the data interpolation. The wave forces and shear stresses have an important influence on nearshore hydrodynamics. In D-Flow FM the wave-induced forces are applied in the momentum equations as source terms. This leads to the following expression for the wave-averaged momentum equation in D-Flow FM:

$$\frac{\partial \langle \vec{u} \rangle}{\partial t} + adv(\langle \vec{u} \rangle) + g\nabla\langle \zeta \rangle + \frac{1}{\rho}\nabla\langle \vec{\tau_b} \rangle + 2\Omega \times \langle \vec{u} \rangle = \vec{F} \tag{G.9}$$

where $\vec{\tau_b}$ denotes the bed shear stress and $\vec{F} = [F_x, F_y]$ represents the substituted wave forces.
The bed shear stress consists of a wave-related part and a current-related part. The bed shear stress due to the current-related part is mainly a function of the square of the current velocity and to a friction coefficient. The wave-related part is proportional to the square of the orbital velocity and to a wave friction factor. The wave orbital velocity $\hat{u}$ is given by linear wave theory:

$$\hat{u} = \frac{1}{4}\sqrt{\pi}\frac{H_{rms}\omega}{\sinh(kh)} \tag{G.10}$$

where H_{rms} represents the root-mean-square wave height, ω the radian frequency, k the wave number and h the water depth.

G.3 Sediment module

The transport of sediment is computed in the same way as any other conservative constituent, although the effectiveness of transport (indicated by the Prandtl number) depends on the quantity that is transported. For sediments transport a constant eddy diffusivity is used, that is equal to the eddy viscosity (i.e. a Prandtl number of 1.0).
The sediment transport and morphology module distinguishes two types of sediment fractions. For cohesive sediment the 'mud' fraction is used and for non-cohesive sediment the 'sand' fraction. Cohesive sediment is only transported as suspended load, which is computed based on the advection-diffusion equation:

$$\frac{\partial c}{\partial t}+\frac{\partial uc}{\partial x}+\frac{\partial vc}{\partial y}+\frac{\partial (w-w_s)c}{\partial z}-\frac{\partial}{\partial x}\left(\epsilon_{s,x}\frac{\partial c}{\partial x}\right)-\frac{\partial}{\partial y}\left(\epsilon_{s,y}\frac{\partial c}{\partial y}\right)-\frac{\partial}{\partial z}\left(\epsilon_{s,z}\frac{\partial c}{\partial z}\right)=0 \quad \text{(G.11)}$$

where:

c	mass concentration of sediment fraction [kg/m^3];
u, v and w	flow velocity components [m/s];
$\epsilon_{s,x}$, $\epsilon_{s,y}$ and $\epsilon_{s,z}$	eddy diffusivities of sediment fraction [m^2/s];
w_s	settling velocity [m/s];

The local flow velocities and eddy diffusivities are based on the results of the hydrodynamic computations. The advection-diffusion equation is solved using boundary conditions. For each open boundary a boundary condition should be prescribed by the user. At the free surface and at the bed the boundary conditions are set by the sediment module. The vertical diffusive flux through the free surface is set to zero for all conservative constituents (except heat, if applicable). For suspended sediment the water surface boundary condition is given by:

$$-w_s c-\epsilon_{s,z}\frac{\partial c}{\partial z}=0, \qquad \text{at } z=\zeta \text{ (free surface)} \quad \text{(G.12)}$$

The exchange of material with the bed is modelled by calculating the sediment fluxes from the water column to the bed and vice versa. These fluxes are then applied to the water column by means of a sediment source and/or sink term and to the bed as well in order to account for morphological updating. The boundary condition at the bed is given by:

$$-w_s c-\epsilon_{s,z}\frac{\partial c}{\partial z}=D-E, \qquad \text{at } z=z_b \text{ (bed level)} \quad \text{(G.13)}$$

where E is the erosion flux and D the deposition flux (both in kg/m^2/s). For cohesive sediment fractions these fluxes between the water column and the bed are calculated with the Partheniades-Krone formulations (Partheniades, 1965):

$$E=\begin{cases} M\left(\frac{\tau_{b,max}}{\tau_{cr,e}}-1\right), & \text{when } \tau_{b,max}>\tau_{cr,e} \\ 0, & \text{when } \tau_{b,max}\leq\tau_{cr,e} \end{cases} \quad \text{(G.14)}$$

$$D=\begin{cases} w_s c\left(1-\frac{\tau_{b,max}}{\tau_{cr,d}}\right), & \text{when } \tau_{b,max}<\tau_{cr,d} \\ 0, & \text{when } \tau_{b,max}\geq\tau_{cr,d} \end{cases} \quad \text{(G.15)}$$

where:

M	user-defined erosion parameter [kg/m^2/s];
$\tau_{b,max}$	maximum bed shear stress [N/m^2] due to current and waves;
$\tau_{cr,e}$	user-defined critical shear stress for erosion [N/m^2];
w_s	settling velocity [m/s];
c	average sediment concentration [m/s];
$\tau_{cr,d}$	user-defined critical shear stress for deposition [N/m^2];

At open inflow boundaries the concentration needs to be specified. A 'Thatcher-Harleman' return time can be used to simulate the re-entry of material that flowed out of the model after the flow reverses direction. Moreover, a Neumann boundary condition can be used to set the sediment concentration at the boundary equal to that just inside the model domain (zero concentration gradient).

Appendix H

Memo FM tests cohesive sediment

Memo

Aan
Johan Reyns

Datum
6 juli 2016

Aantal pagina's
4

Van
Bob Smits

E-mail
bob.smits@deltares.nl

Kopie aan
Katherine Cronin

Onderwerp
FM tests cohesive sediment transport & morphology

---

1. Introduction

This memo describes a test that was performed to assess the behaviour of cohesive sediment transport and the morphological updating of the bed level in Delft3D Flexible Mesh (FM). Two cases were tested: in the first case only tidal flow was used (D-Flow FM standalone) and in the second case tidal flow was combined with waves. The results obtained with FM are compared to results of the validated Delft3D model (D3D).

2. Model set-up

A simple 2DH model of 3 km x 3 km was tested for flow standalone and for flow coupled with waves. A rectangular grid of 30 by 30 cells was used, hence a cell size of 100 m. The bathymetry has a constant slope from -1.0 m in the North to -0.3 m in the South.

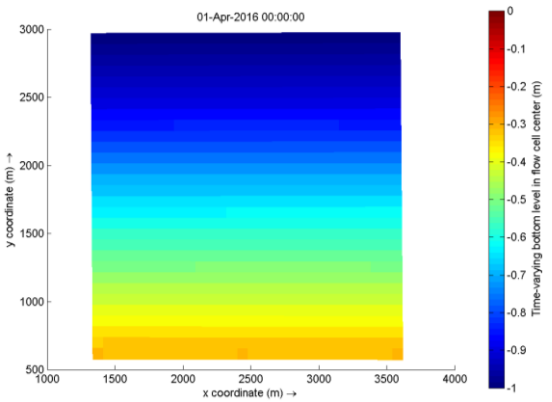

The only open boundary is located on the North. Here, a tidal boundary was applied with an amplitude of 0.3 m. For the wave model, a wave boundary was applied with waves coming from the North, a significant wave height of 0.3 m and a peak period of 4.4 s. A breaker parameter (γ) of 0.78 was used. A wind of 10 m/s from the North was applied in the entire domain, both for the cases with and without waves. A Manning roughness coefficient of 0.015 was used.

The Krone-Partheniades formulations were used to compute sediment transport. A mud fraction (cohesive sediment) was applied with a settling velocity of 0.1 mm/s. The critical shear stress for erosion was set at 0.25 Pa, whereas the critical shear stress for sedimentation was set at 1000 Pa to allow sedimentation to occur throughout the domain. An initial mud concentration of 1.0 g/L was applied, along with 1.0 g/L at the boundaries. A morphological upscaling factor of 15 was used, so that the resulting bed changes are multiplied by a factor 15.

For comparison D3D computations were performed with the same settings.

3. Results

First, the standalone flow model will be considered. The final bed level and sediment thickness are shown in the figures on page 3. The final bed level and cumulative erosion/sedimentation for the

D3D-Flow computation are shown on the right for comparison. No erosion occurred for this case. Some accretion (~7 cm) was observed at the boundary. D3D gives a similar sedimentation pattern, with a bit more accretion (~10 cm) at the boundary.

For the second case, coupled flow and waves, the results are shown in the figures on page 4. In the FM simulations, only erosion can be observed from the final bed level and again it is limited to the cells near the boundary. In the D3D results, the erosion at the boundary is less severe and the erosion is more spread over the entire domain.

4. Discussion

The results from Flexible Mesh give reasonable results that show similar sedimentation and erosion as the Delft3D runs (both in magnitude and in spatial patterns).

Nevertheless, some differences still exist, that cannot fully be explained form this test. In the flow case, the differences in bed level change are small and may be caused by differences in hydrodynamic spinup.

For the coupled flow-wave case, due to erosion, larger bed gradients occur for FM than for D3D. This might be caused by differences in bed shear stresses, which result from the hydrodynamic computations.

5. Conclusions

The behaviour of cohesive sediment transport and morphological updating of the bed level was tested for Delft3D Flexible Mesh, for flow standalone and coupled flow and waves cases. The results were compared to results of the validated Delft3D model and were found to give reasonable sedimentation and erosion results. Additional research is necessary to further improve the results.

FM

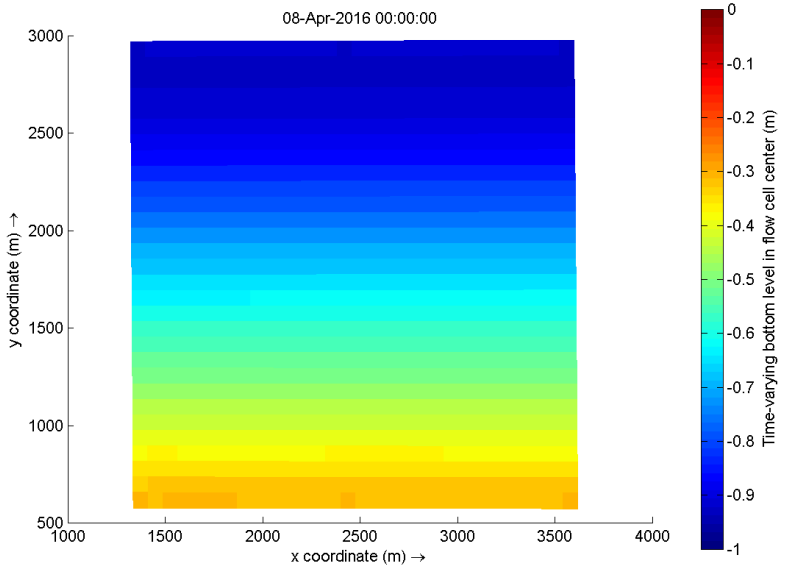
08-Apr-2016 00:00:00
y coordinate (m) →
x coordinate (m) →
Time-varying bottom level in flow cell center (m)

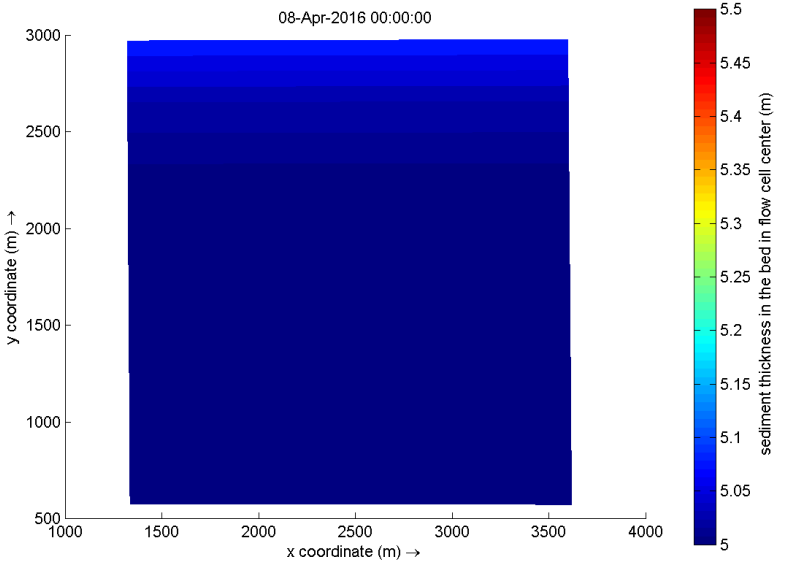
08-Apr-2016 00:00:00
y coordinate (m) →
x coordinate (m) →
sediment thickness in the bed in flow cell center (m)

D3D

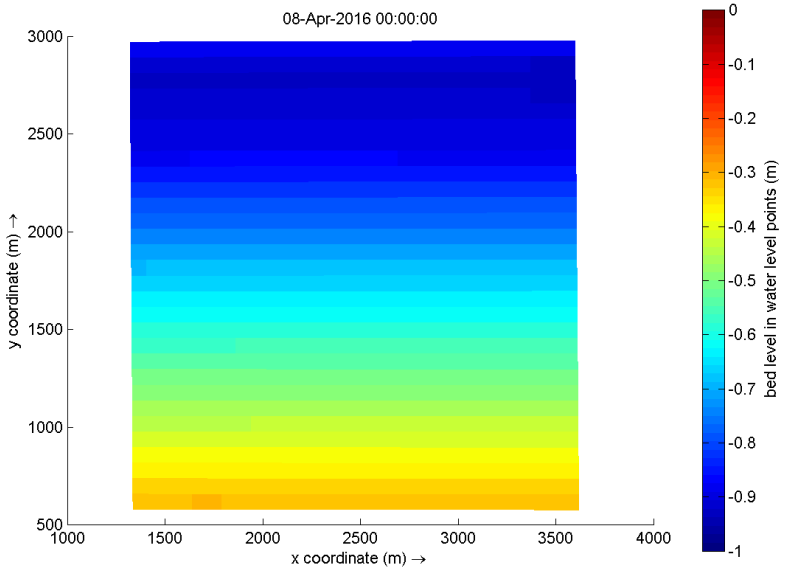
08-Apr-2016 00:00:00
y coordinate (m) →
x coordinate (m) →
bed level in water level points (m)

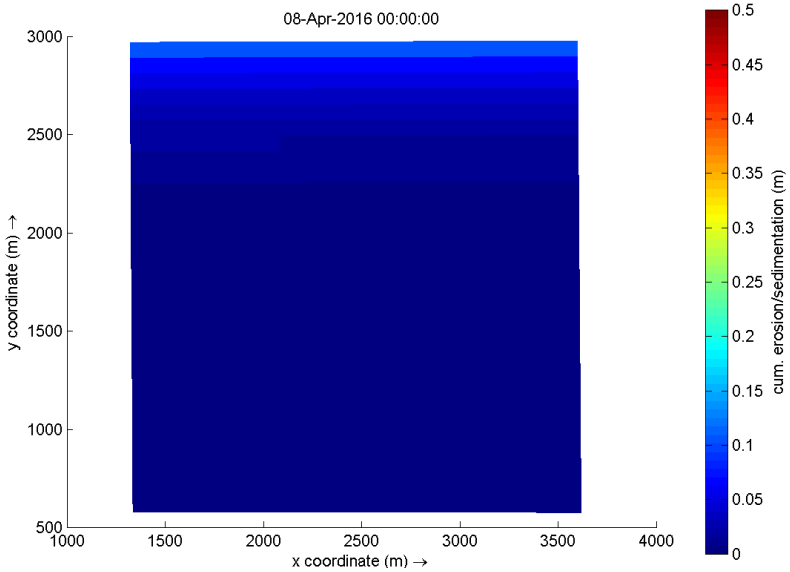
08-Apr-2016 00:00:00
y coordinate (m) →
x coordinate (m) →
cum. erosion/sedimentation (m)

FM

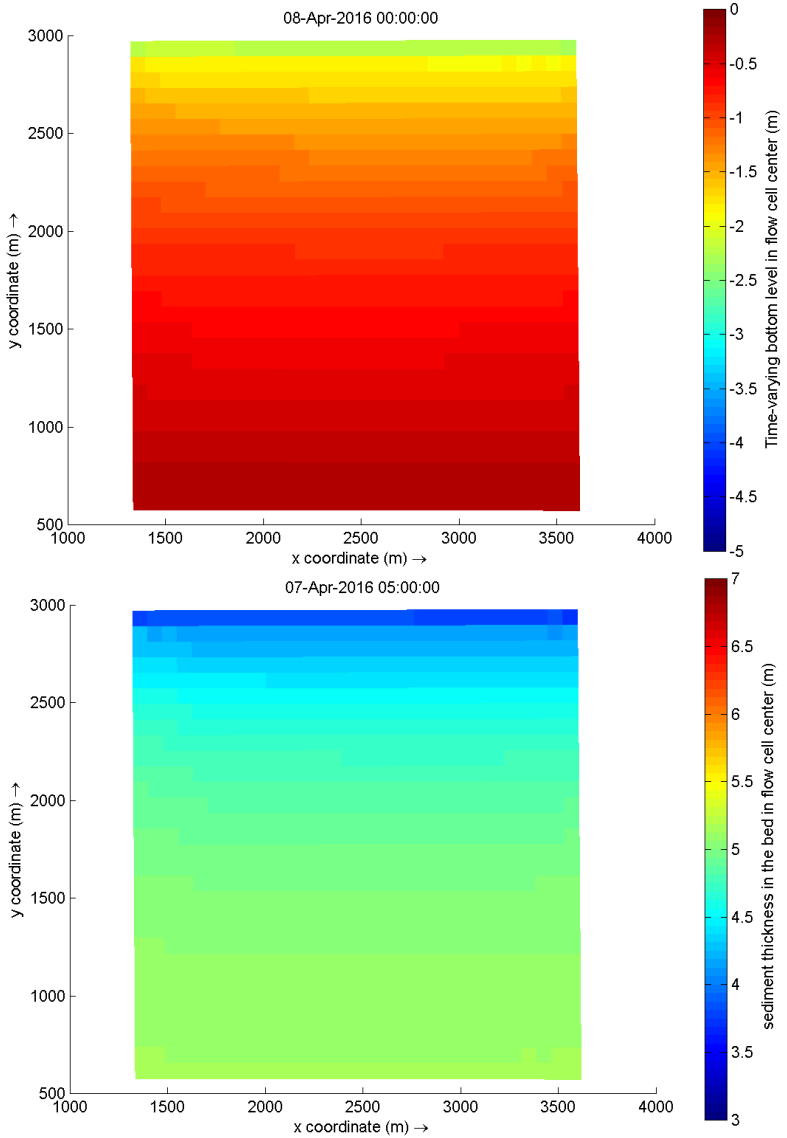
08-Apr-2016 00:00:00
y coordinate (m) →
x coordinate (m) →
Time-varying bottom level in flow cell center (m)
07-Apr-2016 05:00:00
y coordinate (m) →
x coordinate (m) →
sediment thickness in the bed in flow cell center (m)

D3D

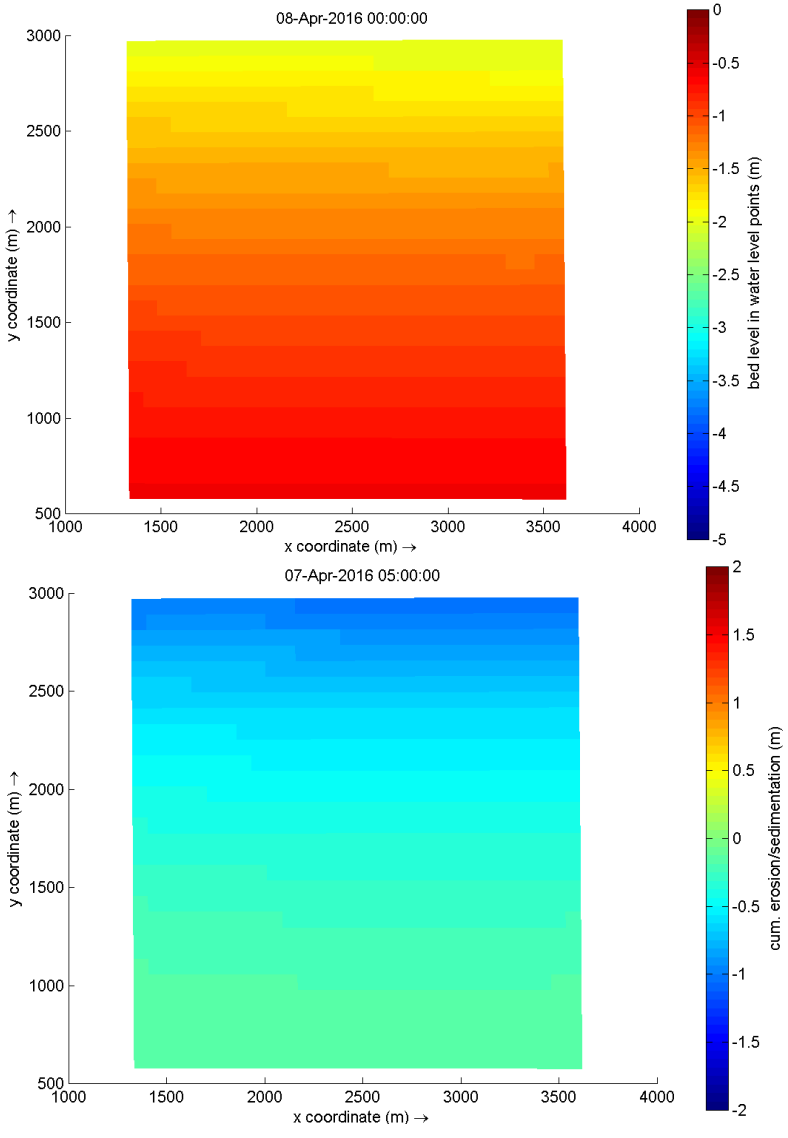
08-Apr-2016 00:00:00
y coordinate (m) →
x coordinate (m) →
bed level in water level points (m)
07-Apr-2016 05:00:00
y coordinate (m) →
x coordinate (m) →
cum. erosion/sedimentation (m)

Appendix I

Results test cases

This appendix contains additional figures of the results from section 6.2.

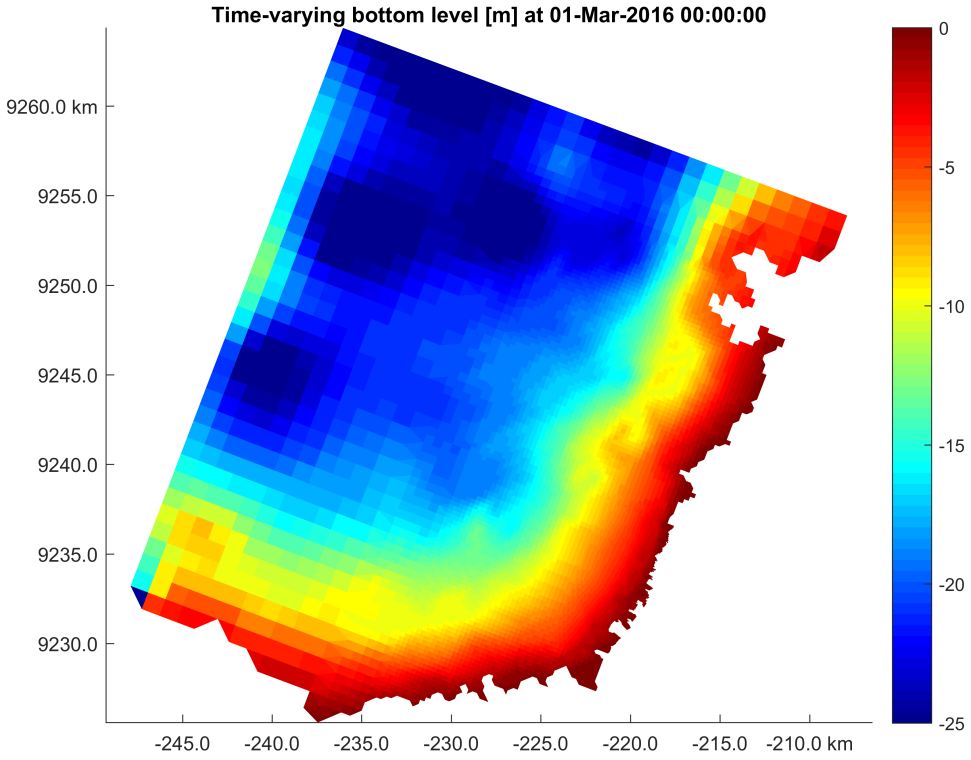

Figure I.1: Resulting bed level [m] compared to MSL in entire domain after a simulation of three months with the monsoon scenario (domain)

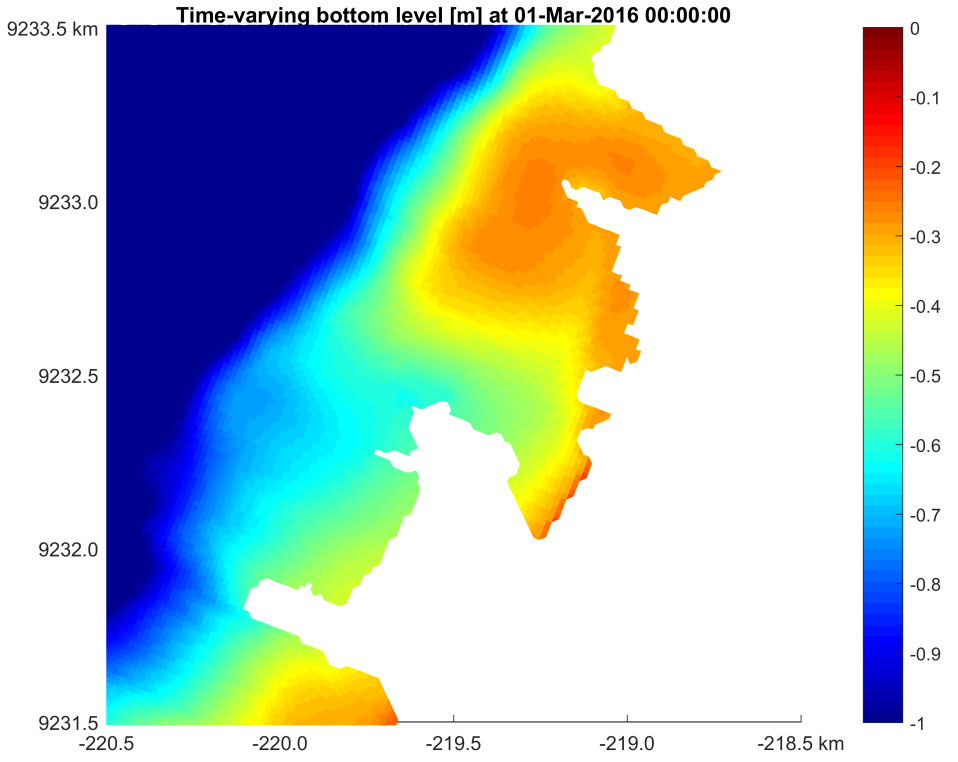

Figure I.2: Zoom of resulting bed level [m] compared to MSL after a simulation of three months monsoon scenario without dams

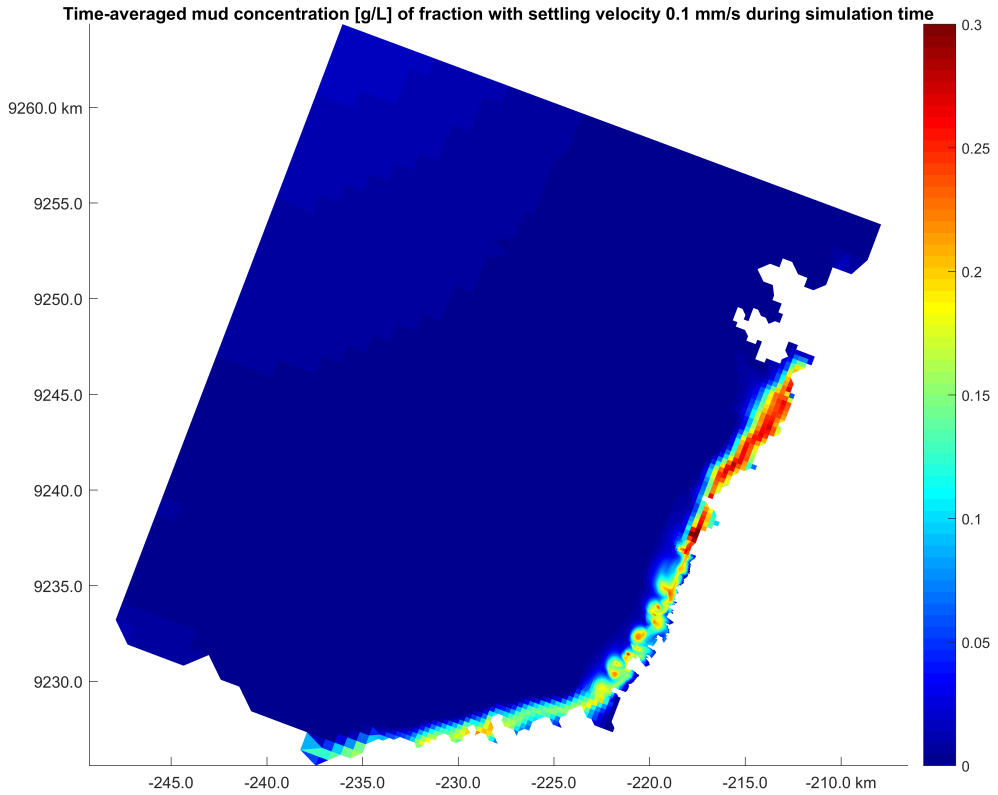

Figure I.3: Time-averaged concentration [g/L] of fraction with settling velocity of 0.1 mm/s for a simulation with the monsoon scenario without dams (domain)

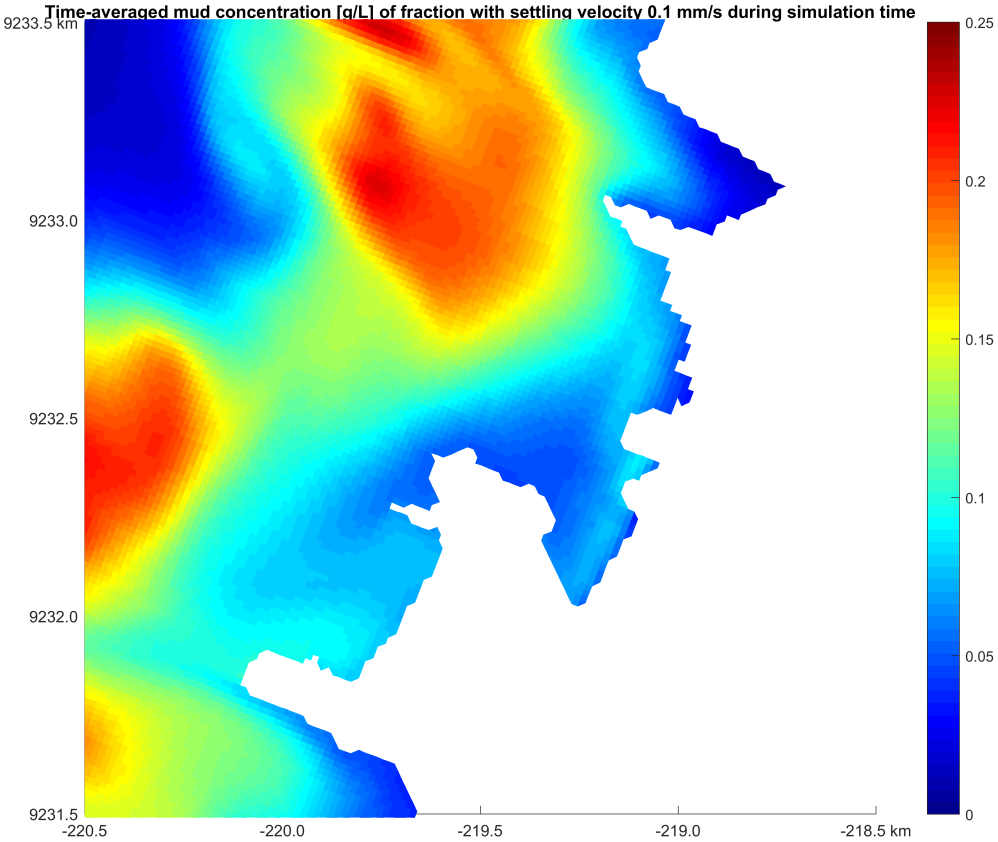

Figure I.4: Zoom of time-averaged concentration [g/L] of fraction with settling velocity of 0.1 mm/s for a simulation with the monsoon scenario without dams

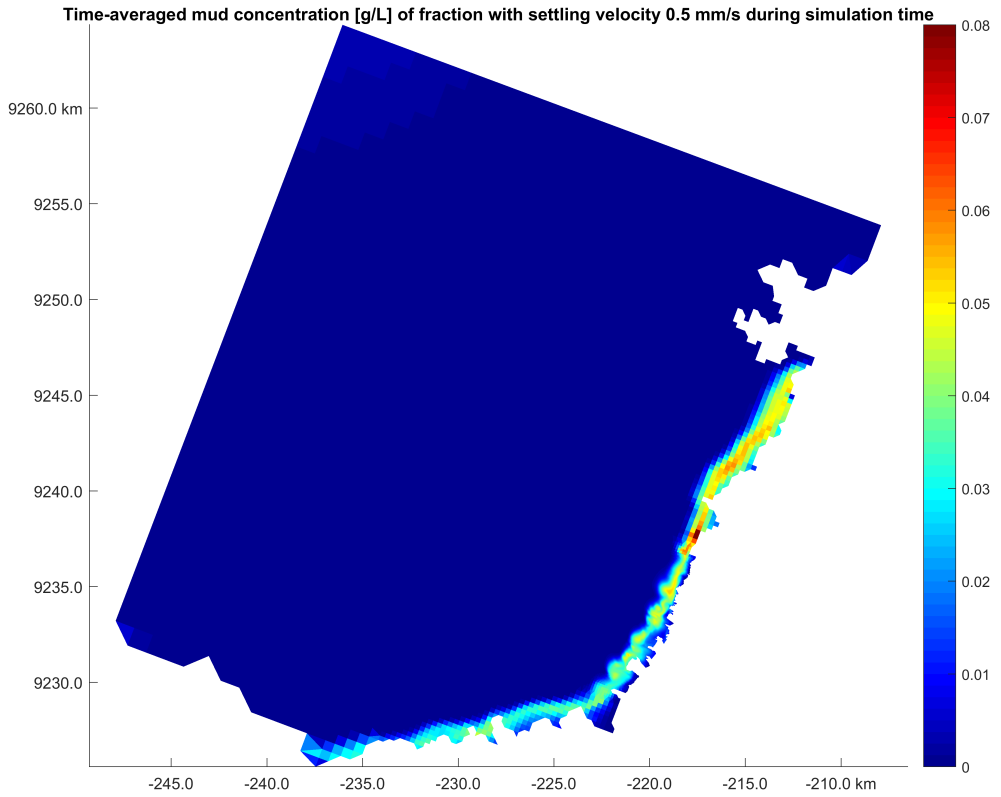

Figure I.5: Time-averaged concentration [g/L] of fraction with settling velocity of 0.5 mm/s for a simulation with the monsoon scenario without dams (domain)

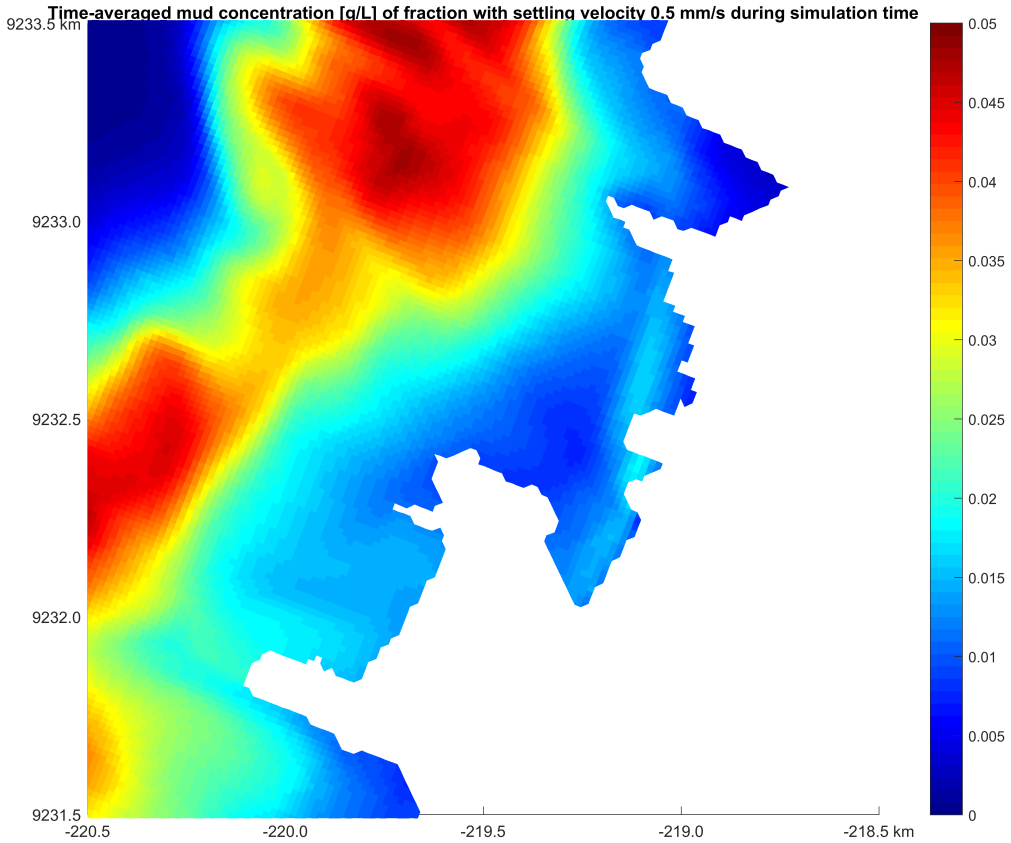

Figure I.6: Zoom of time-averaged concentration [g/L] of fraction with settling velocity of 0.5 mm/s for a simulation with the monsoon scenario without dams

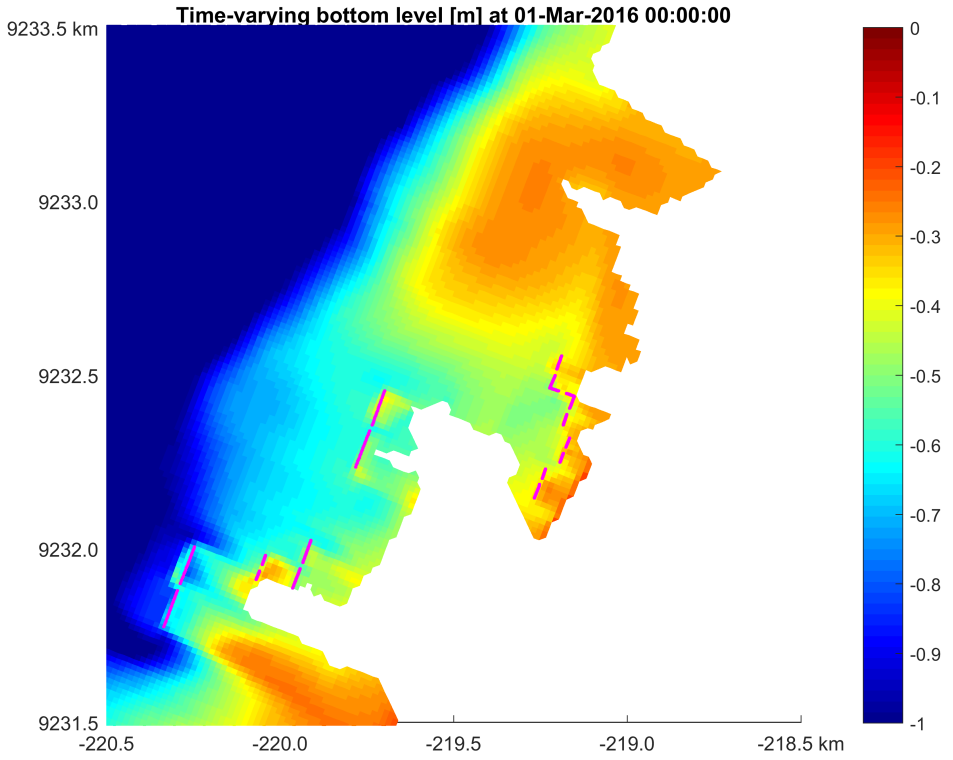

Figure I.7: Zoom of resulting bed level [m] compared to MSL after a simulation of three months monsoon scenario with Ecoshape dams

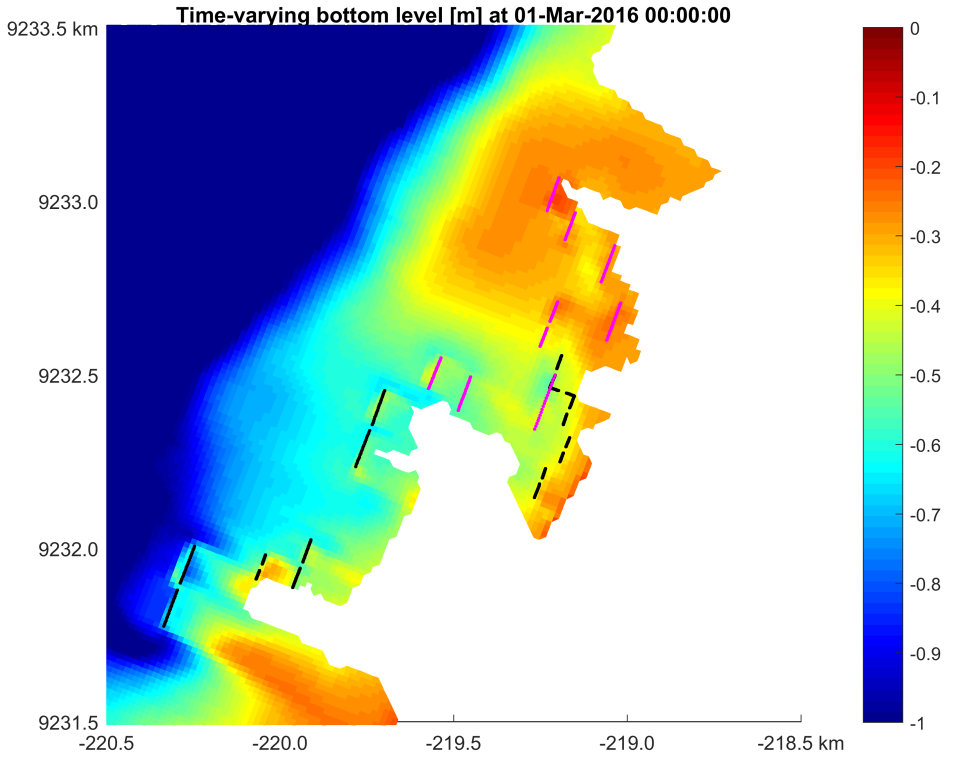

Figure I.8: Zoom of resulting bed level [m] compared to MSL after a simulation of three months monsoon scenario with MMAF and Ecoshape dams

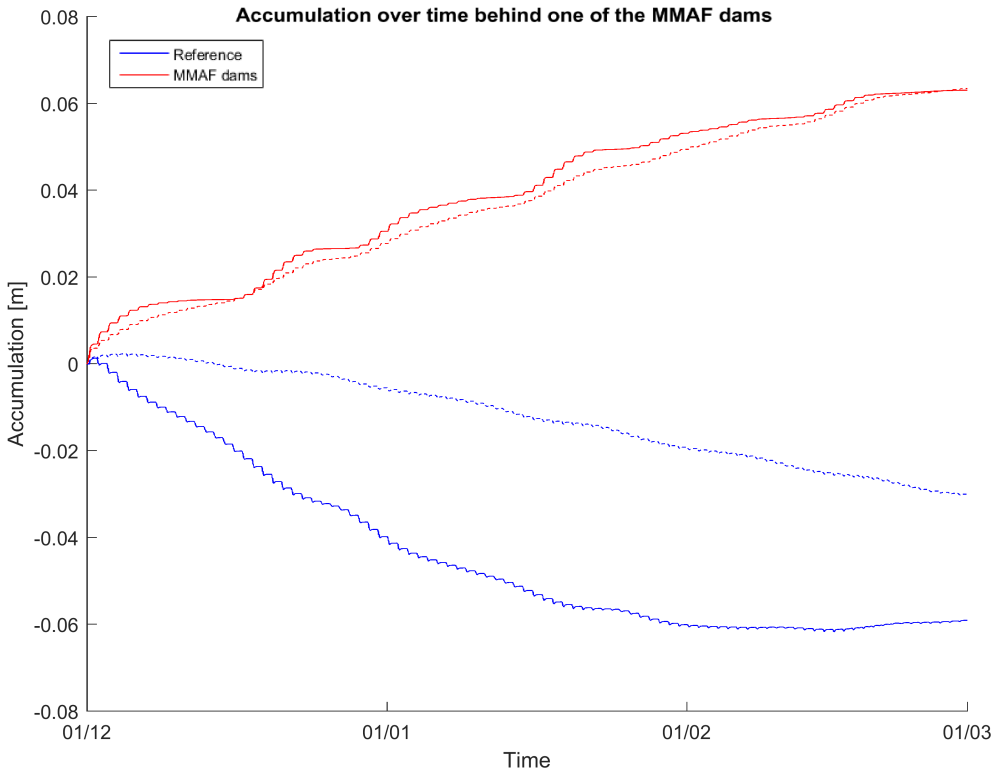

Figure I.9: Accumulation [m] over time behind one of the MMAF dams for a simulation of three months with the monsoon scenario

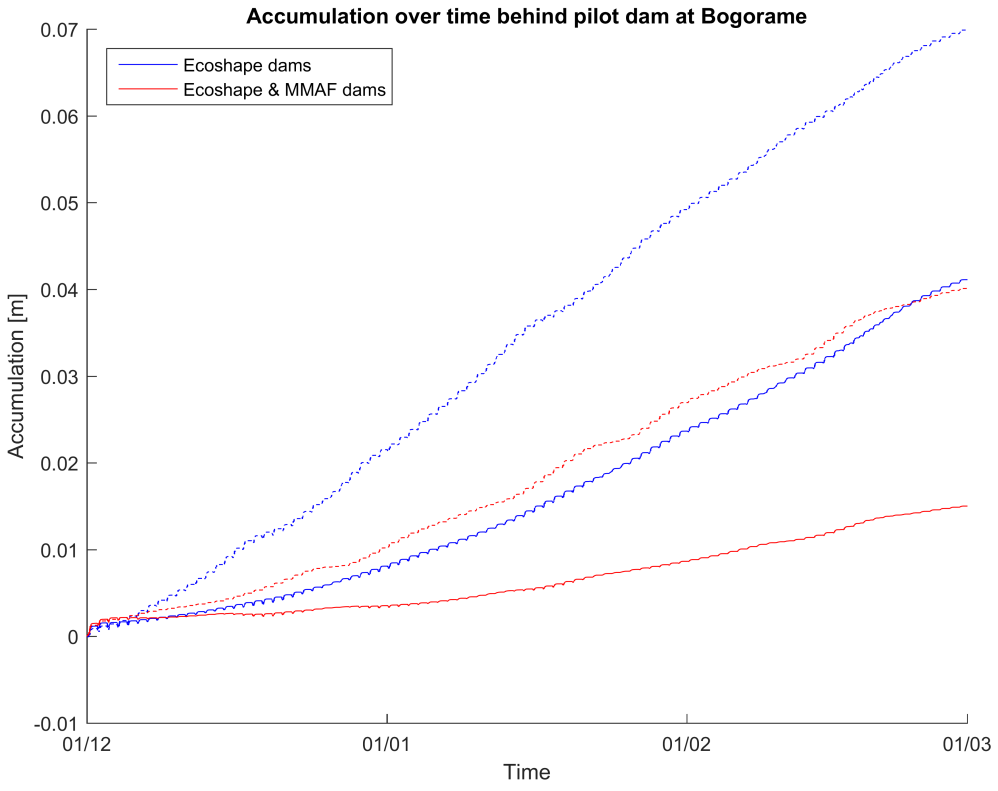

Figure I.10: Accumulation [m] over time behind pilot dam constructed by Ecoshape at Bogorame for a simulation of three months with the monsoon scenario

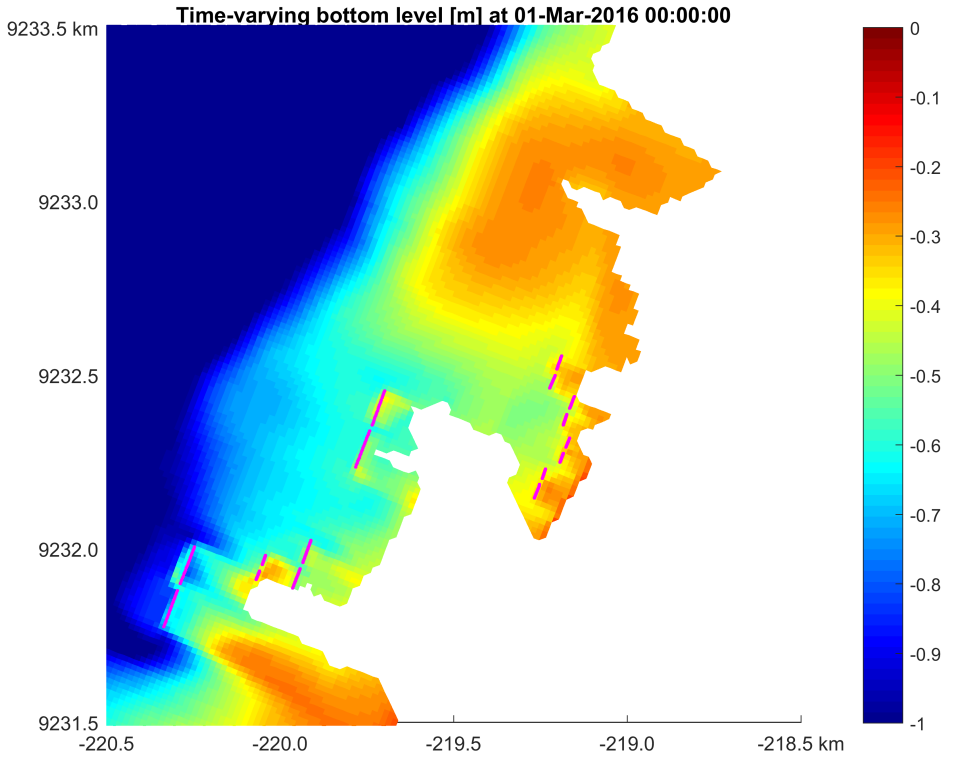

Figure I.11: Zoom of resulting bed level [m] compared to MSL after a simulation of three months monsoon scenario without side dams

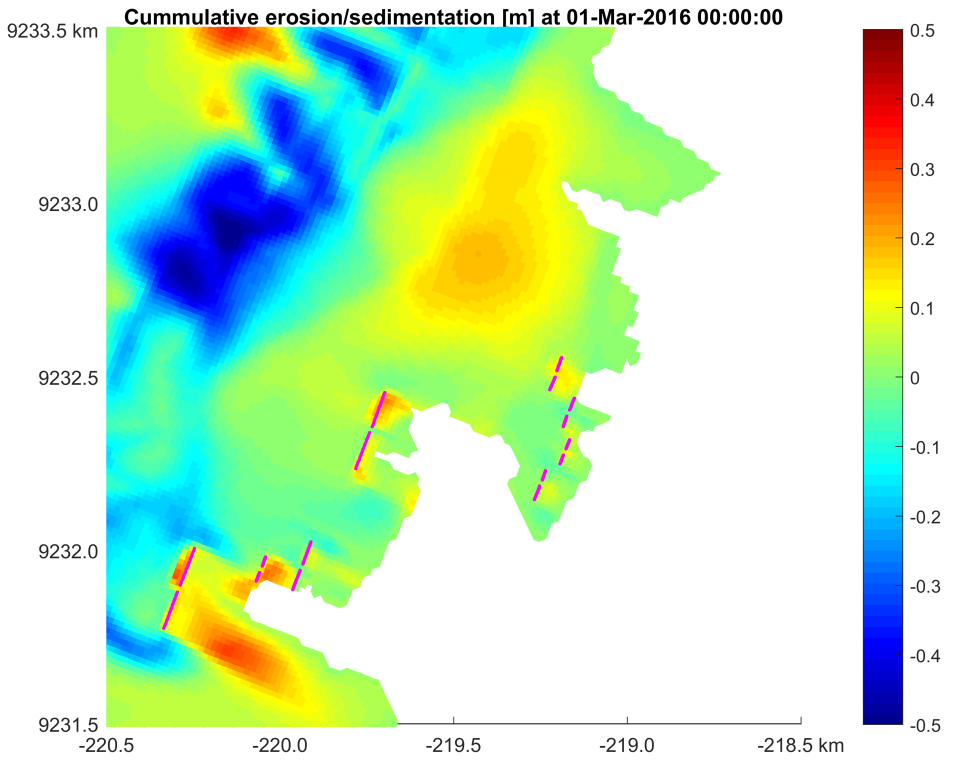

Figure I.12: Zoom of cumulative erosion and sedimentation [m] after a simulation of three months monsoon scenario without side dams

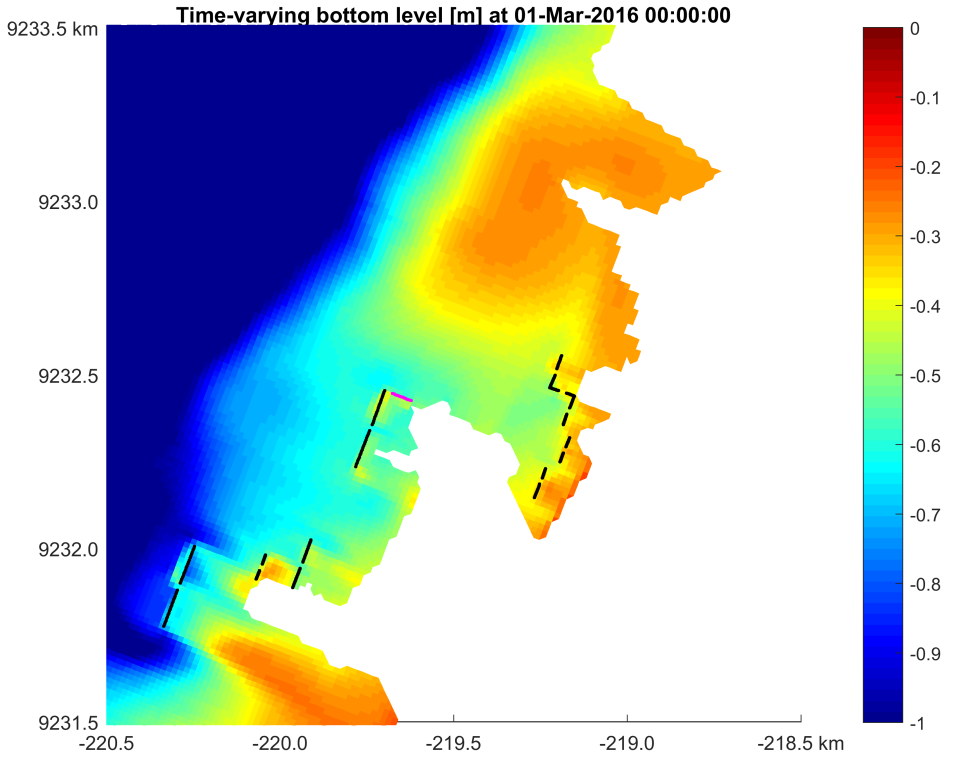

Figure I.13: Zoom of resulting bed level [m] compared to MSL after a simulation of three months monsoon scenario with an extra side dam

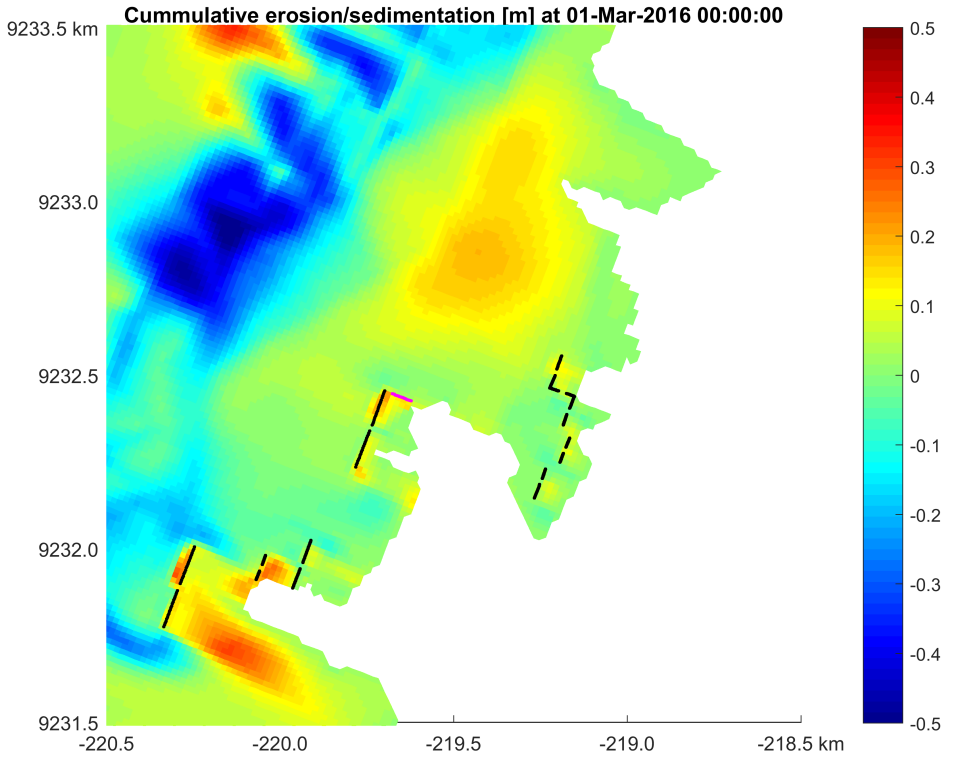

Figure I.14: Zoom of cumulative erosion and sedimentation [m] after a simulation of three months monsoon scenario with an extra side dam

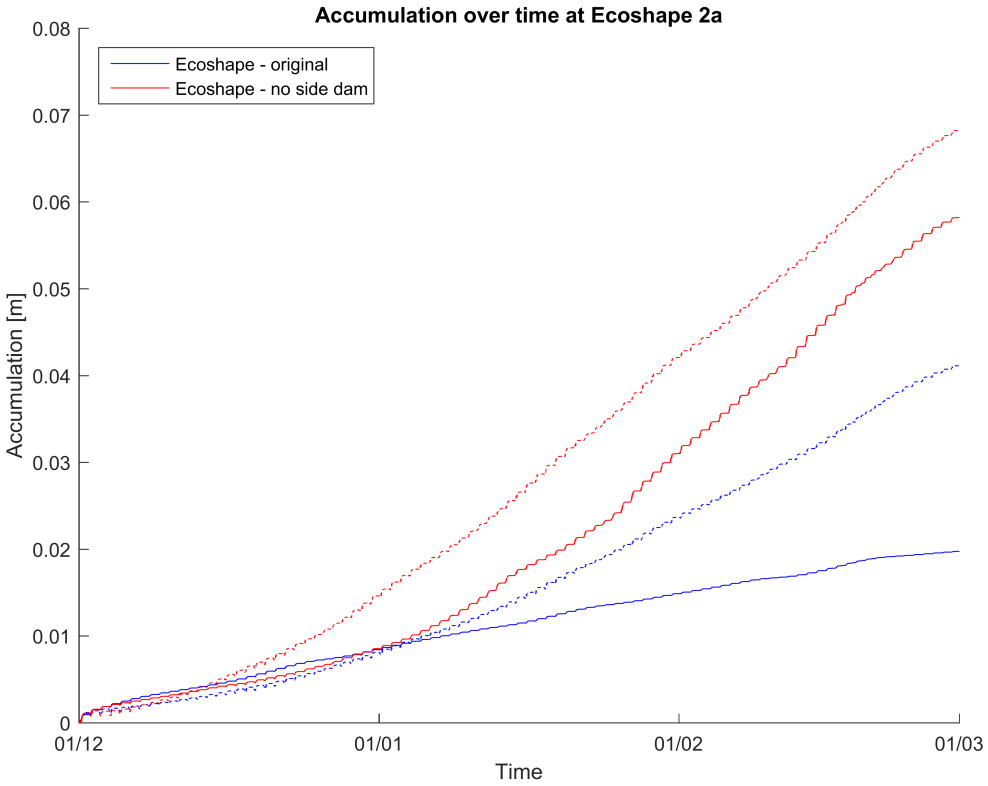

Figure I.15: Accumulation [m] over time where side dam was removed for a simulation of three months with the monsoon scenario

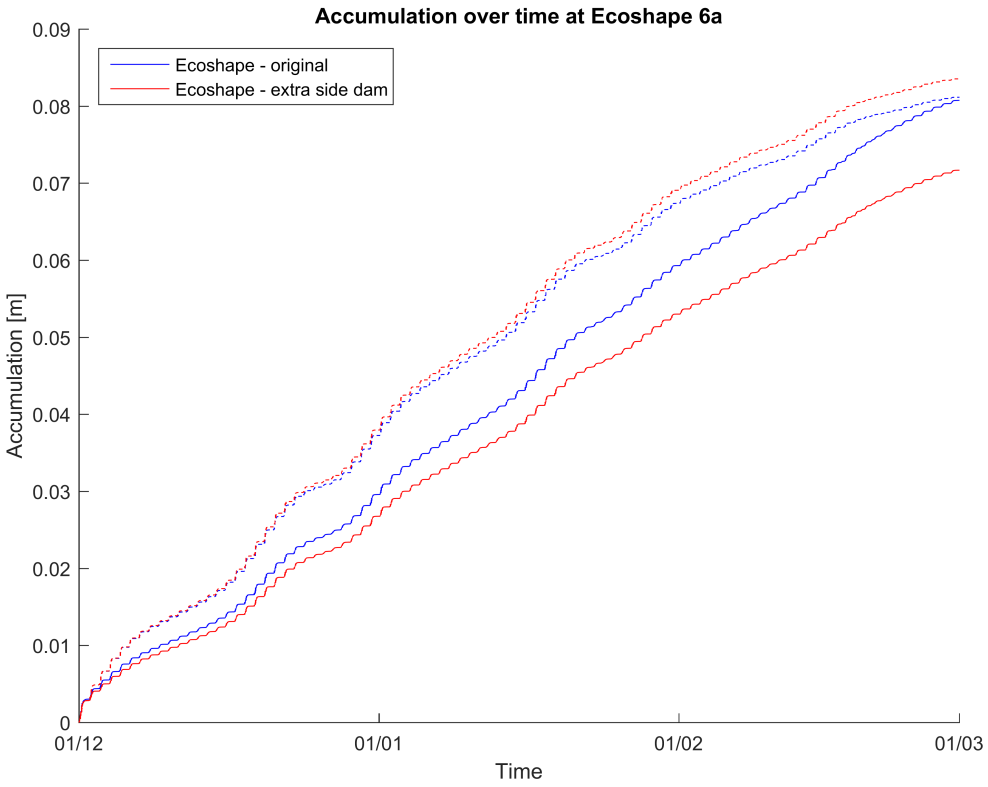

Figure I.16: Accumulation [m] over time where side dam was added for a simulation of three months with the monsoon scenario

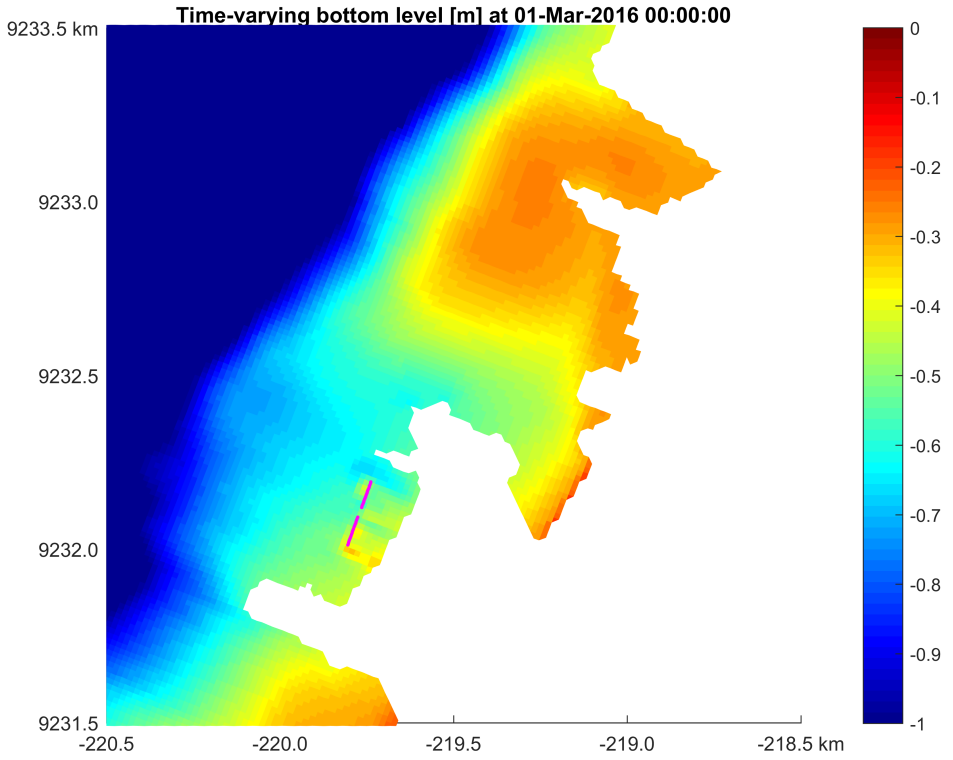

Figure I.17: Zoom of resulting bed level [m] compared to MSL after a simulation of three months monsoon scenario with an extra dam at 100 m from the shore

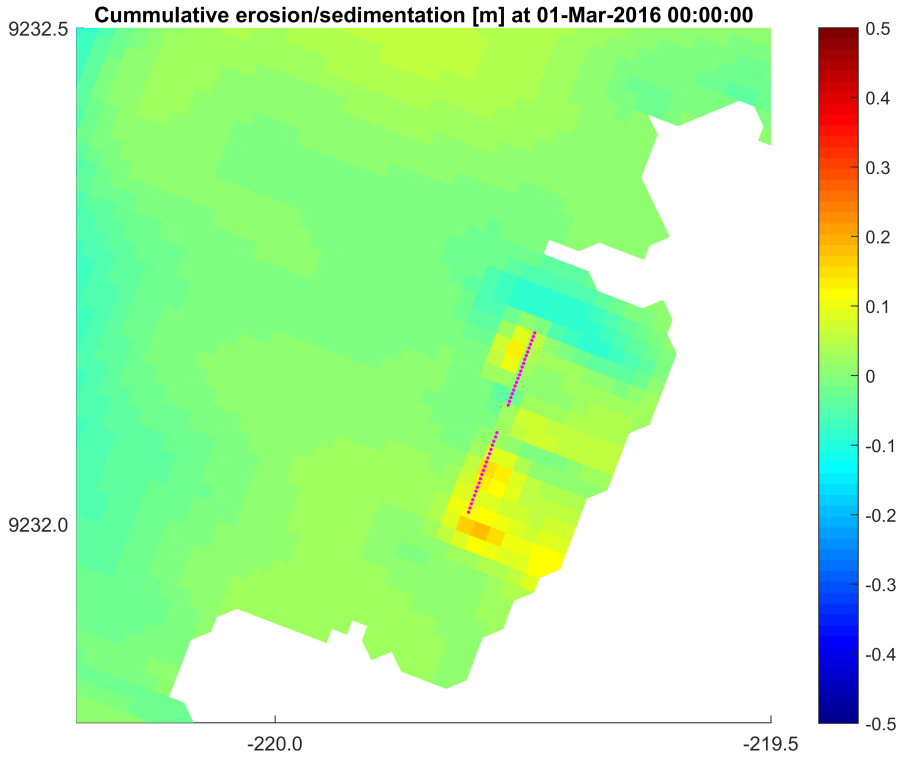

Figure I.18: Zoom of cumulative erosion and sedimentation [m] after a simulation of three months monsoon scenario with an extra dam at 100 m from the shore

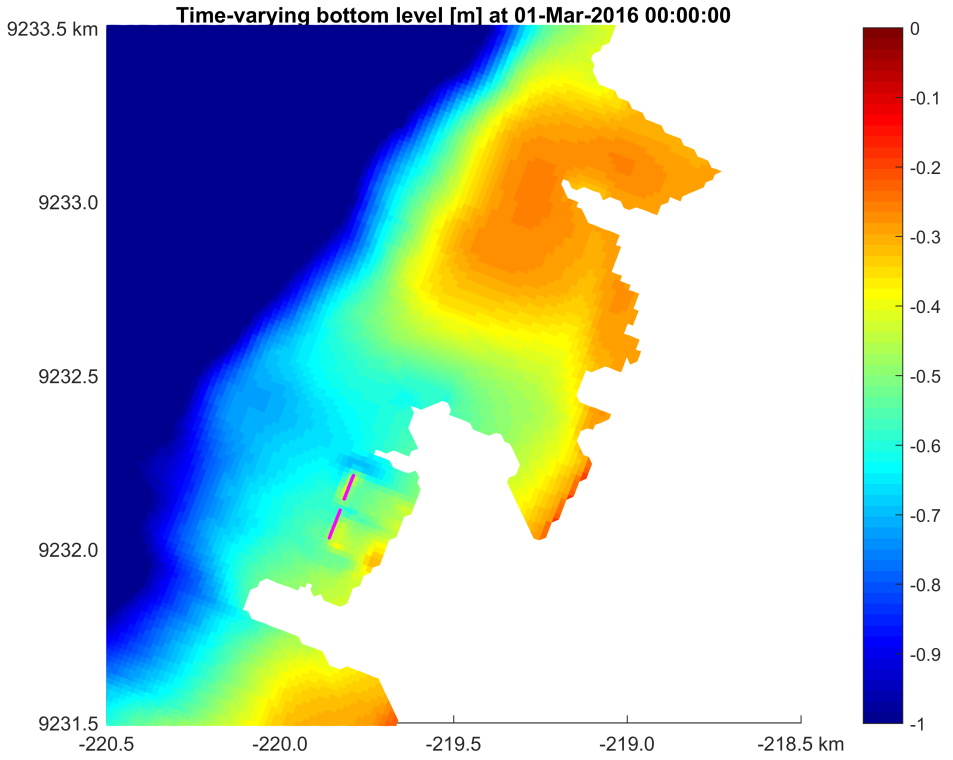

Figure I.19: Zoom of resulting bed level [m] compared to MSL after a simulation of three months monsoon scenario with an extra dam at 150 m from the shore

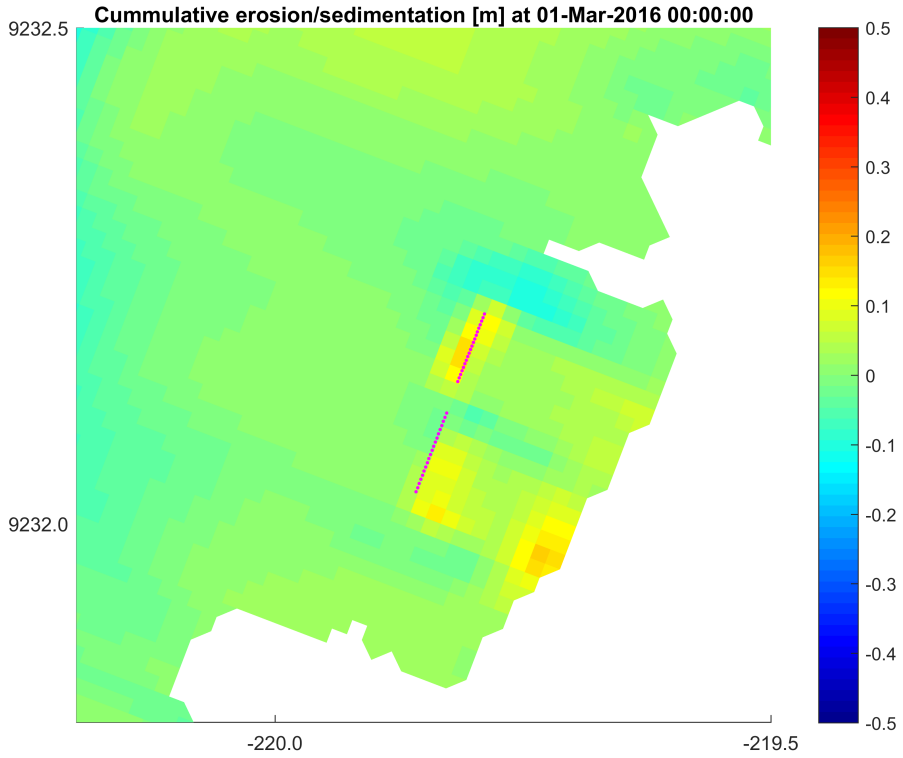

Figure I.20: Zoom of cumulative erosion and sedimentation [m] after a simulation of three months monsoon scenario with an extra dam at 150 m from the shore

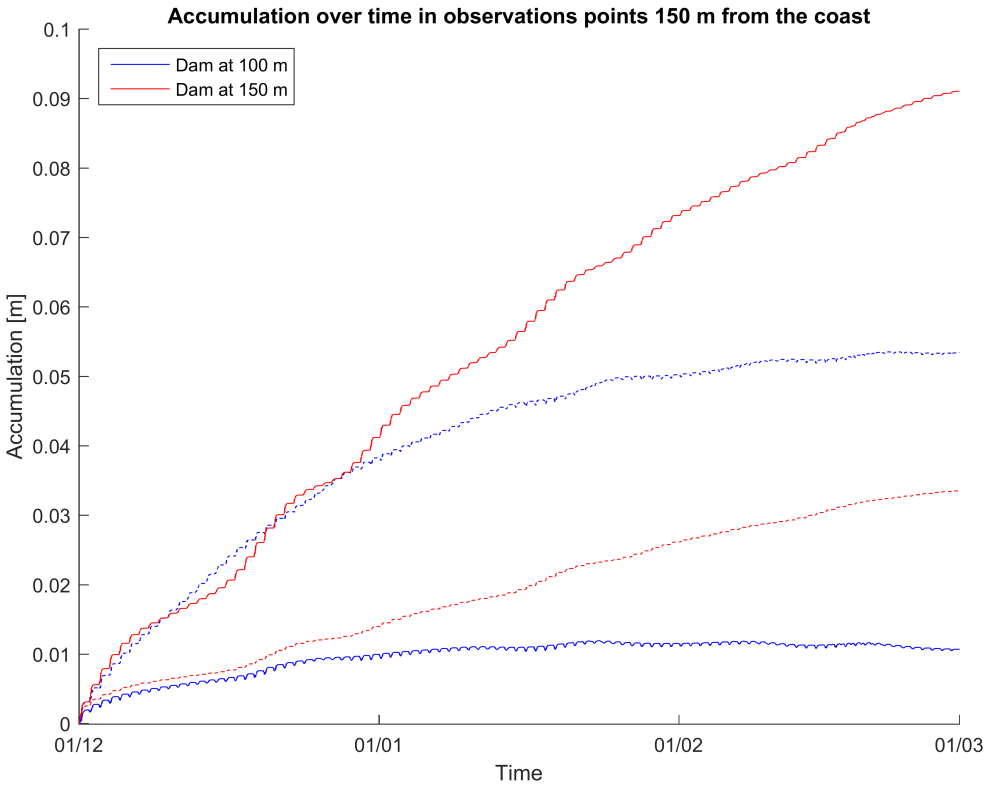

Figure I.21: Accumulation [m] over time for a simulation of three months with the monsoon scenario in an observation point 150 m from the coast

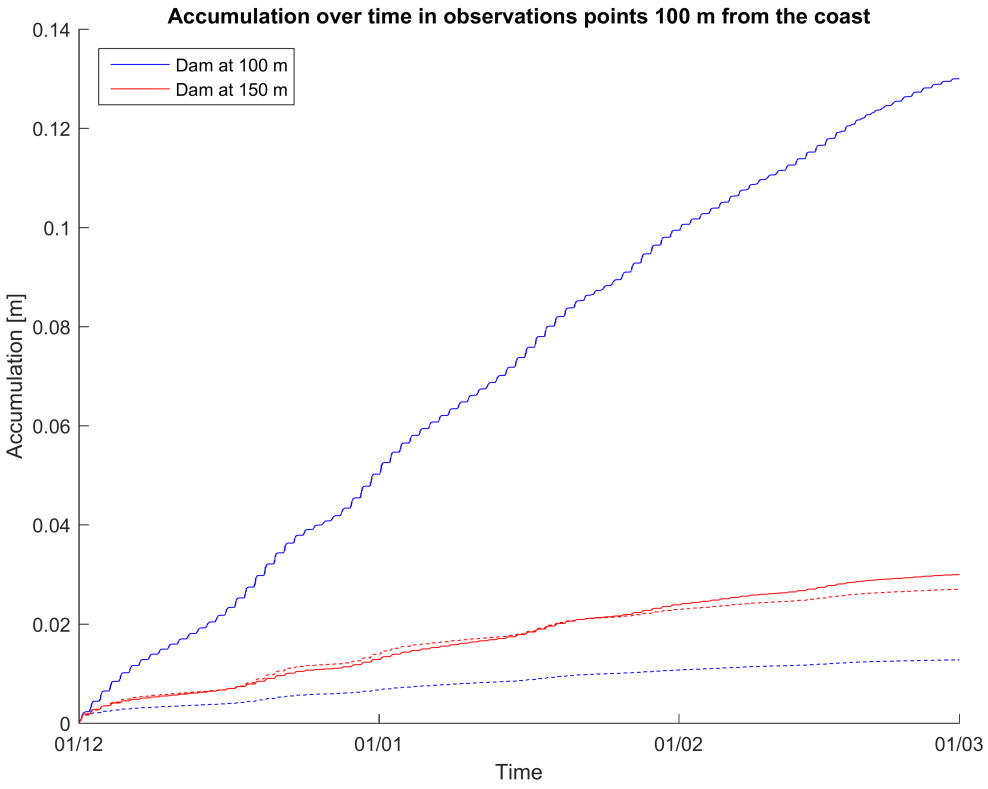

Figure I.22: Accumulation [m] over time for a simulation of three months with the monsoon scenario in an observation point 100 m from the coast

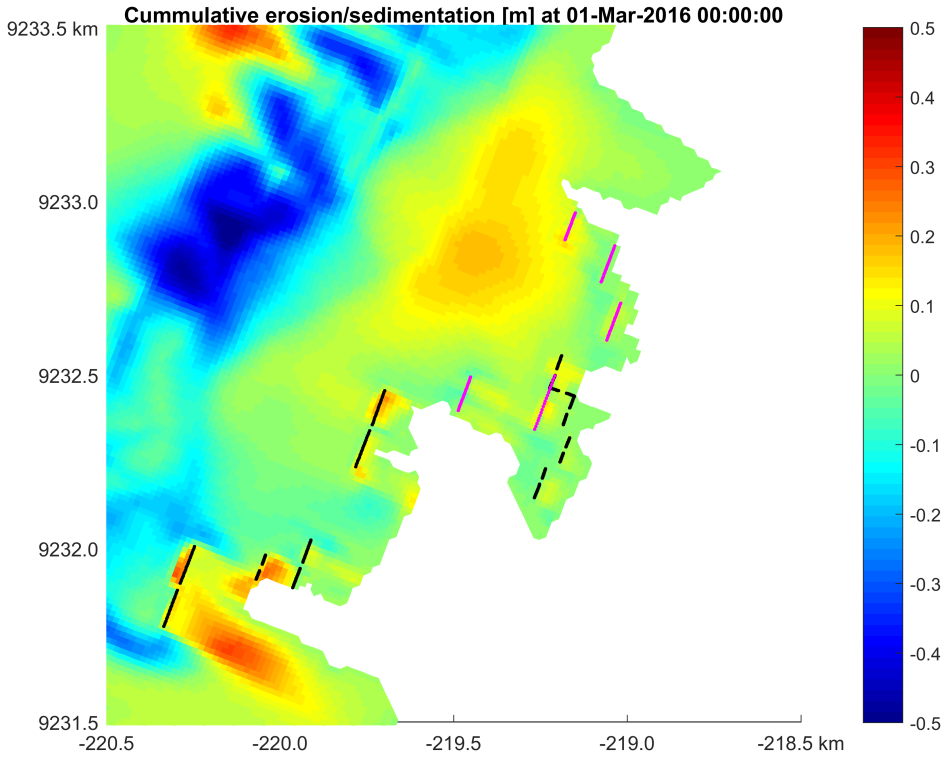

Figure I.23: Zoom of cumulative erosion and sedimentation [m] after a simulation of three months monsoon scenario with altered MMAF dams

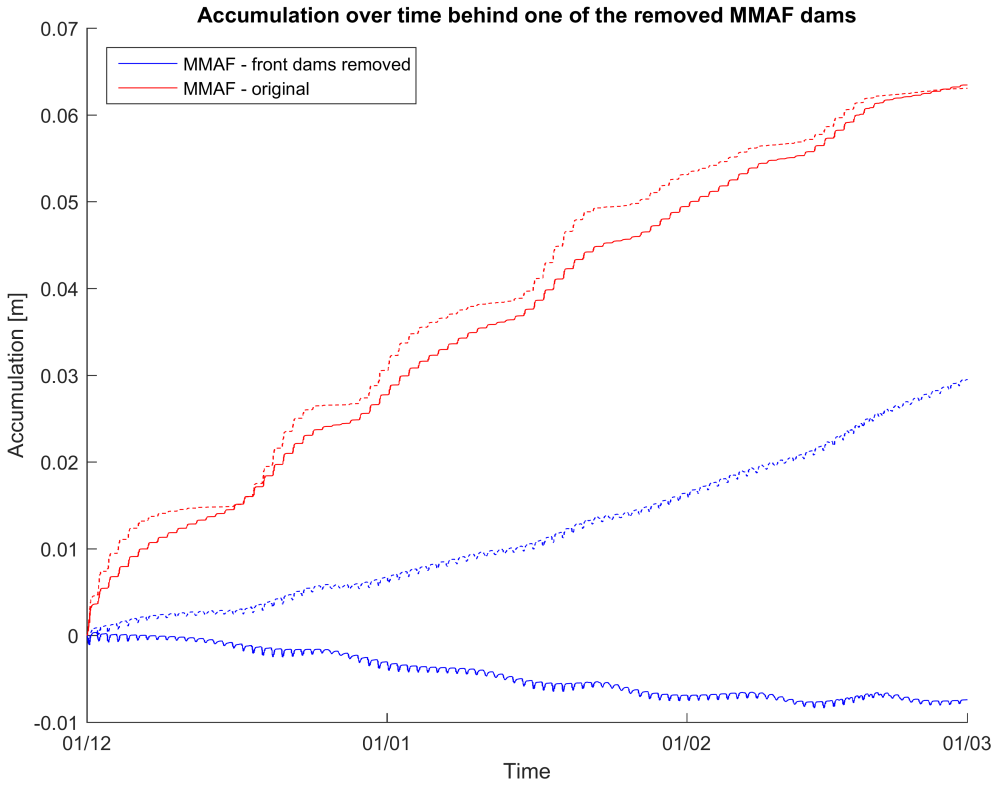

Figure I.24: Accumulation [m] over time where MMAF dam was removed for a simulation of three months with the monsoon scenario

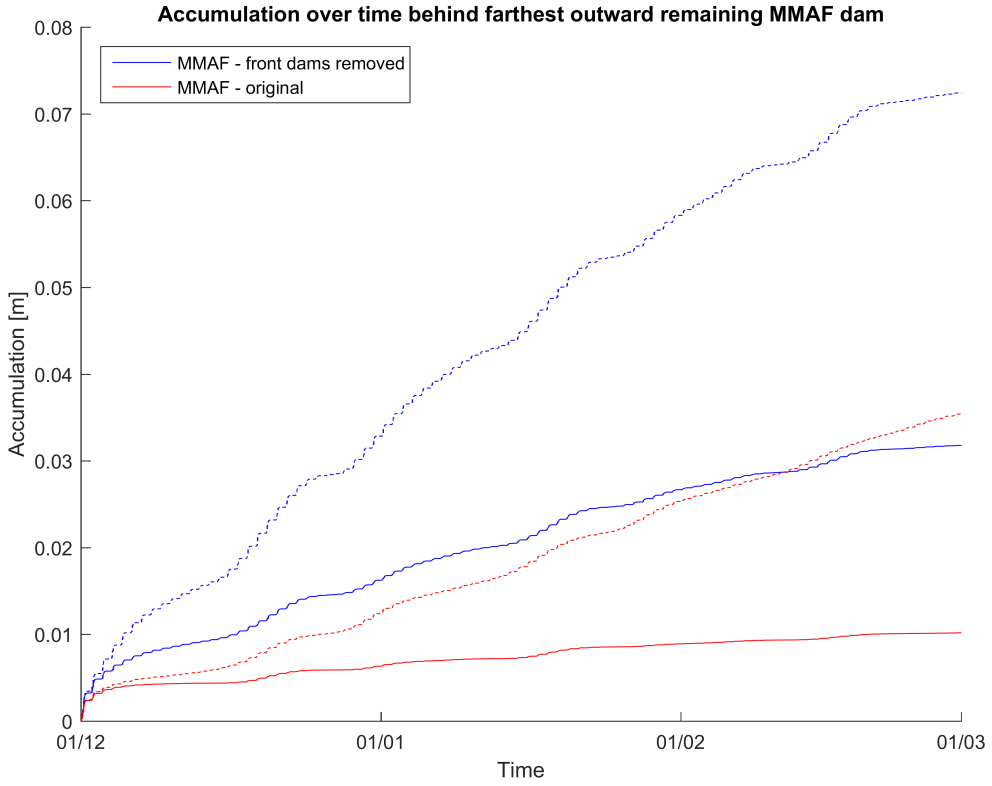

Figure I.25: Accumulation [m] over time behind farthest outward located remaining dam for a simulation of three months with the monsoon scenario

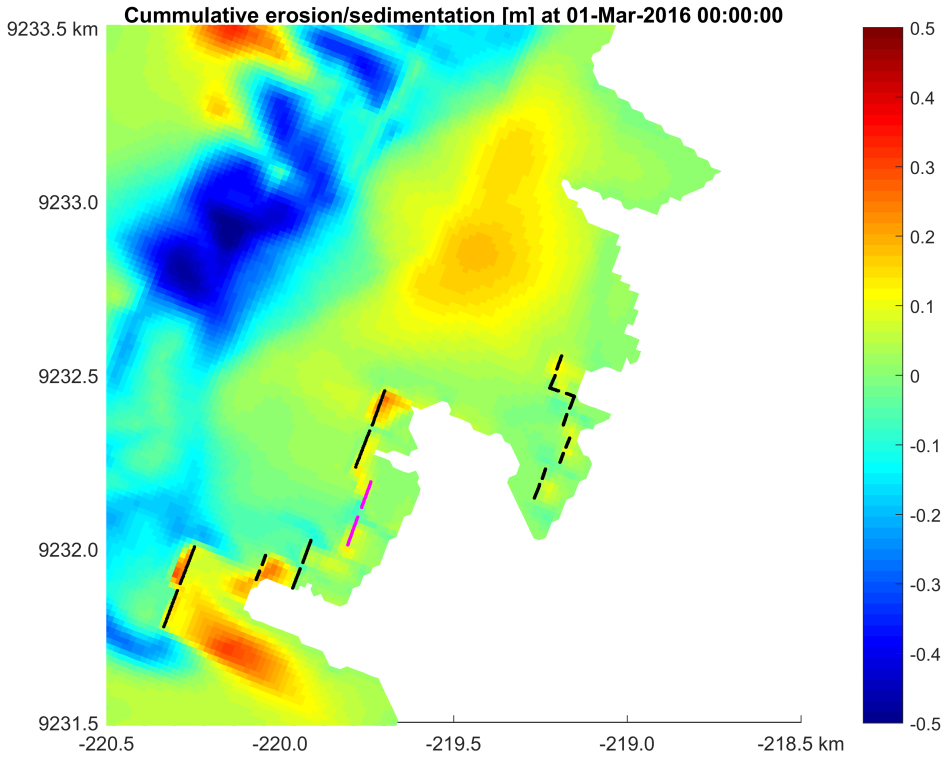

Figure I.26: Zoom of cumulative erosion and sedimentation [m] after a simulation of three months monsoon scenario with Ecoshape dams and dam added at 100 m from shore

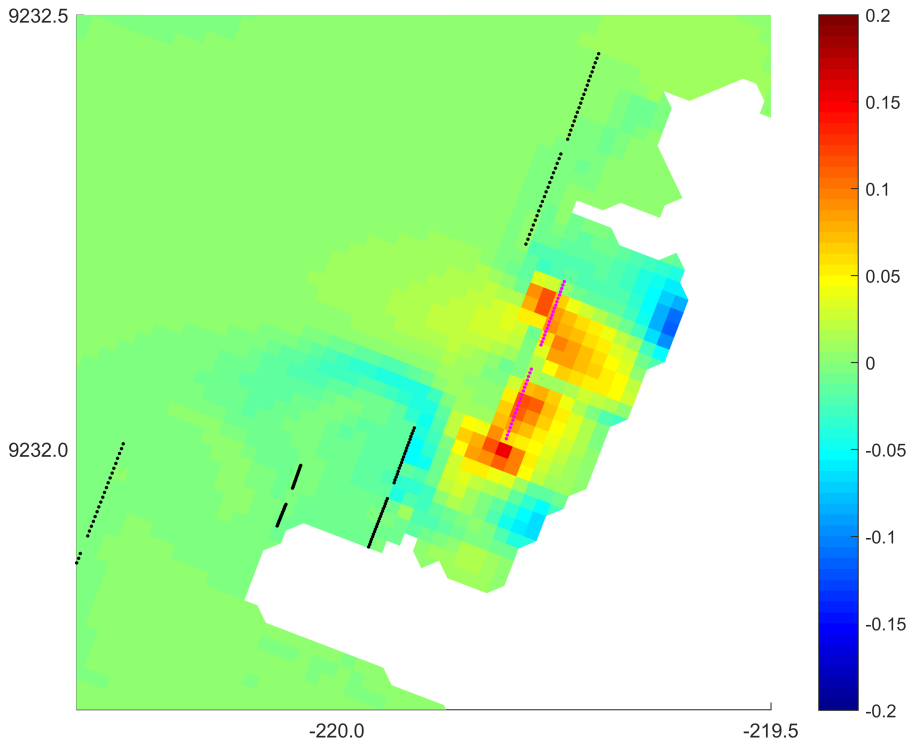

Figure I.27: Difference in remaining bed level [m] of Ecoshape dams with dam added at 100 m from shore compared to the original Ecoshape case

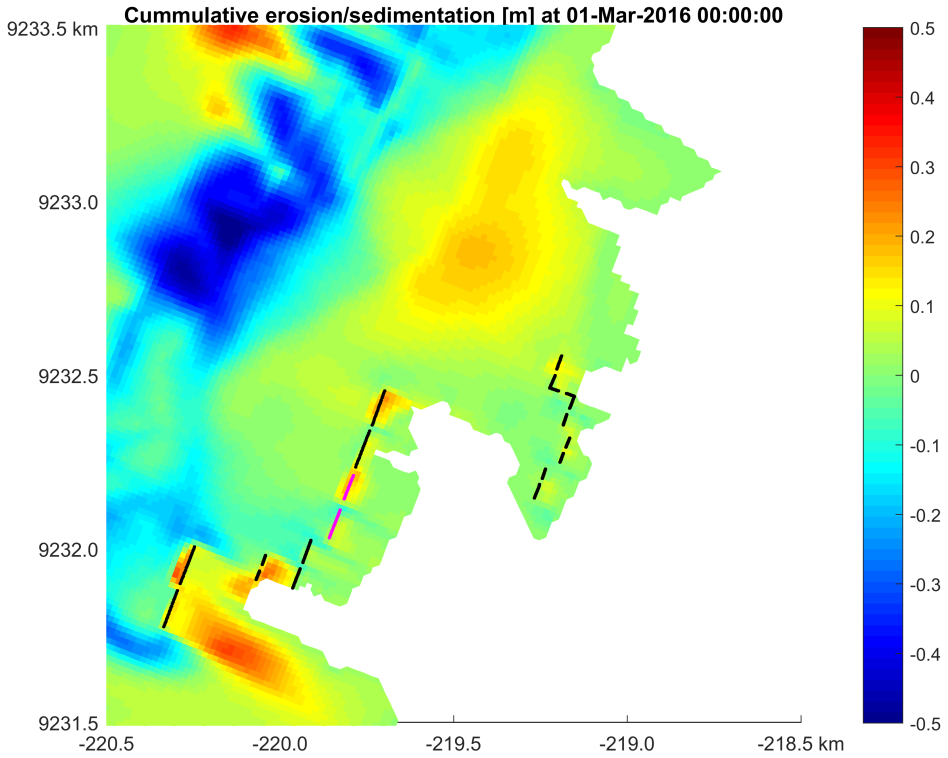

Figure I.28: Zoom of cumulative erosion and sedimentation [m] after a simulation of three months monsoon scenario with Ecoshape dams and dam added at 150 m from shore

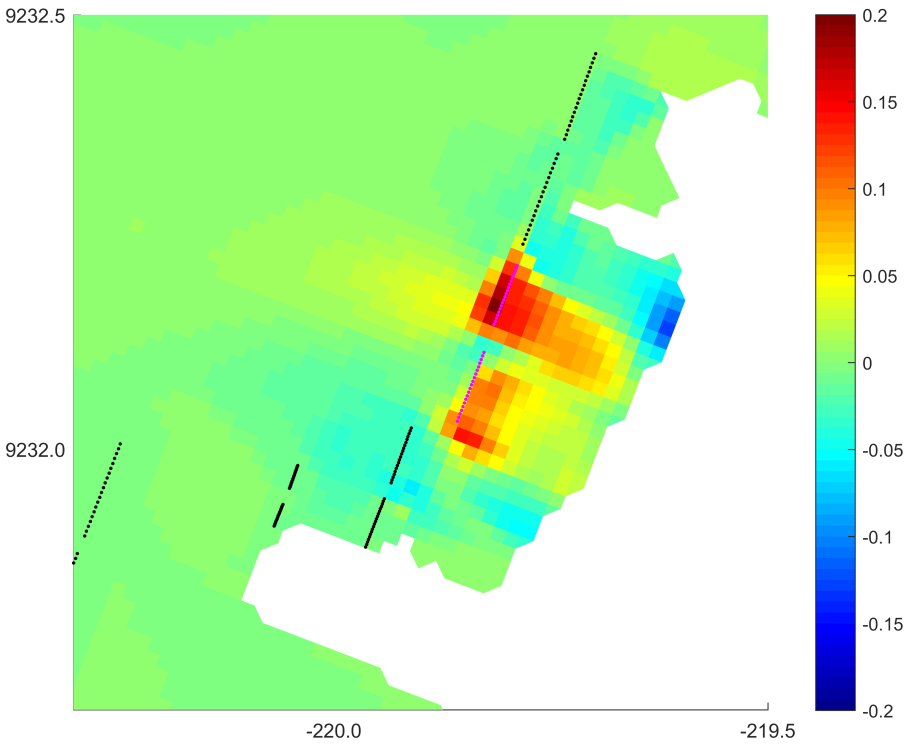

Figure I.29: Difference in remaining bed level [m] of Ecoshape dams with dam added at 150 m from shore compared to the original Ecoshape case

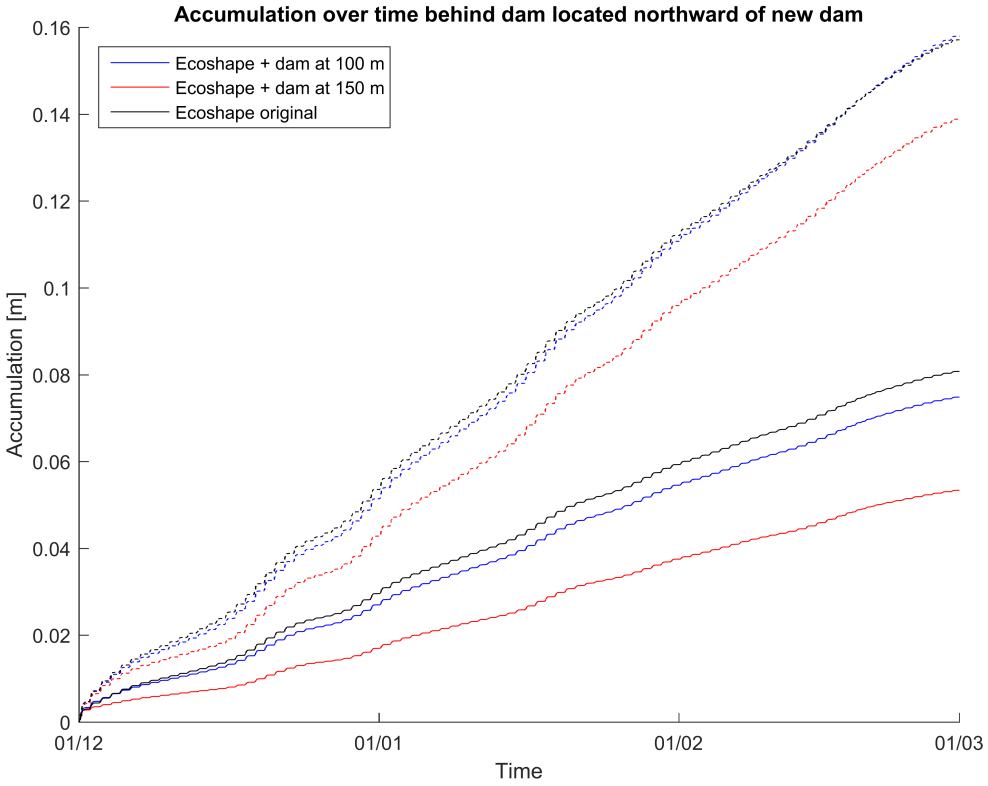

Figure I.30: Accumulation [m] over time behind dam located northward of added dam for a simulation of three months with the monsoon scenario

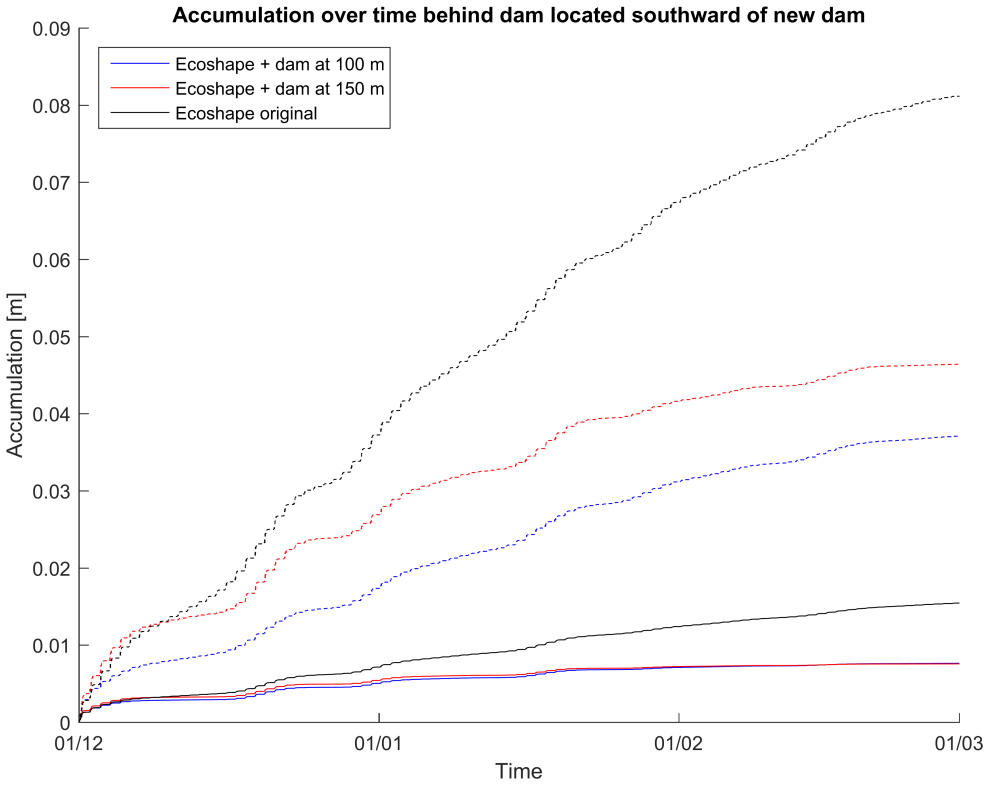

Figure I.31: Accumulation [m] over time behind dam located southward of added dam for a simulation of three months with the monsoon scenario

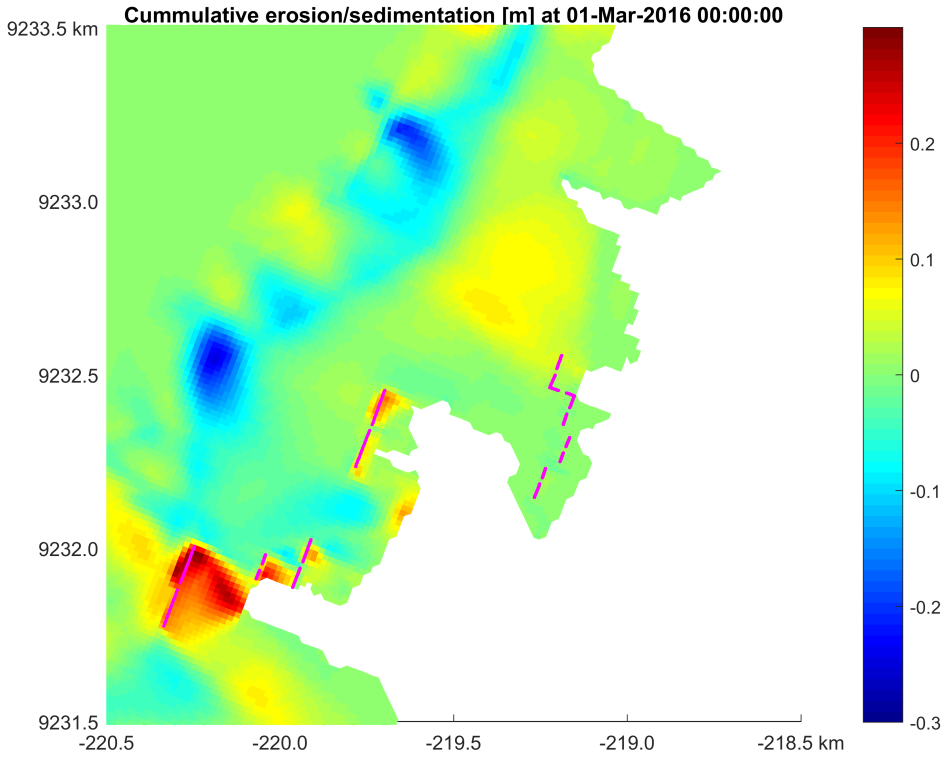

Figure I.32: Zoom of cumulative erosion and sedimentation [m] after a simulation of three months SW monsoon scenario with waves coming from the North

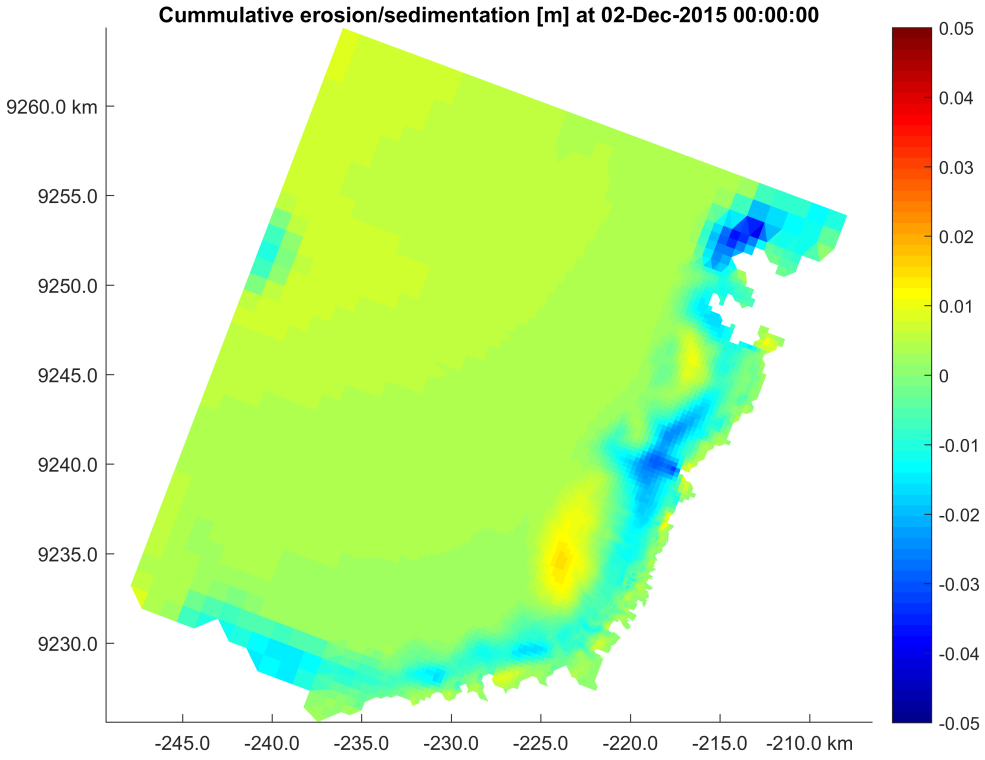

Figure I.33: Cumulative erosion and sedimentation [m] after a simulation of one day storm scenario with 2.1 m significant wave height (domain)

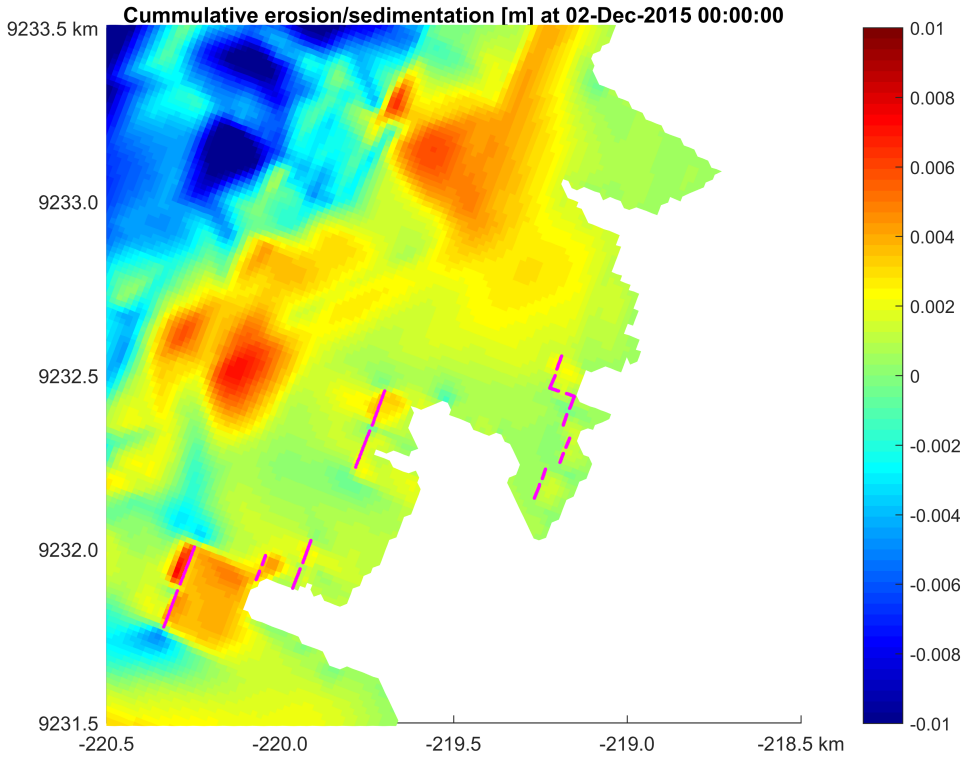

Figure I.34: Zoom of cumulative erosion and sedimentation [m] after a simulation of one day storm scenario with 2.1 m significant wave height

Appendix J

Results sensitivity analysis

This appendix contains the figures of the sensitivity analysis from section 6.3.

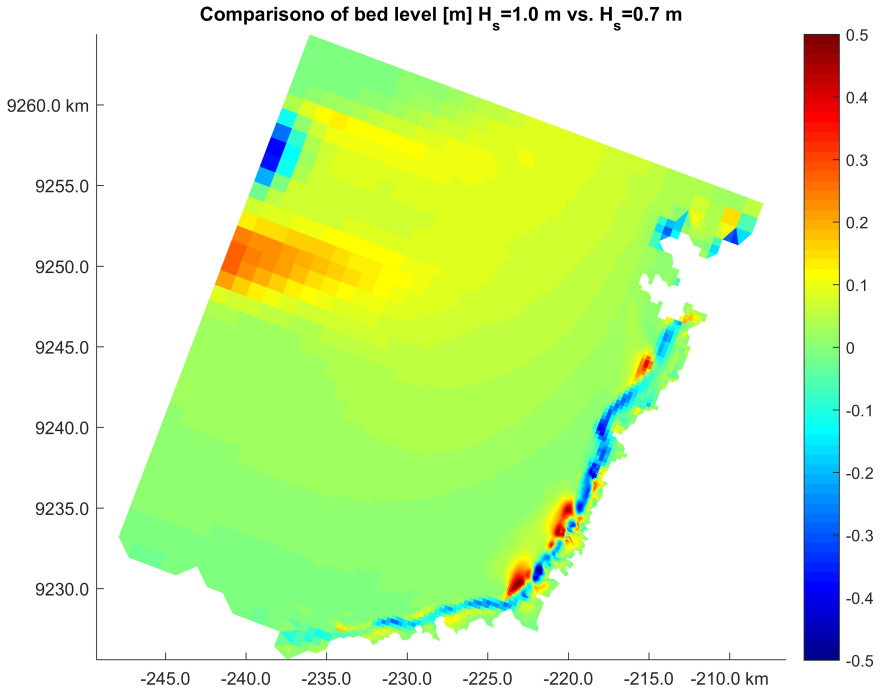

Figure J.1: Comparison of resulting bed levels with larger wave height and original (domain)

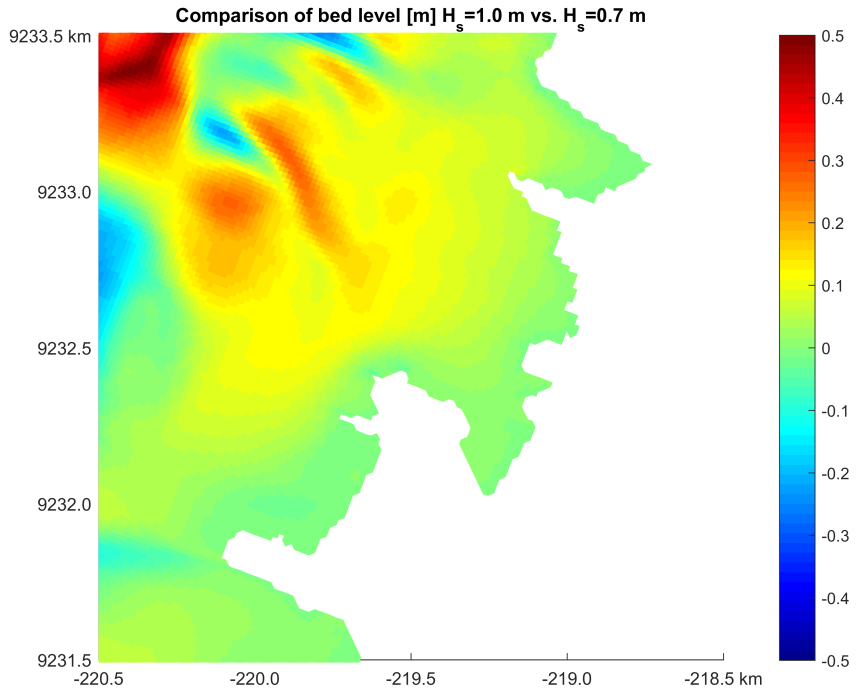

Figure J.2: Comparison of resulting bed levels with larger wave height and original (zoom)

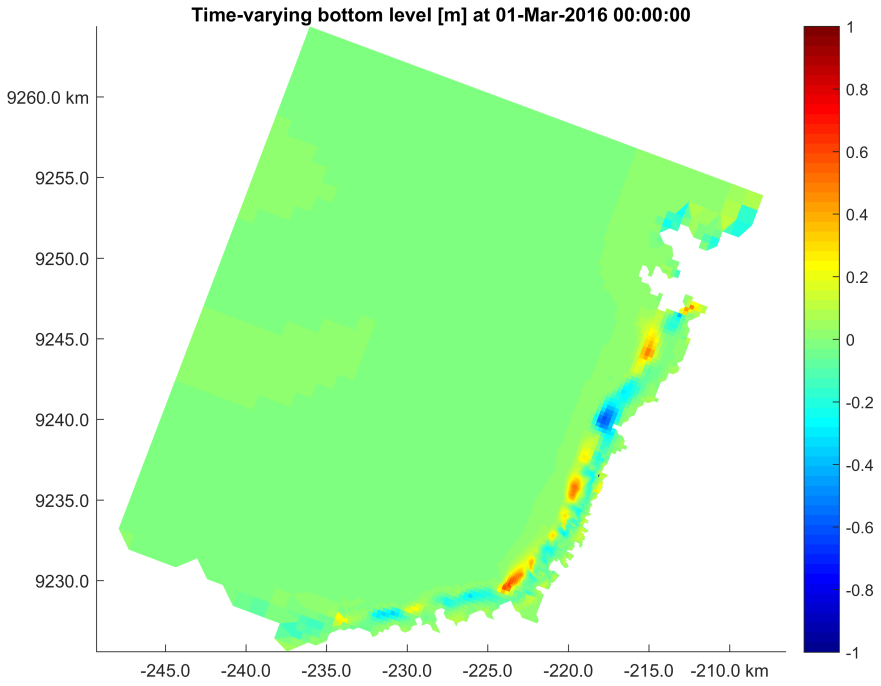

Figure J.3: Cumulative erosion and sedimentation at location of dams for reference case (no dams)

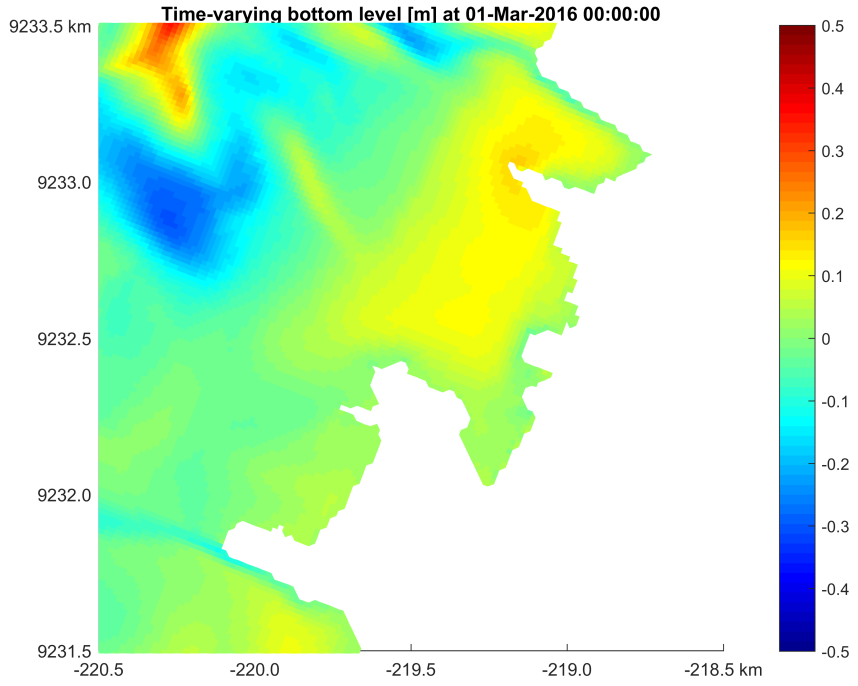

Figure J.4: Comparison of resulting bed levels with smaller viscosity and diffusivity to original (zoom)

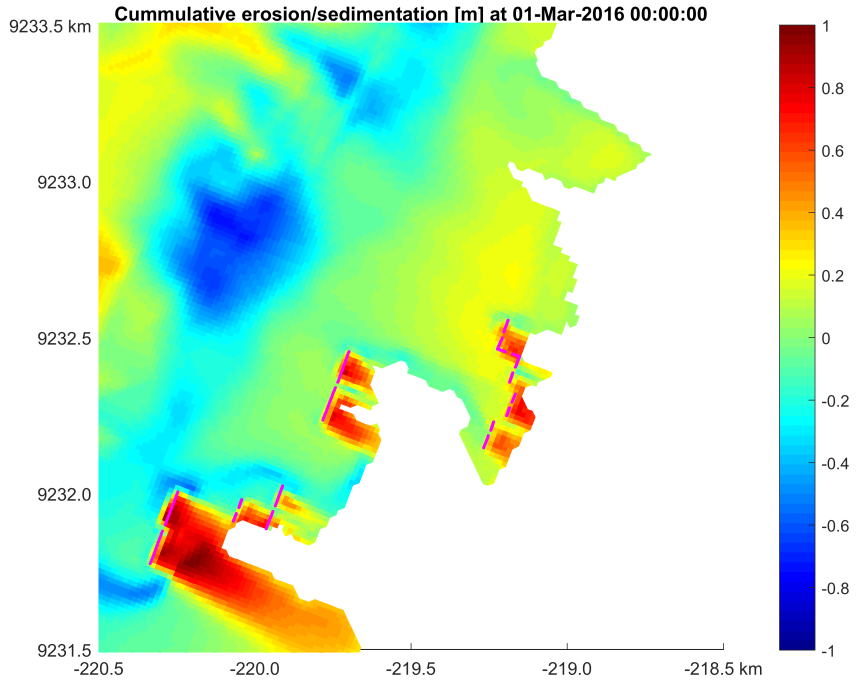

Figure J.5: Cumulative erosion and sedimentation at location of dams with critical shear stress of 0.25 Pa

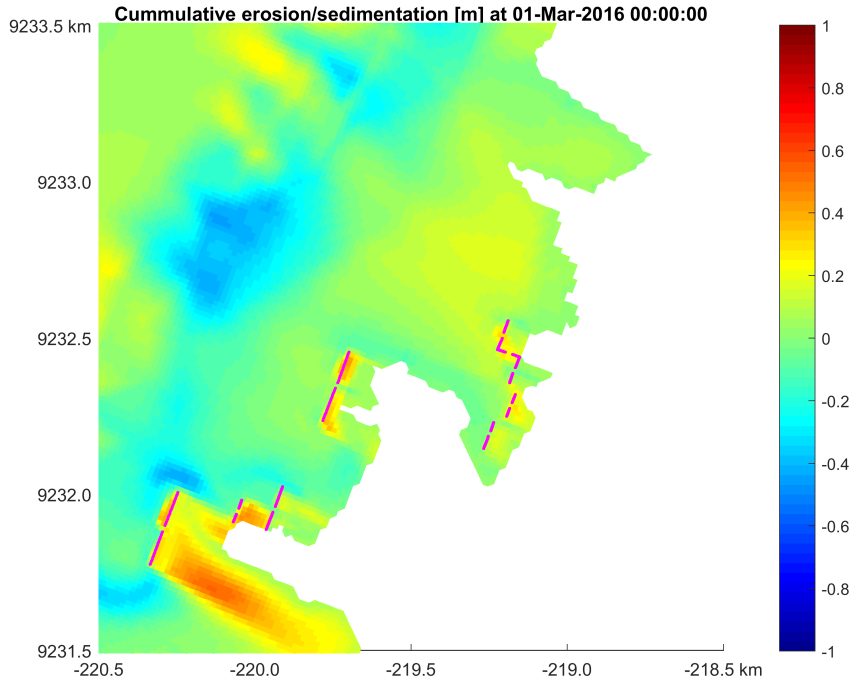

Figure J.6: Cumulative erosion and sedimentation at location of dams with critical shear stress of 0.50 Pa